Coordination Chemistry Reviews 438 (2021) 213623

Contents lists available at ScienceDirect

Coordination Chemistry Reviews

journal homepage: www.elsevier.com/locate/ccr

Review

Electrochemistry of fullerene/transition metal complexes: Three decades of progress

Alan L. Balch [a], Krzysztof Winkler [b,*]

[a] Department of Chemistry, University of California, Davis, Davis, CA 95616, USA
[b] Department of Chemistry, University of Bialystok, 15-245 Bialystok, Poland

ARTICLE INFO

Article history:
Received 4 August 2020
Accepted 21 September 2020
Available online 14 November 2020

Keywords:
Fullerenes
Metal complexes electrochemistry
Fullerenes coordination properties
Fullerene-transition metal macromolecular structures

ABSTRACT

This review is focused on the electrochemical properties of fullerene complexes of transition metals. In the first part of the review, the coordination properties of fullerenes are briefly overviewed. Metal complexes (polypyridyl complexes of transition metals, metallocenes, metalloporphyrins) that are covalently attached to the fullerene cage through the linkers are also briefly described. The η^2-C_{60} complexes of transition metals exhibit electrochemical activity related to the fullerene cage reduction and metal center oxidation. Upon reduction and oxidation, η^2-C_{60} complexes of transition metals are usually unstable and the metal-fullerene bond is cleaved. More stable electrochemical behavior was reported for η^2-C_{60} complexes of transition metal clusters. Fullerene moieties bonded into dimers through metal clusters can communicate electronically between themselves. The η^2-C_{60} coordination is also responsible for the formation of electrochemically active fullerene coordination polymers. These macromolecular systems show electrochemical activity at negative potentials and a n-doped properties. The metal-fullerene bond in polymers is much more stable under electroreduction conditions in comparison to the η^2-C_{60} complexes. The η^5-C_{60} complexes with a half-sandwich or sandwich structure also exhibit electrochemical activity in negative potential range related to the ferrocene cage reduction and in positive potentials due to the metal center oxidation. In contrast to η^2-fullerene complexes, the η^5-fullerene complexes of transition metals are much more robust under electrochemical conditions. The electrochemical properties of transition metal complexes in which the metal center is coordinated to the chelating ligand covalently linked to the fullerene moiety are important for understanding the photochemical performance of these systems. The electrochemical behavior of these complexes are usually combination of electrochemical properties of formed dyads and triads. The electronic communication between redox sites in the ground state depends on the complex geometry, distance between electrochemically active centers, and the nature of the linker.

Contents

* Corresponding author.
E-mail address: winkler@uwb.edu.pl (K. Winkler).

https://doi.org/10.1016/j.ccr.2020.213623
0010-8545/

1. Introduction

The chemical functionalization of fullerenes is a key factor in developing new compounds for potential application in different fields of science and technology. The preparation of first fullerene complexes of Pt(0) [1] and Ir(I) [2], triggered intensive exploration of exohedral transition metal coordination to the outer surfaces of fullerenes, particularly the abundant C_{60} and C_{70} [3–7]. In the reaction with transition metals, the fullerene cage can be considered as a two-electron donor, but one with a strong π-back bonding component that resembles electron-deficient alkene ligands [1].

Progress in the organic functionalization of fullerenes allows the production of a variety of organometallic fullerene derivatives with different structures and physicochemical properties. Also, the polyhedral structure of fullerenes contains a large number of coordination sites and provides a wide diversity of coordination modes to metal centers. Early work was focused on the metallofullerenes in which fullerene moieties were coordinated to the metal center in η^2-fashion. Different metals and metal clusters were bonded to the C_{60} and C_{70} to form a variety of organometallic derivatives of fullerenes [2,3] and this work has continued as outlined in the next section. Additional research focused on the formation of coordination polymers in which fullerene moieties were incorporated into a polymeric network by coordination to metal centers in η^2-fashion [8,9].

Fullerenes are also ideal molecular platform suited for the formation of complexes in which different organometallic moieties, (metalloporphyrins, metallocenes, polypyridyl metal complexes, and others) are bonded to the metal centers through different linkers [4,10]. The physicochemical properties of such structures can be controlled by the nature of organometallic moiety and the nature of the linker. Fullerenes multifunctionalized with organometallic centers can also form a variety of macromolecular systems [11].

Research focused on fullerene organometallic complexes is an important area within fullerene chemistry due to potential applications in bioanalysis, electronics, energy storage and optical devices, catalysis, and other fields of technology [12–14]. These practical applications are very often related to the electrochemical properties of organometallic complexes. C_{60}, the most abundant fullerene, is an electron-deficient spherical polyolefin that exhibits excellent electron-accepting properties. C_{60} is able to accumulate up to six electrons [15]. Its electrochemical properties can be tuned by the chemical modification of the carbon sphere [16]. The improvement of the electron-accepting features of fullerenes may result in the improvement of the intra- and intermolecular charge transfer processes [17,18]. Coordination of electron-rich metal fragments to a fullerene results in electronic modification of fullerene cluster and, consequently, its electrochemical properties. Bonding of electron-accepting fullerenes to metal complex units that exhibit electron-donating properties is another approach to form very interesting structures from a photophysical point of view in transmitting and processing solar energy [18–20]. The intramolecular electron transfer expected for these systems can be controlled by the structure and the distance of the linkers separating the electron-accepting and electron-donating parts of the macromolecular system and by the electrochemical properties of these two centers.

The review is focused on the electrochemical properties of complex fullerene-transition metal systems. In the first part, a short introduction to the coordination chemistry of fullerenes and transition metals is presented. Next, the electrochemical behavior of fullerenes and complexes in which transition metals are directly bonded to ferrocene moiety are described. At the end of this section of the review, the electrochemistry of coordination fullerene polymers is presented. Finally, the electrochemical properties of fullerenes with covalently bonded transition metal complexes' redox centers will be summarized. Special attention will be focused on the metalloporphyrin, metallocenes, and polypyridyl complexes containing fullerene derivatives.

2. Brief introduction to the coordination chemistry of fullerenes

2.1. Fullerenes as ligands

Many transition metal complexes coordinate to C_{60} and other larger fullerenes in an η^2-fashion, using a relatively localized double bond at a 6:6 ring junction of the fullerene as a two-electron donor. The structures of three complexes of this type, (η^2-C_{60})Pt(PPh_3)$_2$ (***1***) [1]; (η^2-C_{70})Ir(CO)Cl(PPh_3)$_2$ (***2***) [2]; and (η^2-D_{2d}(23)-C_{84})Ir(CO)Cl(PPh_3)$_2$ (***3***) [21] are shown in Fig. 1. For C_{60}, the situation is rather simple, addition of a Pt(PPh_3)$_2$ unit occurs at a 6:6 ring junction to form a mono-addition product. With C_{70} the situation is more complex, since there are four different 6:6 ring junctions. In this case, the addition of Ir(CO)Cl(PPh_3)$_2$ occurs at the pole of the oblong C_{70} cage to the ring junction with the highest pyramidalization of the carbon atoms. For addition to an even larger fullerene, C_{84}, additional issues come into play. There are 24 isomers of the C_{84} cage that obey the isolated pentagon rule (IPR), whereas for C_{60} and C_{70} there is only one isomer that obeys the IPR [22]. The IPR requires that each of the 12 pentagons on a fullerene surface be surrounded by five hexagons. All known empty cage fullerenes obey the IPR. The material produced in the usual arc generation

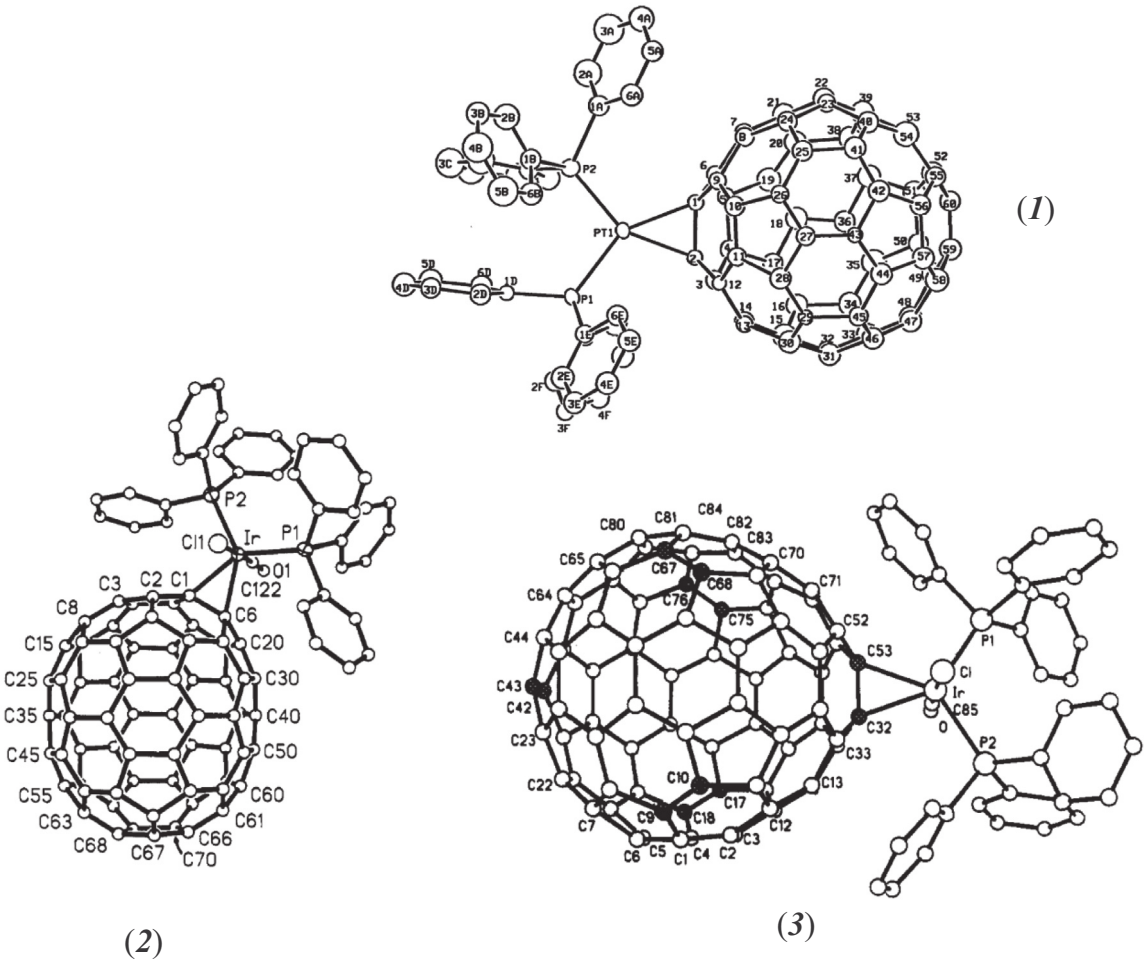

Fig. 1. The crystallographically determined structures of three η^2-complexes. (η^2-C_{60})Pt(PPh_3)$_2$ (***1***). Reproduced with permission from Ref. [1]. Copyright@1991, American Association for the Advancement of Science. (η^2-C_{70})Ir(CO)Cl(PPh_3)$_2$ (***2***). Reproduced with permission from Ref. [2]. Copyright@1991, American Chemical Society. (η^2-D_{2d}(23)-C_{84})Ir(CO)Cl(PPh_3)$_2$ (***3***) Reproduced with permission from Ref. [21]. Copyright © 1994, American Chemical Society.

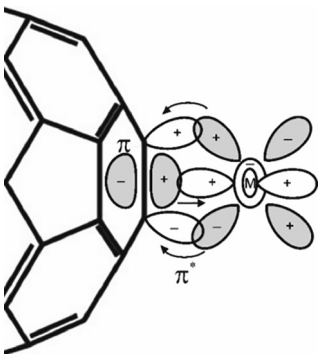

Fig. 2. The graphic representation of η^2-C_{60} – metal bond formation.

of fullerenes contains a mixture of several C_{84} isomers of which two with D_2 (22) and D_{2d} (23) symmetry are the most abundant and most stable [23]. The adduct isolated from a mixture of isomers of C_{84}, (η^2-D_{2d}(23)-C_{84})Ir(CO)Cl(PPh_3)$_2$, involved the C_{84} isomer with the highest localization of the π-bonding [21].

The η^2-type coordination of fullerene moiety to the metallic center is the most common form of fullerene-metal bonding. This type of fullerene-metal coordination is similar to the bonding of olefins to the metal center (Fig. 2). However, the electron-deficient properties of fullerene reduces the possibility of coordination of higher-valent metal ions. The η^2-C_{60} complexes of transition metal are largely limited to low oxidation states of metal center (0 or + I). The bonding of fullerene to the transition metal center can be described using the Dewar-Chatt-Duncanson back-donation model [24,25]. The donor bonding orbital is mainly generated from the HOMO of fullerene cage. The shift of the electron density from the fullerene to the metal center during the σ-bond formation may favor reduction of the fullerene moiety. In the back bonding donation, electron density is transferred from the HOMO of metal center to the LUMO of fullerene moiety. The relatively high electron affinity of the fullerene cage is responsible for strong back-donation bonding. This type of metal-fullerene interaction results in increase of negative charge on the fullerene cage and may disfavor reduction of fullerene moiety. This effect can be additionally enhanced by surface distortion of the fullerene cage and a lowered degree of π-electron conjugation. In general, the reduction potentials of η^2-C_{60} complexes of transition metals are determined by these two factors, which are not easy to separate.

More than one transition metal complex can bind to a single C_{60} or C_{70} molecule. Such multiple additions can readily result in the formation of isomers. For the addition of two similar groups to

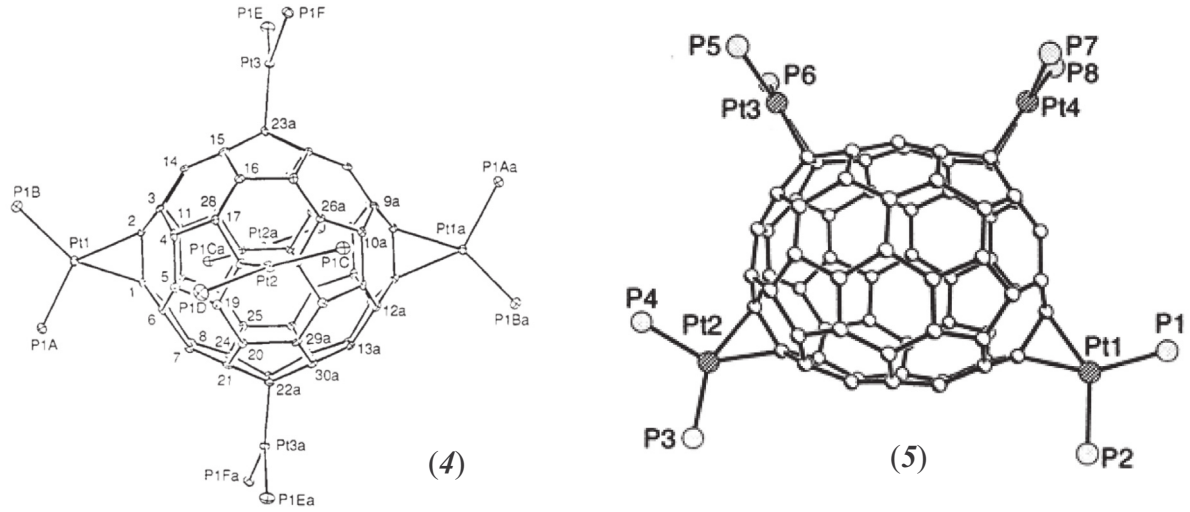

Fig. 3. The crystallographically determined structures of left $C_{60}\{Pt(PEt_3)_2\}_6$ (***4***) with the ethyl groups omitted. Reproduced with permission from Ref. [28]. Copyright@1991, American Chemical Society, and right $C_{70}\{Pt(PPh_3)_2\}_4$ (***5***) with the phenyl groups omitted. Reproduced with permission from Ref. [26]. Copyright © 1996, Wiley-VCH Verlag.

C_{60} there are eight possible regioisomers, and the complexity increases if more groups are added to the fullerene. A double addition product of C_{60} with two $Ir(CO)Cl(PPhMe_2)_2$ groups at opposite ends of the fullerene in *trans*-1 position has been crystallographically characterized, as has a double addition product of C_{70} [26,27]. In the case of addition of $Pt(PR_3)_2$ to fullerenes, the reaction is reversible and some rather symmetrical multiple addition products of C_{60} and C_{70} have been crystallized as seen in Fig. 3. $C_{60}\{Pt(PEt_3)_2\}_6$ (***4***) has six platinum atoms arranged in a nearly octahedral fashion about a C_{60} molecule [28]. The addition of four $Pt(PPh_3)_2$ groups to C_{70} produced the adduct $C_{70}\{Pt(PPh_3)_2\}_4$ (***5***) with C_{2v} symmetry [29]. Further developments in placing multiple metal ions about a C_{60} core have led to the creation of a series of copper(I) complexes that involve groups of six, twelve and twenty four copper(I) ions surrounding the fullerene [30]. Fig. 4 shows the structure of one member of the series with two $(C_3F_7CO_2Cu)_3(\mu\text{-}H_2O)CuO_2CC_3F_7)_3$ (***6***) units coordinated to the fullerene. As the drawing shows, each copper(I) ion is attached to the fullerene in an η^2-fashion.

Metal clusters can also be affixed to C_{60} and C_{70} [31]. The hexagonal face capped cluster, $Ru_3(CO)_9(\mu_3\text{-}\eta^2,\eta^2,\eta^2\text{-}C_{60})$ (***7***), shown in Fig. 5 is a prime example [32,33]. The compound was obtained by heating $Ru_3(CO)_{12}$ with C_{60} and resulted in the replacement of three carbonyl groups by three olefinic units within a hexagonal face of the fullerene. Although the overall structure is rather complicated, each attachment of a ruthenium atom to the fullerene can be viewed simply as an η^2 coordination of an olefinic unit at a 6:6 ring junction of the fullerene to the ruthenium.

Fullerenes that utilize a pentagonal face as an equivalent for a cyclopentadienide ligand have been obtained by the organocuprate

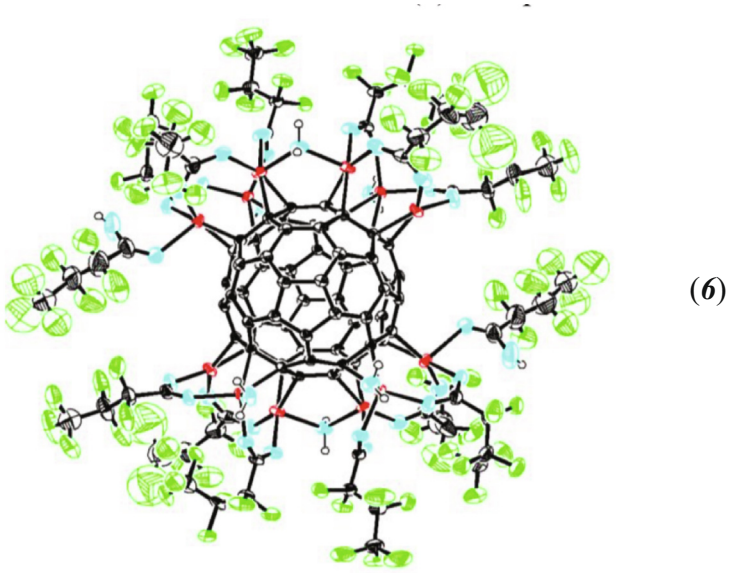

Fig. 4. Twelve copper(I) ions surrounding C_{60}. The crystallographically determined structure of $C_{60}@\{(C_3F_7CO_2Cu)_3(\mu\text{-}H_2O)CuO_2CC_3F_7)_3\}_2$ (**6**). Atom colors: copper, red; carbon, black, fluorine, green; oxygen, blue. Reproduced with permission from Ref. [30]. Copyright © 2020, American Chemical Society.

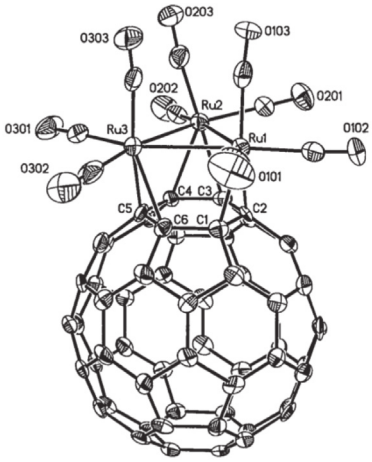

(7)

Fig. 5. The structure of face-capped $Ru_3(CO)_9(\mu_3\text{-}\eta^2,\eta^2,\eta^2\text{-}C_{60})$ (***7***) as determined by single crystal X-ray diffraction. Reproduced with permission from Ref. [32]. Copyright © 1996, American Chemical Society.

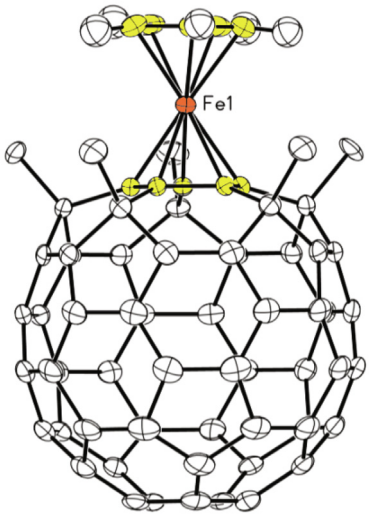

(8)

Fig. 6. The structure of the buckyferrocene hybrid $(\eta^5\text{-}C_{60}Me_5)Fe(\eta^5\text{-}C_5H_5)$ (***8***) as determined by single crystal X-ray diffraction from data in Ref. [35]. Copyright © 2002, American Chemical Society.

addition shown in Scheme 1 [34]. The reaction adds five alkyl or aryl groups to the fullerene in such a fashion that a pentagon is electronically isolated from the rest of the cage but available for η^5-coordination to a metal. Using this strategy, Nakamura and coworkers prepared the buckyferrocene hybrid $(\eta^5\text{-}C_{60}Me_5)Fe(\eta^5\text{-}C_5H_5)$ (***8***) seen in Fig. 6 [35] along with other η^5-bonded complexes such as $(\eta^5\text{-}C_{60}Me_5)Ru(\eta^5\text{-}C_5H_5)$ and $(\eta^5\text{-}C_{70}Me_3)Fe(\eta^5\text{-}C_5H_5)$.

In contrast to the high frequency of formation of η^2-complexes of fullerenes, η^1-C_{60} complexes with a metal bound to only one carbon atom of the fullerene are relatively rare. The photolysis of the metal–metal bound dimers, $\{Re(CO)_5\}_2$ or $\{(\eta^5\text{-}C_5H_5)Ru(CO)_2\}_2$ in the presence of C_{60} forms the η^1-C_{60} adducts, η^1-$C_{60}\{Re\{(CO)_5\}_2$ [36] and η^1-$C_{60}\{Ru\{(\eta^5\text{-}C_5H_5)(CO)_2\}_2$ [37,38], respectively. While η^1-$C_{60}\{Re\{(CO)_5\}_2$ was too unstable in solution to crystallize, η^1-$C_{60}\{Ru\{(\eta^5\text{-}C_5H_5)(CO)_2\}_2$ could be obtained in crystalline form [37]. The structure of η^1-$C_{60}\{Ru\{(\eta^5\text{-}C_5H_5)(CO)_2\}_2$ (***9***) is shown in Fig. 7. The two organo-ruthenium units are attached to opposite ends of a hexagonal face of the fullerene but are still quite close to one another as the space filling diagram shows. Encapsulation of C_{60} by silver(I) nitrate produces $C_{60}\{Ag(NO_3)\}_5$ with a network of silver(I) and nitrate ions that surround the carbon cage. The silver(I) ions engage in η^1-bonding to the fullerene carbon atoms [39].

The substituted fullerene C_{60} in Scheme 1 can also function as an η^1-ligand with an appropriate metal. Thus, reaction of K[(*p*-tolyl)$_5C_{60}$] with $ClAu(PPh_3)$ produced $(\eta^1\text{-}C_{60}(p\text{-}tol_5)Au(PPh_3)$ (***10***) whose structure is shown in Fig. 8 [40,41]. Interestingly, the copper(I) analog, $(\eta^5\text{-}C_{60}(p\text{-}tol_5)Cu(PPh_3)$, exhibits η^5-coordination with the copper ion centered above the pentagonal face of the fulleride.

Endohedral metallofullerenes are molecules comprised of a closed fullerene cage that encapsulates one or more metal atoms [42–44]. Additionally, clusters of metal atoms and main groups atoms can be found inside suitably sized carbon cages such as in $Sc_3N@I_h\text{-}C_{80}$ [45], $Sc_4O_2@I_h\text{-}C_{80}$ [46], and $Sc_2S@C_2(10528)\text{-}C_{72}$ [47]. Endohedral metallofullerenes have a rich electrochemical behavior but are formed in relatively low yield. As a consequence, major efforts are needed to isolate and purify these novel molecules. Exohedral transition metal adducts of endohedral fullerenes are rarely studied, probably because the endohedral fullerenes are available in such small amounts. But there are a few exceptions.

Treatment of $[Li@C_{60}](PF_6)$ with $Ir(CO)Cl(PPh_3)_2$ produced the η^2-adduct, $[\eta^2\text{-}Li@C_{60}]Ir(CO)Cl(PPh_3)_2(PF_6)$ (***11***), whose structure is shown in Fig. 9 [48,49]. In this adduct, the iridium-fullerene interaction is stronger than in the corresponding empty cage adduct, η^2-$(C_{60})Ir(CO)Cl(PPh_3)_2$ [50]. $[Li@C_{60}](PF_6)$ also reacts with platinum(0) complexes to form adducts such as $[\eta^2\text{-}Li@C_{60}]Pt\{1,1'\text{-bis(diphenylphosphino)ferrocene}\}^+$ (***12***), whose structure is also shown in Fig. 9. Notice that in both structures shown in Fig. 9,

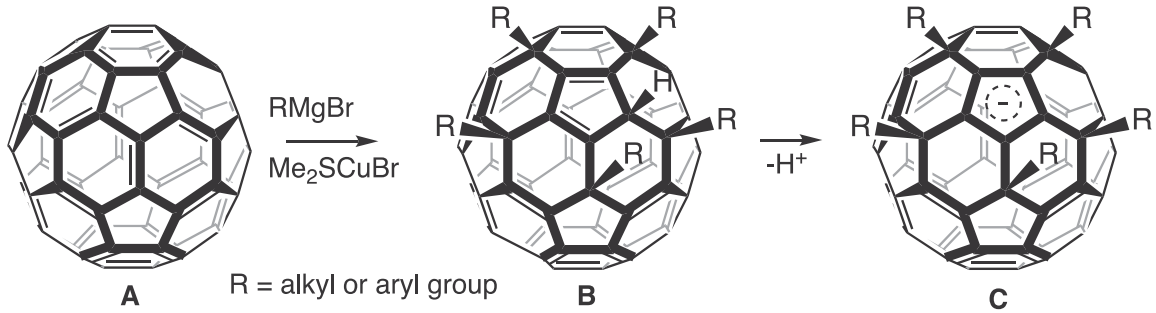

Scheme 1. The organocuprate addition to attach five alkyl or aryl groups to C_{60}.

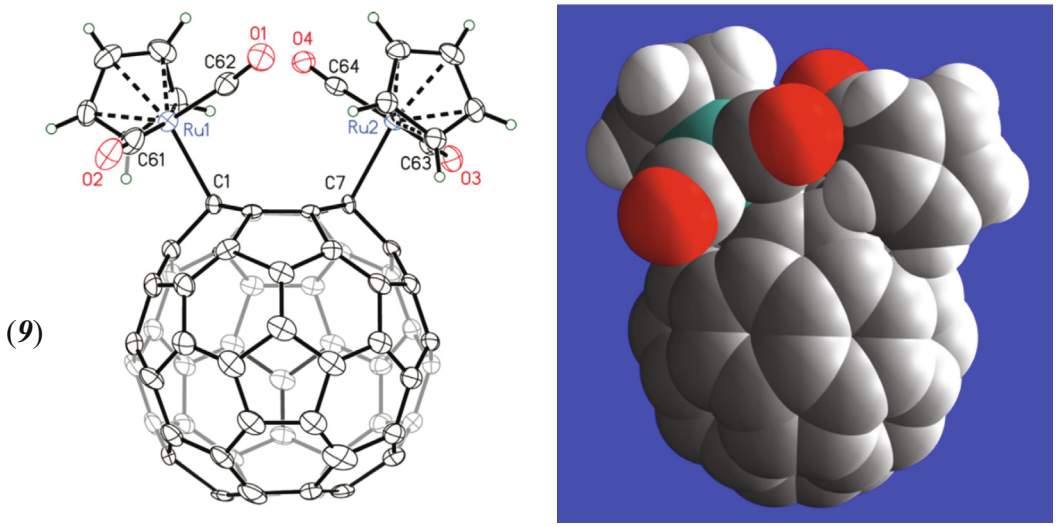

(*9*)

Fig. 7. The structure of η^1-C_{60}{Ru{(η^5-C_5H_5)(CO)$_2$}$_2$ (***9***) as determined by single crystal X-ray diffraction. The drawing on the right shows space filling contours that emphasize the close proximity of the two organo-ruthenium groups. Reproduced with permission from Ref. [37]. Copyright © 2014, American Chemical Society.

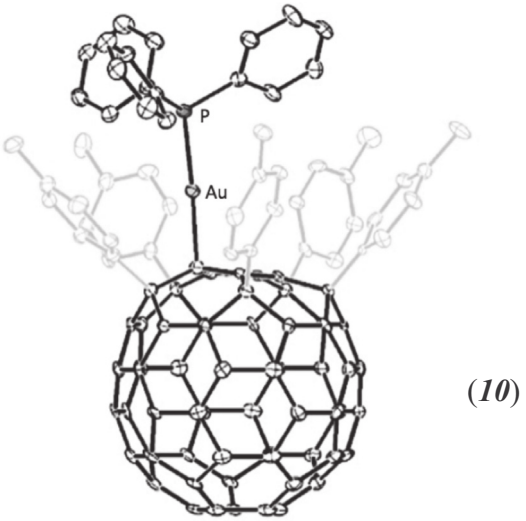

(*10*)

Fig. 8. The structure of (η^1-C_{60}*p*-tol$_5$)Au(PPh$_3$) (10) as determined by single crystal X-ray diffraction reproduced with permission from Ref. [40]. Copyright © 2011, American Chemical Society.

the Li^+ ion is localized in a single position near the site of bonding to the external metal. In $[Li@C_{60}]^+$, the lithium ion is freely moving within the cage [51].

The photochemical reaction between $W(CO)_4(Ph_2PC_2H_4PPh_2)$ and $Sc_3N@I_h$-C_{80} produces the adduct, (η^2-$Sc_3N@I_h$-C_{80})$W(CO)_3$(-$Ph_2PC_2H_4PPh_2$) (***13***), whose structure is shown in Fig. 10 [52]. The tungsten atom is bonded to carbon atoms at a 6:6 ring junction of the endohedral fullerene.

Under appropriate conditions, endohedral metallofullerenes can also form η^1-bound complexes with transition metals. Photolysis of {$Re(CO)_5$}$_2$ in the presence of the paramagnetic endohedral fullerene $Y@C_{2v}(9)$-C_{82} produces the η^1-bonded, diamagnetic complex, η^1-($Y@C_{2v}(9)$-C_{82})$Re(CO)_5$. Two views, (***14***) and (***15***), of its structure are shown in Fig. 11 [53].

Endohedral metallofullerenes can also bind metal clusters. The reaction of $Sc_2C_2@C_{3v}(8)$-C_{82} with $(\mu$-H)$_3$Re$_3$(CO)$_{11}$(NCMe) produced [(η^2,η^2-$Sc_2C_2@C_{3v}(8)$-C_{82})(μ-H)$_3$Re$_3$(CO)$_9$] (***16***), whose structure is given in Fig. 12 [54]. In an interesting development, reactions of the cluster (μ-H)$_3$Re$_3$(CO)$_{11}$(NCMe) with mixtures of fullerenes including $Sc_2@C_{3v}(8)$-C_{82}, $Sc_2C_2@C_{2v}(5)$-C_{80}, $Sc_2O@C_s(6)$-C_{82}, $C_2(17)$-C_{86}, and $C_s(16)$-C_{86} have been shown to yield adducts and to be useful in the separation of these molecules [55]. Further crystallographic characterization of these adducts would be a welcome addition to the field.

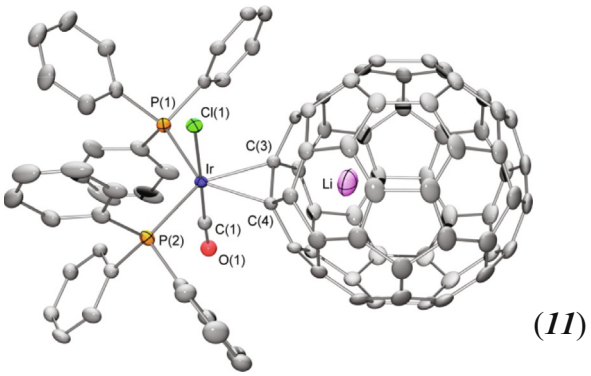

(*11*)

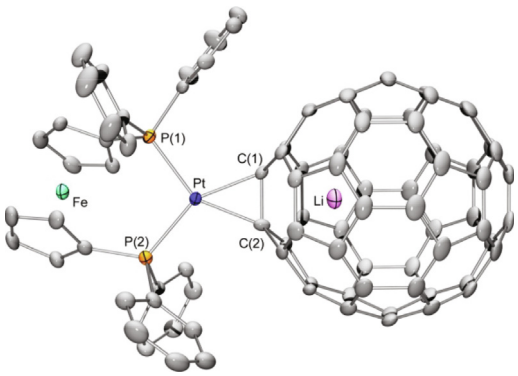

(*12*)

Fig. 9. Drawings of the cations: [(η^2-Li@C_{60})Ir(CO)Cl(PPh$_3$)$_2$]$^+$ (***11***) and [η^2-Li@C_{60}]Pt{1,1′ -bis(diphenylphosphino)ferrocene}$^+$ (***12***). Hydrogen atoms and the anions are not shown for simplicity. Reproduced with permission from Ref. [48]. Copyright © 2013, American Chemical Society.

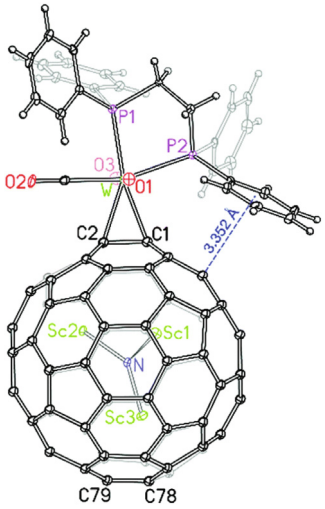

(*13*)

Fig. 10. Drawing of (η^2-$Sc_3N@I_h$-C_{80})$W(CO)_3(Ph_2PC_2H_4PPh_2)$ (***13***) reproduced with permission from Ref. [52]. Copyright © 2016, Royal Society of Chemistry.

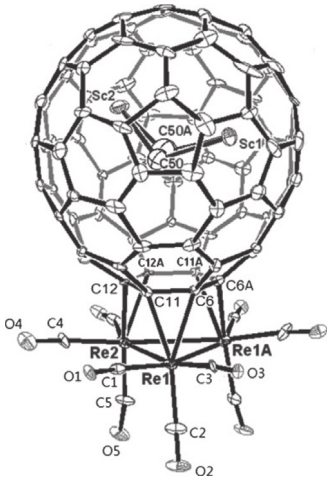

(*16*)

Fig. 12. The structure of {(η^2,η^2,η^2-$Sc_2C_2@C_{3v}(8)$-C_{82})(μ-H)$_3Re_3(CO)_9$} (***16***) as determined by X-ray crystallography reproduced with permission from Ref. [54]. Copyright © 2012, Wiley-VCH Verlag.

2.2. Metal-coordinating ligands attached to fullerene

In addition to direct coordination of transition metals to fullerenes and endohedral metallofullerenes, ligating groups can be appended to the surfaces of these fullerenes that allow attachment of metals to specifically designed external sites with control over the distance of the metal to the fullerene. This topic has been reviewed [56]. Fig. 13 shows a few examples of such ligands where specific sites for metal bonding have been covalently attached to the fullerene. Further examples will be discussed in the context of their electrochemical behavior later in this article.

It is also possible to have a hybrid situation in which a coordinating group covalently appended to a fullerene binds a metal that is also bound to the fullerene surface. Fig. 14 shows two examples of such a situations [57,58].

3. Electrochemistry of pristine fullerenes.

The fullerenes, C_{60} and C_{70}, are strong electron acceptors but weak electron donors. A partial molecular orbital diagram for the frontier orbitals for C_{60} is shown in Fig. 15 [59]. The HOMO is a five-fold degenerate h_u orbital, while the LUMO is a three-fold degenerate t_{1u} orbital that can accommodate up to six added electrons. Fig. 16 shows cyclic voltammograms and differential pulse voltammetry for C_{60} and for C_{70} in a toluene/acetonitrile mixture with tetra(*n*-butyl)ammonium hexafluorophosphate as supporting electrolyte at 10° C [60]. Six one-electron, reversible reduction waves are seen for both fullerenes. These reductive processes produce stable anions. These anions have been isolated in various solid forms. The properties of these anionic fulleride salts have been reviewed [61,62]. In particular, the alkali metal fullerides such as K_3C_{60} have remarkable conducting and superconducting properties [62–65]. Recently, hydrocarbon soluble magnesium salts of the fulleride ions $(C_{60})^{n-}$ (n- = 2-, 4-, and 6-) have been isolated and crystallographically characterized [66].

While C_{60} is readily reduced, it is difficult to oxidize, and the resulting cations are highly reactive [67,68]. Cyclic voltammograms of C_{60} in carefully dried dichloromethane solution with tetra(*n*-butyl)ammonium hexafluoroarsenate as supporting electrolyte reveals three reversible, one-electron oxidation waves at 1.27, 1.74 and 2.14 V vs Fc^+/Fc [69].

(*14*)

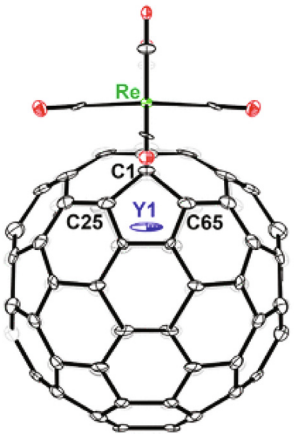

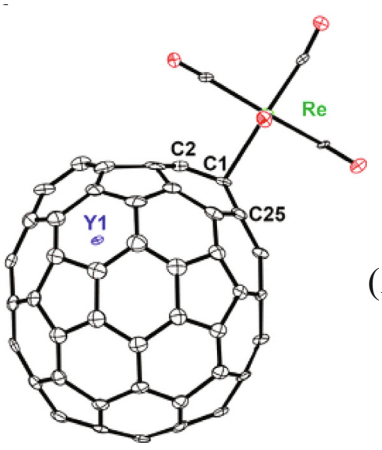

(*15*)

Fig. 11. Two drawings (***14***) and (***15***) of η^1-(Y@$C_{2v}(9)$-C_{82})$Re(CO)_5$. Thermal contours are at 0.30 probability. The CS_2 solvate molecule and Y positional disorder are not shown for simplicity. Reproduced with permission from Ref. [53]. Copyright © 2019, American Chemical Society.

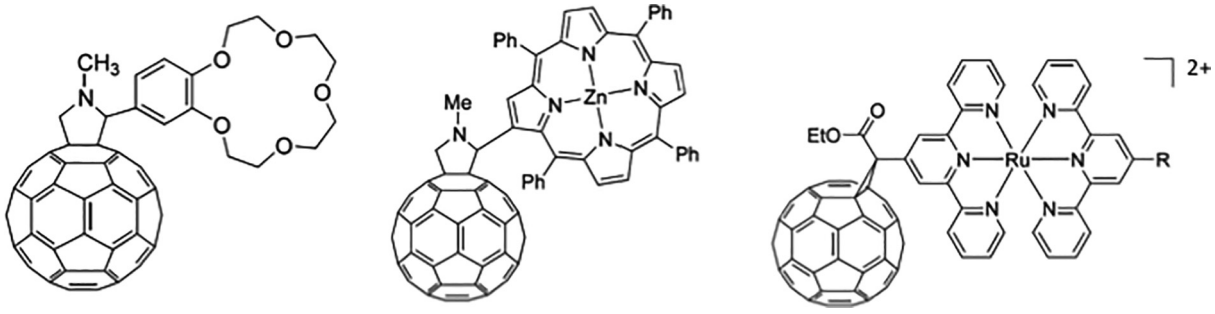

Fig. 13. Three examples of C_{60} with ligating groups covalently attached.

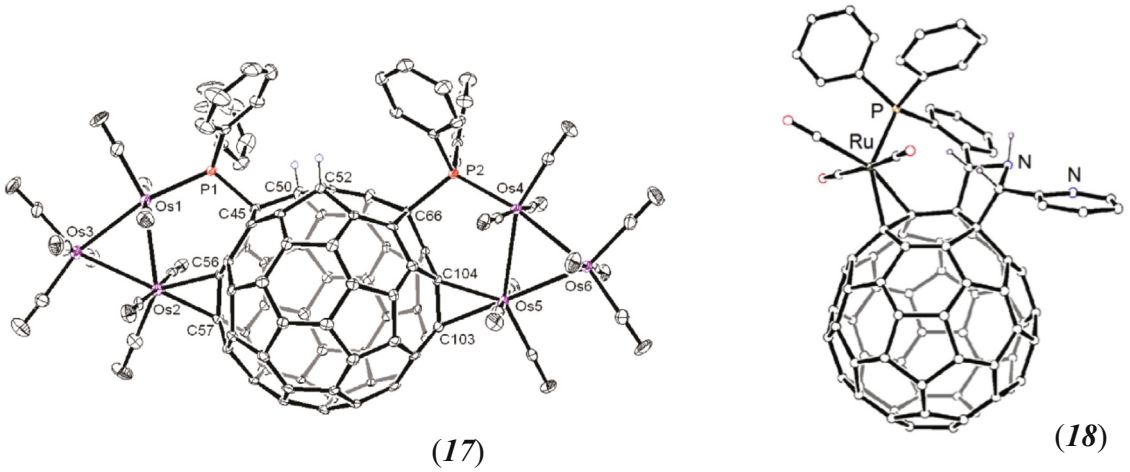

(*17*) (*18*)

Fig. 14. Two examples of C_{60} with ligating groups, which bind metal complexes that are also coordinated to the fullerene cage. Structure of $(Os_3(CO)_{10})_2(\mu,\mu,\eta^3,\eta^3\text{-}(PPh_2)_2(H)_2C_{60})$ (***17***). Reproduced with permission from Ref. [57]. Copyright @ 2011, American Chemical Society. Structure of $Ru(CO)_3[\eta^3\text{-}PPh_2(o\text{-}C_6H_4)(o\text{-}C_5H_4N)(C_2H_3NC_{60})]$ (***18***). Reproduced with permission from Ref. [58]. Copyright © 2017, Elsevier.

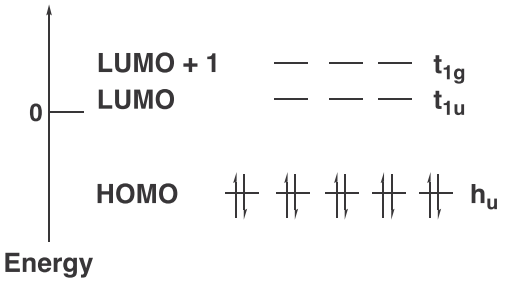

Fig. 15. The frontier molecular orbitals for I_h-C_{60}.

4. Electrochemistry of complexes with direct coordination of fullerenes to transition metals

4.1. Complexes of η^2- fullerene coordination to the metal center

4.1.1. η^2-fullerene complexes of group 10 metals

The η^2-type fullerene complexes of zero-valent platinum(***19***), palladium (***20***), and nickel (***21***) have been extensively investigated [70,71]. The exemplary crystal structure of $(\eta^2\text{-}C_{60})Pt(PPh_3)_2$ is shown in Fig. 1. These are also historically very important studies. Fagan and co-workers reported the electrochemical behavior of these fullerene complexes for the first time. In the negative potential range, the fullerene cage involved reduction steps are observed as seen in Scheme 2 and Fig. 17. The potentials of these redox processes are shifted by ca. 300–350 mV toward more negative potentials in comparison to the corresponding potentials for pristine fullerene reduction (see Table 1). Such significant shifts of reduction potentials of these complexes result from the π-back electron transfer from the metal to the fullerene cage and therefore a significant increase of electron density within the fullerene ligand. The nature of the metal atoms and the organic groups bound to phosphorus do not influence the potentials for fullerene reduction. The stability of the complex upon reduction depends on the negative potential limit. In the time window of experiment (sweep rate was 0.2 Vs^{-1}), reversible electrochemical behavior was observed for the exchange of the first electron. The second and third reduction processes were accompanied by the following chemical reaction of complex decomposition. Scheme 2 describes the electrochemical processes for η^2-type fullerene complexes of zero-valent metals (Ni, Pd, and Pt). The reduction potential of the complex depends also on the number of metal centers bounded to the fullerene cage (Table 1) [70,71]. The addition of each metal unit results in a similar shift of the complex reduction potential in the range of 30 to 40 mV. Such behavior indicates that each metal unit transfers the same electron density to the fullerene cage during complex formation.

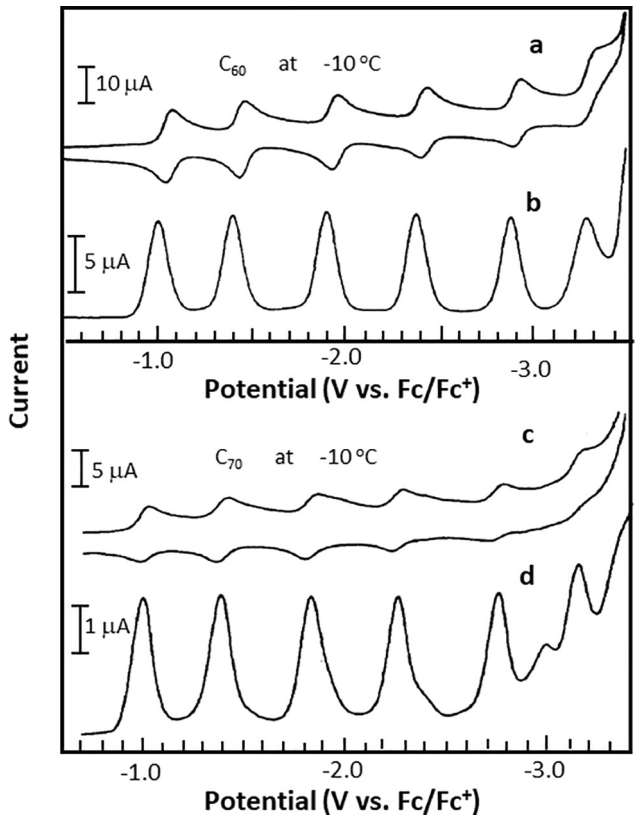

Fig. 16. Cyclic voltammetry (traces a and c) and differential pulse voltammetry (traces b and d) for C_{60} and C_{70} in toluene/acetonitrile solution with $[(n\text{-}Bu)_4N]PF_6$ as supporting electrolyte at 10 °C reproduced with permission from Ref. [60]. Copyright © 1992, American Chemical Society.

In the positive potential range, irreversible oxidation processes for η^2-fullerene complexes of Ni, Pd, and Pt are observed as seen in Fig. 18 [71]. The number of oxidation steps depends on the number of metal centers coordinated to the fullerene moiety. The addition of each metal-containing group shifts the oxidation potential of the complex toward less positive values [71]. The oxidation potential also depends on the nature of metal indicating that HOMO orbitals located on metal centers are involved in these oxidation processes. Additionally, the oxidation potentials for the complexes correlate with the standard potentials of M/M^{2+} (M = Ni, Pd, and Pt) redox couples. The oxidation process, like the reduction process, results in the complex decomposition. In the case of multimetallic complexes, each two-electron oxidation process is followed by a cleavage of metal-fullerene bound (Scheme 3).

Similar voltammetric behavior was observed for η^2- [60] fullerene complexes of Pd(0) (***22***) and Pt(0) (***23***) that contain chiral 2,3-O,O'-isopropylidene-2,3-dihydroxy-1,4-bis(diphenyl-phosphanyl) butane (diop) [72]. For these complexes, it was reported that the rate of fullerene-metal cleavage processes can be lowered at low temperatures.

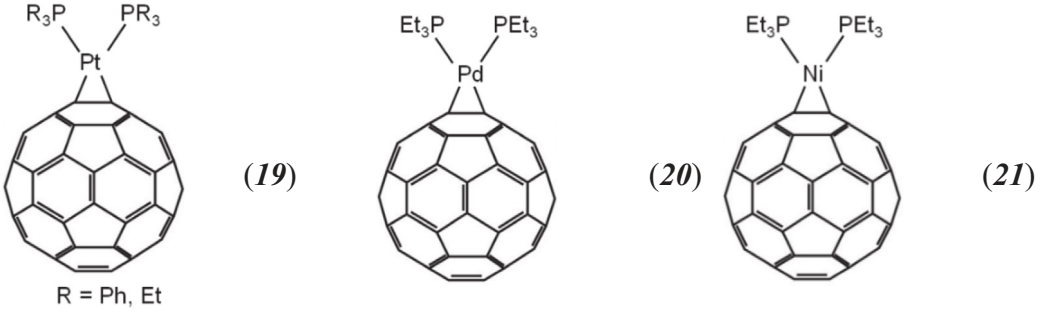

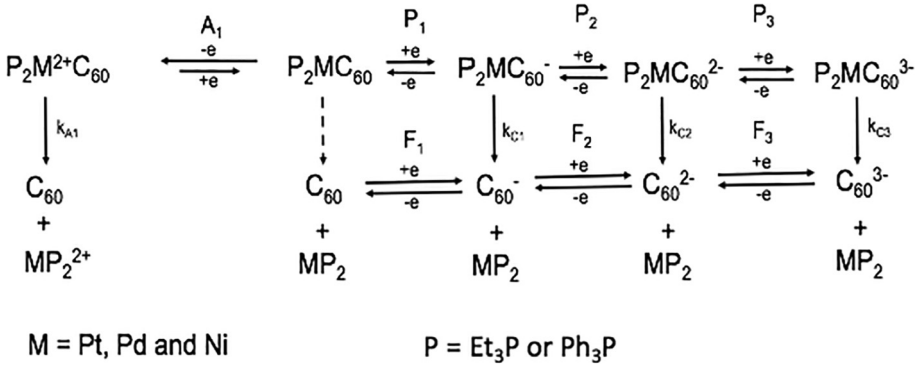

Scheme 2. Electrode processes for η^2-C_{60} complexes of platinum, palladium and nickel.

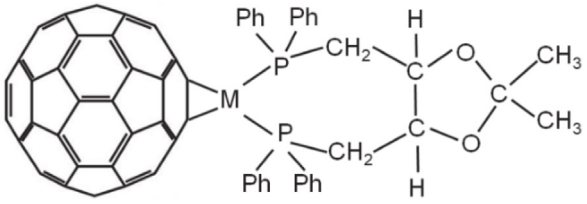

M = Pd (*22*)

M = Pt (*23*)

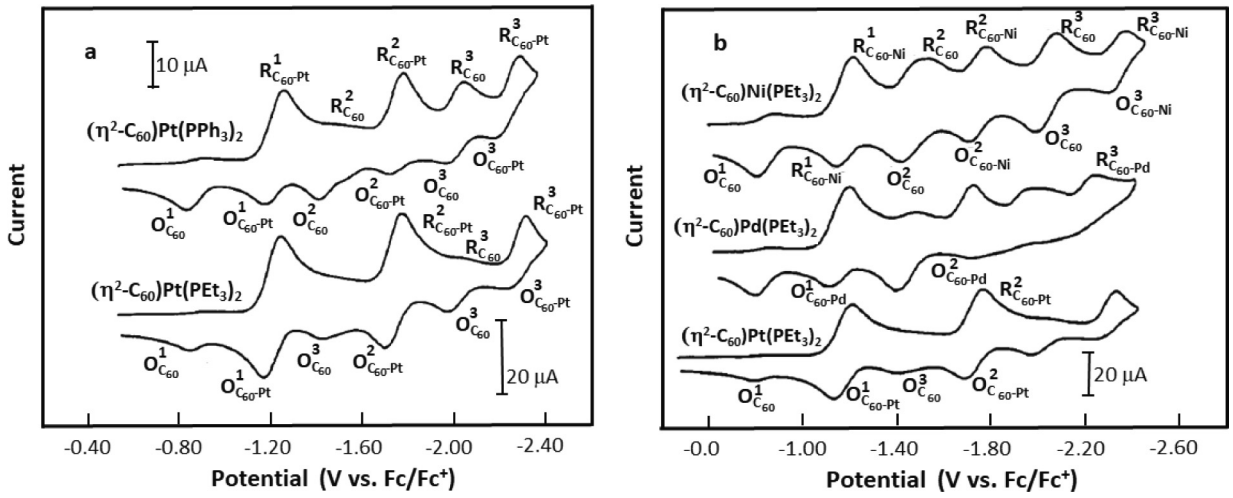

Fig. 17. Comparison of cyclic voltammograms of (a) $(\eta^2\text{-}C_{60})Pt(PPh_3)_2$ and $(\eta^2\text{-}C_{60})Pt(PEt_3)_2$, and (b) $(\eta^2\text{-}C_{60})M(PEt_3)_2$ (M = Ni, Pd, Pt) in tetrahydrofuran containing 0.2 M $[(n\text{-}Bu)_4N]PF_6$, platinum disk working electrode, scan rate was 0.2 V s^{-1}, ambient temperature. Reproduced with permission from Ref. [70]. Copyright © 1992, American Chemical Society.

Table 1
Redox potentials of C_{60} and η^2-C_{60} complexes of platinum, palladium and nickel in tetrahydrofuran.

Compound	Redox potential in V vs. Fc/Fc^+				
	E_{ox}[a]	R_1	R_2	R_3	Ref.
C_{60}		−0.86	−1.44	−2.00	[70]
$(\eta^2\text{-}C_{60})Pt(PPh_3)_2$		−1.21	−1.75	−2.23	[70]
$(\eta^2\text{-}C_{60})Pt(PEt_3)_2$	+0.35	−1.20	−1.73	−2.27	[70,71]
$(\eta^2\text{-}C_{60})[Pt(PEt_3)_2]_2$	+0.40 + 0.18	−1.51			[70,71]
$(\eta^2\text{-}C_{60})[Pt(PEt_3)_2]_3$	+0.40 + 0.21–0.06	−1.93			[70,71]
$(\eta^2\text{-}C_{60})[Pt(PEt_3)_2]_4$		−2.31			[70]
$(\eta^2\text{-}C_{60})Pd(PEt_3)_2$		−1.18	−1.69	−2.23	[70]
$(\eta^2\text{-}C_{60})Ni(PEt_3)_2$	+0.09	−1.20	−1.74	−2.32	[70]

[a] peak potential of irreversible oxidation process.

The η^2-fullerene palladium(0) and platinum(0) dimers (***24***) – (***26***) in which η^2-fullerene-metal moieties were connected with *trans*-1,1′-bis(diphenylphosphanyl)ethylene (dppet) linkers have been used to examine possibility of electronic communication between fullerene moieties [73]. The voltammetric behavior of the homometallic complex (***24***) and the heterometallic complex (***26***) are shown in Fig. 19. The voltammogram of complex (***24***) exhibits four two-electron reduction peaks (Fig. 19a). The complex does not show any electronic communication effects but is stable upon reduction in the potential range for four fullerene cage reduction steps. The heterometallic dimer (***26***) exhibits more complex behavior. Six one-electron reduction steps involve the reduction of the fullerene cages. The potentials for three of them correspond to the reduction potentials of complex (***24***) and are related to the reduction of fullerene moiety bonded to the palladium center. The second sequence of voltammetric peaks corresponds to the reduction of fullerene cage coordinated to platinum center. The larger cathodic shift of fullerene moiety reduction potential indicates the higher coordination ability of Pt with respect to Pd towards fullerene. In contrast to the results reported for Fagan and coworkers [70,71], electrochemical experiments performed for the heterometallic dimer (***26***) [73] indicate that nature of the metal atom influences the amount of electron density transferred to the fullerene center during complexation.

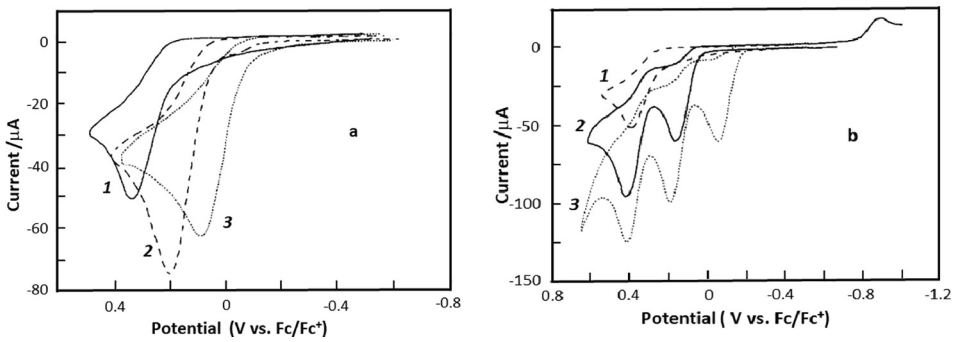

Fig. 18. (a) Cyclic voltammograms of 0.5 mM (η^2-C_{60})$Pt(Et_3P)_2$ (*1*), (η^2-C_{60})$Pd(Et_3P)_2$ (*2*), and (η^2-C_{60})$Ni(Et_3P)_2$ (*3*). (b) Cyclic voltammograms of 0.5 mM (η^2-C_{60})$Pt(Et_3P)_2$ (*1*), (η^2-C_{60})$[Pt(Et_3P)_2]_2$ (***2***), and (η^2-C_{60}) $[Pt(Et_3P)_2]_3$ (***3***) in tetrahydrofuran containing 0.2 M $[(n\text{-}Bu)_4N]PF_6$, platinum disk working electrode, sweep rate was 0.20 V/s, ambient temperature. Reproduced with permission from Ref. [71]. Copyright © 1995, American Chemical Society.

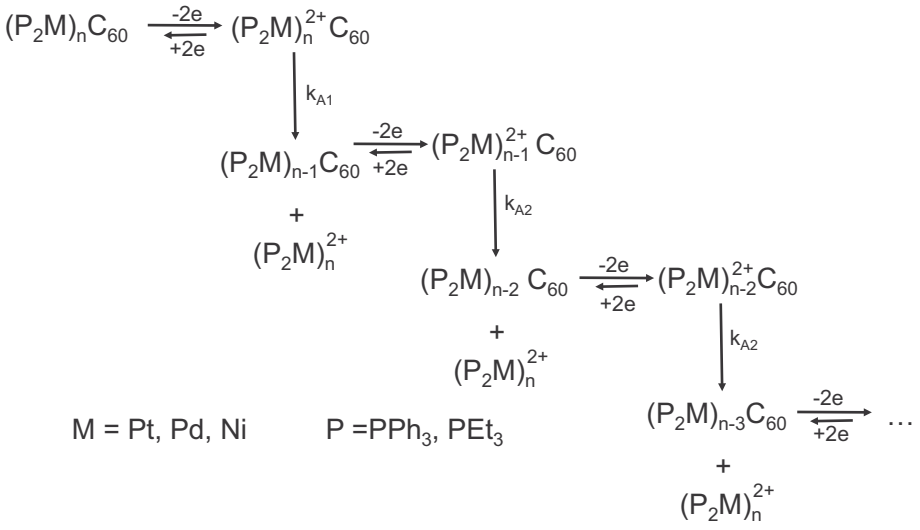

Scheme 3. Oxidative electrode processes for η^2-C_{60} complexes of platinum, palladium and nickel.

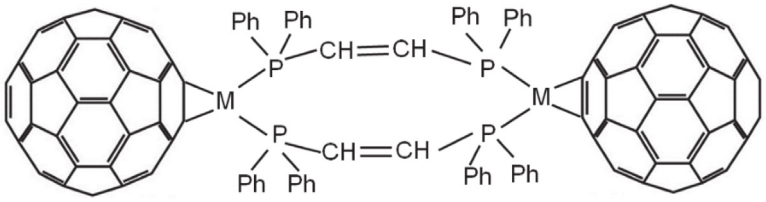

M = Pd (***24***)

M = Pt (***25***)

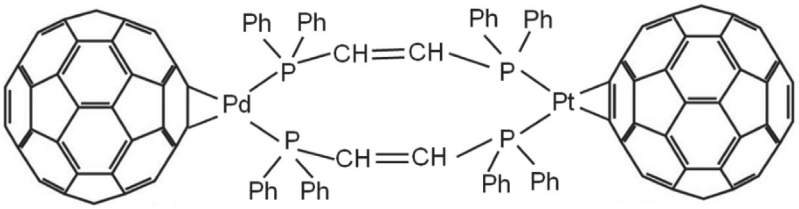

(***26***)

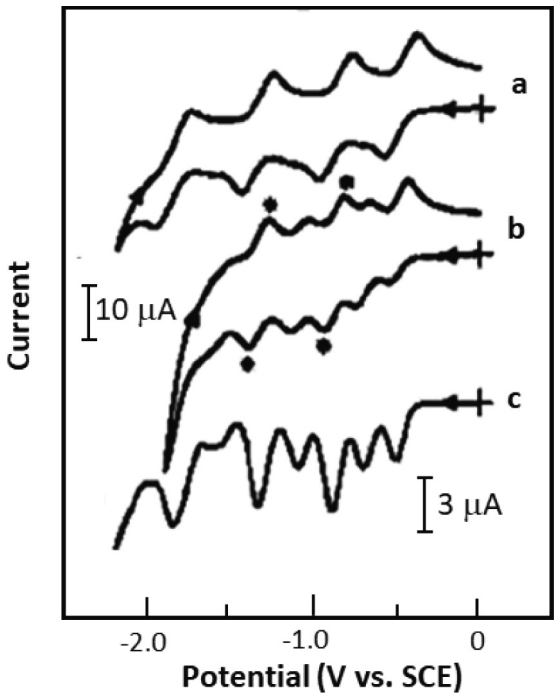

Fig. 19. Cyclic voltammograms recorded at a platinum electrode in 1,2-$Cl_2C_6H_4$ solution containing 0.2 M $[(n\text{-}Bu)_4N]PF_6$ of (a) complex (***24***) (1.1 mM) and (b) complex (***26***) (1.1 mM). (c) Osteryoung square-wave voltammogram of (***26***) (1.1 mM). Scan rates: (a, b) 0.2 V s^{-1}; (c) 0.1 V s^{-1}. Reproduced with permission from Ref. [73]. Copyright © 2006, Wiley-VCH Verlag.

4.1.2. η^2-fullerene complexes of group 9 metals

The electrochemical properties of variety of η^2-fullerene complexes of cobalt, rhodium and iridium were investigated. For exohedral mono- (***27***) - (***30***) and bi-metallic (***31***) - (***35***) hydride complexes of rhodium and iridium with C_{60} and C_{70}, the metal-centered two-electron oxidation processes results in metal-C_{60} bond cleavage [74]. In the negative potential range, electrons were transferred from electrode to the fullerene-located orbitals. Reduction of the fullerene cage coordinated to the metal center was more difficult than the reduction of pristine fullerenes (Table 2). These processes were also followed by loss of the metal unit. In the case of complexes with two metal centers attached to the fullerene unit (***31***) - (***35***), the first reduction processes were observed at potentials more negative than the reduction potential of the monoadducts. These reductions were accompanied by the stepwise metal complex dissociation as shown in Scheme 4 [74]. Such unstable electrochemical behavior was also reported for complexes containing an NO ligand coordinated to the metallic center M(NO)$(PPh_3)_2(\eta^2\text{-}C_{60})$, where M = Co (***36***) and Rh (***37***) [75]. Interpretation of voltammetric results obtained for these complexes was complicated by the low stability of the starting complexes and their decomposition leading to the formation of fullerene and metal complex components. Redox potentials reported for these complexes are shown in Table 2.

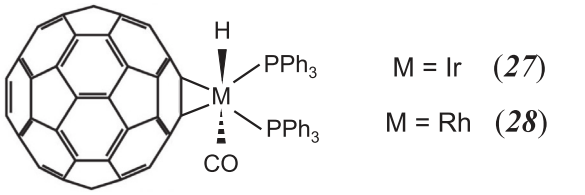

M = Ir (***27***)
M = Rh (***28***)

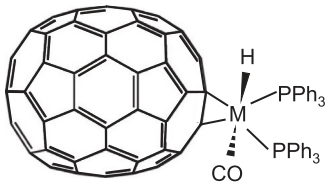

M = Ir (***29***)
M = Rh (***30***)

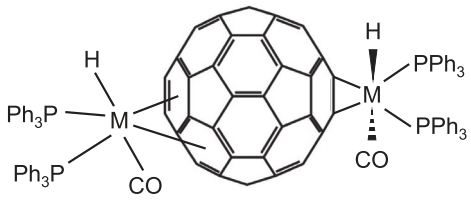

M = Ir (***31***) M = Rh (***32***) M = Ir and Rh (***33***)

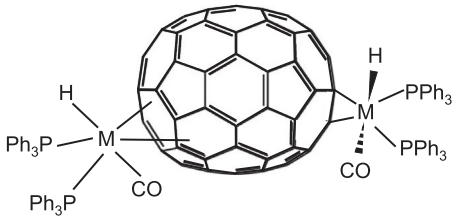

M = Ir (***34***) M = Rh (***35***)

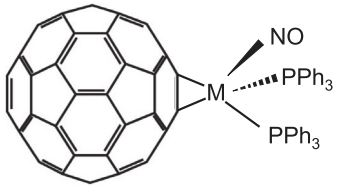

M = Co (***36***)
M = Rh (***37***)

Table 2
Redox potentials of fullerenes C_{60} and C_{70} and selected η^2-C_{60} complexes of iridium, rhodium, and osmium.

Compound	Redox potential in V vs. Fc/Fc^+				
	E_{ox}	$R_{red}^{0/-I}$	$R_{red}^{-I/-II}$	$R_{red}^{-II/-III}$	Ref.
C_{60}[a]		−0.70	−1.30	−1.90	[74]
C_{70}[a]		−0.68	−1.25	−1.76	[74]
(η^2-C_{60})IrHCO(PPh_3)$_2$ (***27***)[a]	+0.82	−1.03	−1.55	−2.14	[74]
(η^2-C_{60})RhHCO(PPh_3)$_2$ (***28***)[a]	+0.73	−0.92	−1.30[c]	−2.20	[74]
(η^2-C_{70})RhHCO(PPh_3)$_2$ (***30***)[a]	+0.73	−0.90	−1.25[c]		[74]
(η^2-C_{60})[IrHCO(PPh_3)$_2$]$_2$(***32***)[a]	+0.82 + 0.60	−1.30	−1.55	−2.14	[74]
(η^2-C_{60})IrRh[HCO(PPh_3)$_2$]$_2$(***33***)[a]	+0.82 + 0.73	−1.25	−1.45	−2.14	[74]
(η^2-C_{60})OsCOCN(t-Bu)(PPh_3)$_2$(***42***)[a]	+0.55	−1.13	−1.69	−2.30	[78]
(η^2-C_{60})OsH(CO)(DiOP) (***43***)[a]		−1.12	−1.67	−2.24	[78]
C_{60}[b]	← ←	−0.86	−1.48	−2.08	[75]
(η^2-C_{60})CoNO(PPh_3)$_2$[b] (***36***)	−0.29	−1.17	−1.72	−2.25	[75]
(η^2-C_{60})RhNO(PPh_3)$_2$[b] (***37***)	+0.35	−1.14			[75]
(η^2-C_{60})RuH(NO)(PPh_3)$_2$ (***46***)		−1.12	−1.70	−2.29	[75]
(η^2-C_{60})Ru(CO)$_4$ (***47***)		−1.13	−1.50		[75]

DiOP = $(PPh_2CH_2CHO_2)_2C(CH_3)_2$
[a] in tetrahydrofuran
[b] in dichloromethane
[c] overlapping peaks

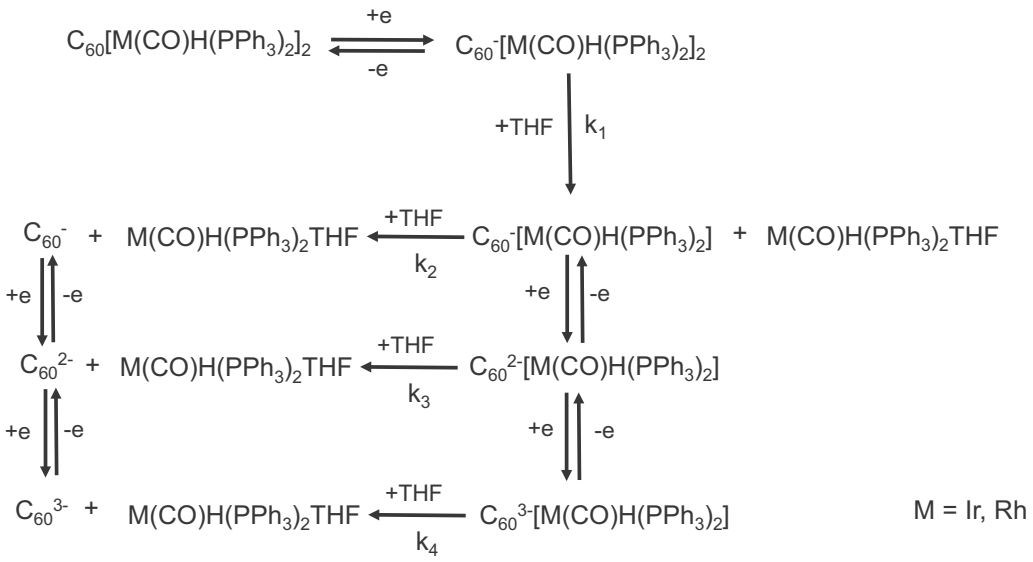

Scheme 4. Electroreduction of bi-metallic hydride complexes of rhodium (***31***) and iridium (***32***) with C_{60}.

Similar behavior was reported for complex containing (η^5-C_9H_7)Ir(CO) bound to the C_{60} in η^2-fashion (***38***). The redox properties of this complex were investigated by electrochemical and spectro-(IR and UV–Vis)electrochemical techniques. Two quasi-reversible reduction steps and irreversible two-electron oxidation process were reported [76]. The IR spectra recorded during reduction of the complex (particularly examination of CO stretch) indicate that reduction process causes only minor changes in the electron density at the metal center. However, the complex oxidation process was accompanied by the irreversible loss of the carbon monoxide ligand from the complex [76].

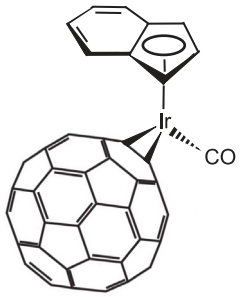

(***38***)

Denisovich and co-workers reported electrochemical properties of the variety of η^2-C_{60} complexes of iridium(I), rhodium(I), and osmium(I) (***39***)–(***45***) [77,78]. All these metallofullerenes exhibited stepwise reduction of the fullerene ligand followed by loss of the metal complex. In all cases, the fullerene cage reduction was more difficult in comparison to the reduction of pristine C_{60}. At positive potentials, metal-centered oxidation processes were also accompanied by complex decomposition. Among the metallofullerenes examined, the osmium complex (***42***) appeared to be the most stable upon reduction [78].

4.1.3. η^2-fullerene complexes of group 8 metals

The electrochemical properties of η^2-C_{60} complexes of ruthenium, $RuH(NO)(PPh_3)_2(\eta^2\text{-}C_{60})$ (***46***) and $Ru(CO)_4(\eta^2\text{-}C_{60})$ (***47***) were investigated [75]. The instability of these complexes in solution, particularly in the case of $Ru(CO)_4(\eta^2\text{-}C_{60})$, complicated their electrochemical analysis. $RuH(NO)(PPh_3)_2(\eta^2\text{-}C_{60})$ was more stable in comparison to its cobalt and rhodium analogs [75]. The redox potentials obtained for these complexes are collected in Table 2. Surprisingly, the redox potentials of $Ru(CO)_4(\eta^2\text{-}C_{60})$, which contains electron-withdrawing CO ligands coordinated to ruthenium, are still more negative, particularly in the case of the first reduction step, than those obtained for pristine C_{60}.

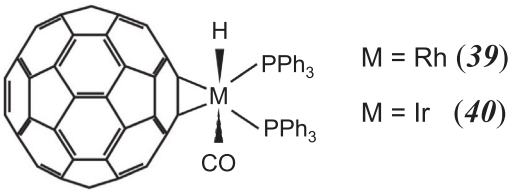

M = Rh (***39***)

M = Ir (***40***)

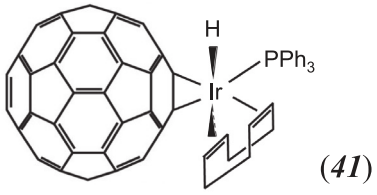

(***41***)

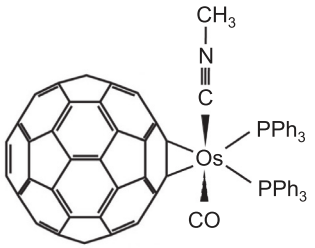

(***42***)

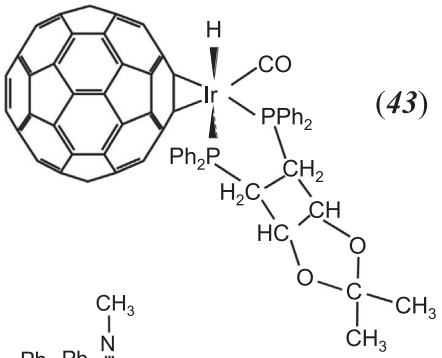

(***43***)

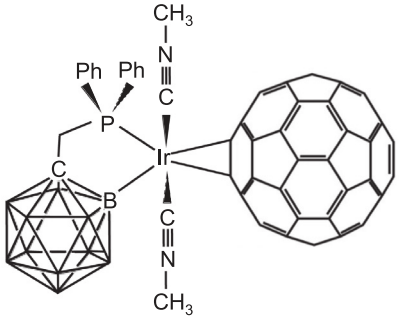

(***44***)

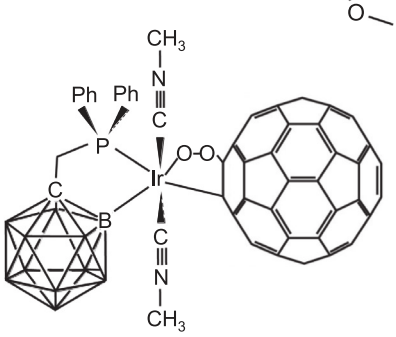

(***45***)

Table 3
Comparison of redox potentials of C_{60} and selected η^2-C_{60} complexes of rhenium, molybdenum, and tungsten.

Compound	Redox potential in V vs. SCE				
	E_{ox}	$R_{red}^{0/-I}$	$R_{red}^{-I/-II}$	$R_{red}^{-II/-III}$	Reference
C_{60}[a]		–058	–0.96	–1.42	[70]
$Re_2H_8(PMe_3)_4(\eta^2,\eta^2\text{-}C_{60})$ (***49***)	–0.07	–0.75	–1.26		[75]
$(\eta^2\text{-}C_{60})Mo(CO)_3$(diop) (***53***)[a]	+0.88	–0.76	–1.11	–1.60	[72]
$(\eta^2\text{-}C_{60})W(CO)_3$(diop) (***54***)[a]	+0.95	–0.78	–1.15	–1.65	[72]
$(\eta^2\text{-}C_{60})W(CO)_3$(dppb) (***59***)[a]		–0.80	–1.14	–1.64	[80]
$(\eta^2\text{-}C_{60})W(CO)_3$(dppe) (***60***)[a]		–0.82	–1.17	–1.65	[80]
$(\eta^2\text{-}C_{60})W(CO)_2$(dbm)(phen) (***61***)[a]		–0.76	–1.17	–1.60	[81]
$(\eta^2\text{-}C_{60})Mo(CO)_2$(dbm)(phen) (***62***)		–0.77	–1.13	–1.60	[81]

[a] in dichloromethane

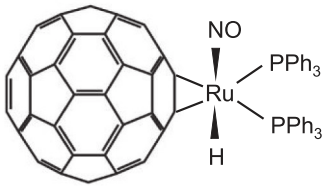

(46)

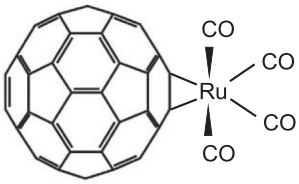

(47)

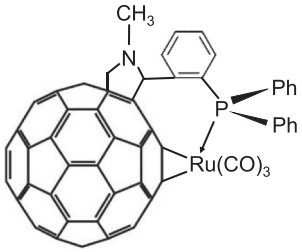

(48)

Two irreversible reduction steps were observed in the voltammograms recorded for the ruthenium complex, $Ru(CO)_3(\eta^3$-$PPh_2(o$-$C_6H_4)(CH_2NMeCH)C_{60})$ (***48***) [79]. It was postulated that the first two-electron reduction process is associated with reduction of ruthenium metal center.

4.1.4. η^2-fullerene complexes of group 7 metals

Much less attention has been focused on the electrochemical behavior of η^2-C_{60} complexed of Group 7 metals. The voltammetric behavior of bimetallic rhenium complexes $Re_2H_8(PMe_3)_4(\eta^2,\eta^2$-$C_{60})$ (***49***) [75], and $(\mu$-$H)Re_2(CO)_5(\mu$-$SSOH)(\mu,\eta^5$-$PPh_2(o$-$C_6H_4)(CH_2$-$NMeCH)C_{60})$ (***50***) [80], and monometallic $HRe(CO)_2(\eta^3$-PPh_2-$(o$-$C_6H_4)(CH_2NMeCH)C_{60})$ (***51***) [80] were reported. The η^2, η^2-C_{60} birhenium (***49***) complex is very unstable. Its two first reduction steps were observed at potentials more negative than the corresponding potentials for C_{60} reduction (Table 3). Stable electrochemical behavior was reported for complexes (***50***) and (***51***) as seen in Fig. 20. However, the voltammetric responses were irreversible. Reduction potentials of the fullerene moieties bonded to two metal atoms are more negative in comparison to the potentials of the corresponding monometallic complexes. In dinuclear complexes, the rhenium atoms were coordinated both directly to the fullerene cage and to the phosphine moiety linked covalently to the fullerene center. For comparison, the voltammetric properties of the bis-rhenium complex, $(\mu$-$H)Re_2(CO)_7(\mu,\eta^3$-$PPh(o$-$C_6H_4)_2(CH_2NMeCH)C_{60})$ (***52***), in which two rhenium atoms are bounded to the fullerene through a phosphine linker were studied [80]. In this case, the reduction potentials of the complex are significantly lower in comparison to those reported for complexes (***50***) and (***51***) that contain rhenium atoms directly coordinated to the fullerene cage. Therefore, the increase of density of negative charge on the fullerene cage and the distortion of the fullerene π-electron conjugation due the metal coordination are major factors that influence the redox properties of these rhenium complexes.

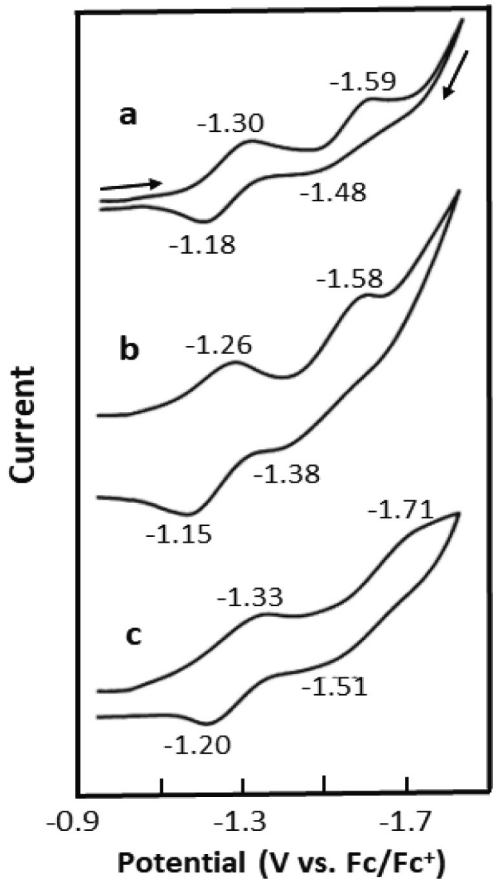

Fig. 20. Cyclic voltammograms for (a) $(o$-$C_6H_4)(CH_2NMeCH)C_{60}$ (1 mM) and η^2-C_{60} complexes of rhenium (b) (***51***) (1 mM), (c) (***52***) (1 mM) in carbon disulfide–dichloromethane (3:2, v/v) containing 0.1 M $[(n$-$Bu)_4N]PF_6$ as supporting electrolite. The potential was scanned at 10 mV s^{-1} at 27 °C, with arrows indicating the direction of potential sweep. Reproduced with permission from Ref. [80]. Copyright 2013, Royal Society of Chemistry.

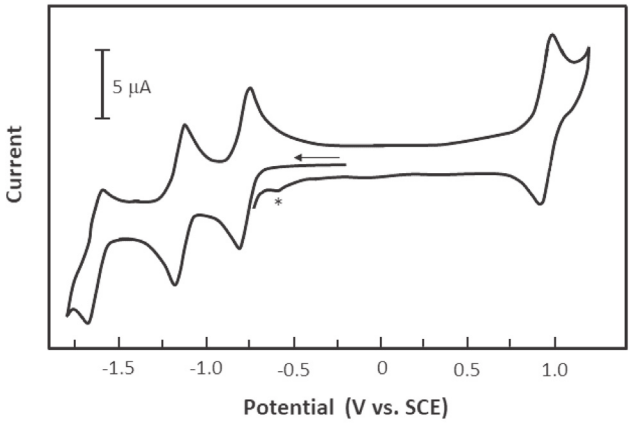

Fig. 21. Cyclic voltammogram on a platinum electrode of a dichloromethane solution containing 0.4 mM $(\eta^2$-$C_{60})W(CO)_3$(diop) (***54***) and . Scan rate 0.2 $V{\cdot}s^{-1}$, T = -20 °C. Reproduced with permission from Ref. [72]. Copyright © 2006, Wiley-VCH Verlag.

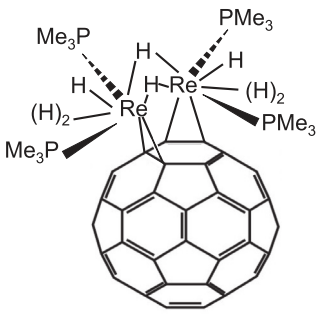

(*49*)

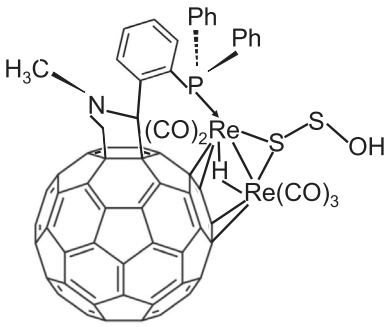

(*50*)

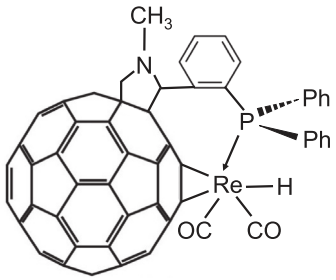

(*51*)

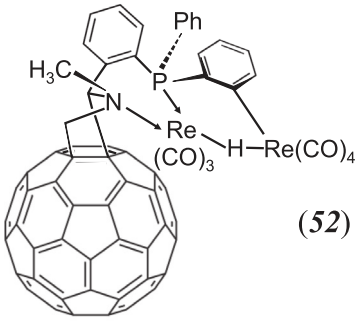

(*52*)

4.1.5. η^2-fullerene complexes of group 6 metals

The η^2-complexes of molybdenum and tungsten, $(\eta^2\text{-}C_{60})M(CO)_3(diop)$ where M = Mo (***53***) and W (***54***), and diop = 2,3-*O*-isopropylidene-2,3-dihydroxy-1,4-bis(diphenylphosphino)-butane exhibit electrochemical activity both in the negative and positive potential ranges [72]. In the negative potential range, the electrode processes are related to reduction of the C_{60} moiety. The reduction waves are shifted toward more cathodic potentials in comparison to the reduction of pristine C_{60} due to the electron density increase on the carbon cage. Reduction of fullerene moiety is followed by the cleavage of metal-C_{60} bonds and complex decomposition. The rate of this reaction increases with the increase in the number of electron transferred to the fullerene moiety. At positive potentials, an irreversible metal-centered one-electron oxidation process was observed. This process was also associated with complex decomposition. The stability of both the electroreduction and electrooxidation products is increased at low temperature. In Fig. 21, the reversible voltammetric behavior of $(\eta^2\text{-}C_{60})W(CO)_3(diop)$ (***54***) in dichloromethane at −20 °C is shown for three successive [60]-fullerene reduction steps and for oxidation of exohedral metal center. A cathodic shift of redox potentials was also reported for the tungsten complex, $W(CO)_4(\eta^3\text{-}PPh_2(o\text{-}C_6H_4)(CH_2NMeCH)C_{60})$, in which the metal center is coordinated through the phosphine group linked covalently to C_{60} and through one 6:6 ring junction of fullerene, (***55***) [79]. The formal potentials for η^2-C_{60} complexes of rhenium, molybdenum, and tungsten are collected in Table 3.

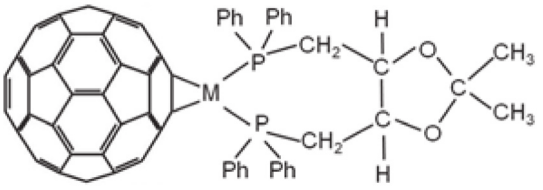

M = Mo (***53***)

M = W (***54***)

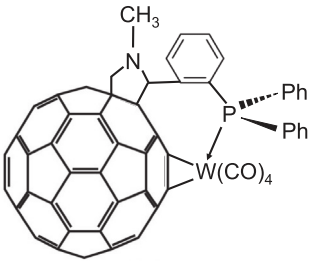

(*55*)

In the case of η^2-C_{60} complexes of molybdenum, tungsten, and chromium with the metal center coordinated by five carbon monoxide ligands (56) – (58), a positive shift of the fullerene cage reduction potential in comparison to the C_{60} reduction potential is observed [81]. Such behavior is attributed to the strong electron-accepting properties of carbonyl ligands and shifting the electron density from the fullerene to the metal center.

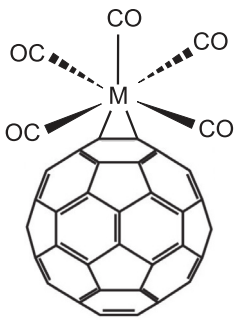

M = Mo (***56***)

M = W (***57***)

M = Cr (***58***)

Replacing a carbon monoxide ligand with an electron-donating 1,2-bis(diphenylphosphno)benzene (dppb) ligand (***59***) or 1,2-bis(diphenylphosphino)ethene (dppe) ligand (***60***) results in a cathodic shift of the fullerene cage reduction potential by *ca.* 200 mV in comparison to pristine fullerene [82]. Stable reversible electrochemical behavior was reported for (η^2-C_{60})W(CO)$_3$(dppb) without any evidence of chemical complications, even at the slow scan rate of 0.02 V s^{-1}.

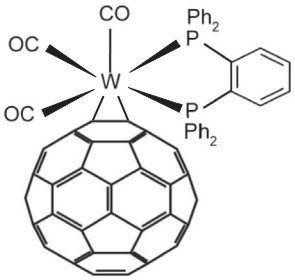

(***59***)

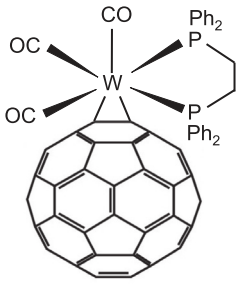

(***60***)

The electrochemical properties of (η^2-C_{60})M(CO)$_2$(dbm)(phen), where M = W (***61***) and Mo (***62***), dbm = dibutylmaleate, and phen = 1,10-phenanthroline, were also investigated [83]. In these cases, significant cathodic shifts of the fullerene cage reduction potentials were reported. Interestingly, the fullerene cage reduction potential is almost unaffected by the nature of metal center. In the case of the molybdenum analog, the effect of the number of metal fragments coordinated to the fullerene cage, (η^2-C_{60})[Mo(CO)$_2$(dbm)(phen)]$_n$, where n = 1–3, was examined [84]. The negative shift of the fullerene cage reduction process increased with the number of molybdenum atoms coordinated to the fullerene cage. These complexes are not stable under electrochemical reduction, and the partial decomplexation of molybdenum-fragment was observed. The rate of the subsequent chemical reactions increases with the number of molybdenum-fragments coordinated to the C_{60}. At negative potentials, the metal center is reduced [84]. This process was followed by the rapid and complete decomposition of the complex. Similar voltammetric behavior was reported for the C_{70} analogs of these C_{60} complexes [84].

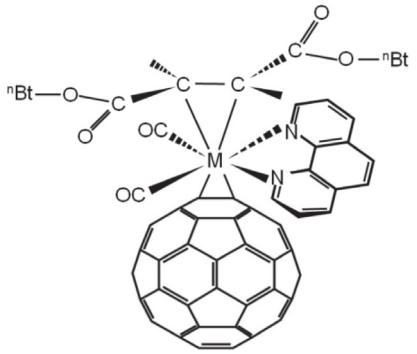

M = W (***61***)

M = Mo (***62***)

Table 4
Comparison of redox potentials of C_{60} and selected C_{60} complexes of metal clusters.

Compound	Redox potential in V vs. Fc/Fc$^+$				
	R_1	R_2	R_3	R_4	Ref.
C_{60}[a]	−1.05	−1.41	−1.87	−2.38	[85]
(η^2-C_{60})Os$_3$(CO)$_{11}$ (***63***)[a]	−1.08	−1.31	−1.61[d]		[85]
(η^2-C_{60})Os$_3$(CO)$_{10}$PPh$_3$ (***64***)[a]	−1.16	−1.44	−1.68[d]		[85]
(η^2-C_{60})Os$_3$(CO)$_9$(PPh$_3$)$_2$ (***65***)[a]	−1.19	−1.25	−1.76[d]		[85]
(μ^3-η^2:η^2:η^2-C_{60})Os$_3$(CO)$_9$ (***66***)[b]	−0.98	−1.33	−1.61	−1.74	[87]
(μ^3-η^2:η^2:η^2-C_{60})Os$_3$(CO)$_8$(PMe$_3$)(***67***)[b]	−1.06	−1.42	−1.93	−1.95	[87]
(μ^3-η^2:η^2:η^2-C_{60})Os$_3$(CO)$_7$(PMe$_3$)$_2$ (***68***)[b]	−1.13	−1.48	−2.09		[87]
(μ^3-η^2:η^2:η^2-C_{60})Re$_3$(μ-H)$_3$(CO)$_9$ (***69***)	−0.95	−1.24	−1.34	−1.73	[90]
(μ^3-η^2:η^2:η^2-C_{60})Re$_3$(μH)$_3$(CO)$_8$(PPh)$_3$(***70***)	−1.04	−1.35	−1.75	−1.77	[90]
(***71***)[c]	−1.18	−1.53	−2.11	−2.11	[91]
(***72***)[c]	−1.13	−1.46	−1.54	−1.88	[91]
(μ^3-η^2:η^2:η^2-C_{60})Rh$_6$(CO)$_9$(dppm) (***77***)[c]	−1.23	−1.58	−1.94[e]	−2.57	[94]
(μ^3-η^2:η^2:η^2-C_{60})Rh$_6$(CO)$_7$(dppm)$_2$(CNR)$_2$(***78***)[c]	−1.35	−1.70	−2.25[e]	−2.71	[94]
C_{60}[b]	−1.19	−1.59	−2.05	−2.54	[92]
(μ^3-η^2:η^2:η^2-C_{60})Ru$_5$C(CO)$_{11}$(PPh$_3$) (***74***)[b]	−1.16	−1.56	−1.93	−2.53	[92]
(μ^3-η^2:η^2:η^2-C_{60})Ru$_5$C(CO)$_{10}$(dppf) (***75***)[b]	−1.20	−1.47	−1.58	−1.97	[92]
(μ^3-η^2:η^2:η^2-C_{60})PtRu$_5$C(CO)$_{11}$(dppe) (***76***)[b]	−1.19	−1.55	−1.92	−2.49	[92]

[a] dichloromethane/toluene
[b] 1,2-dichlorobenzene
[c] chlorobenzene
[d] cathodic peak potential
[e] two-electron proces dppf = 1,1′-bis(diphenylphosphino)ferrocene dppe = 1,2-bis(diphenylphosphino)ethane dppm = 1,2-bis(diphenylphosphino)methane

In conclusion, the electrochemical properties of η^2-C_{60} complexes of transition metals are tuned by the σ-π interaction between metal center and fullerene moieties. The electrochemical behavior of these complexes at positive potentials was related to the oxidation of metal center. The potential of this process depends on the formal potential of M/M^{+n} redox couple. The shift of electron density from the metal center to the fullerene cage in the η^2-C_{60} complexes usually favors this process. Upon oxidation of the metal center, the η^2-bonded transition metals tend to dissociate from the fullerene moiety. This effect is related to the decrease of the metal *d*-orbital electron density and weakening of the π-back donation effect. In the negative potential range, fullerene-centered reduction processes occur. The negative shifts of reduction potentials of these processes caused by appended metal centers are a common feature of η^2-fullerene electrochemistry. The degree of this shift depends only slightly on the metal nature, which indicates that the charge transferred to the fullerene moiety from the metal center is effectively delocalized over the carbon cage. It is likely that disruption of π-electron conjugation due to the coordination of fullerene moiety by the metal complex is responsible for the cathodic shift of the fullerene cage reduction. Anions of η^2-C_{60} complexes of transition metals are unstable and decompose to the pristine fullerene and metal complexes. The rates of these reactions increase with an increase in negative charge localized on the carbon cage.

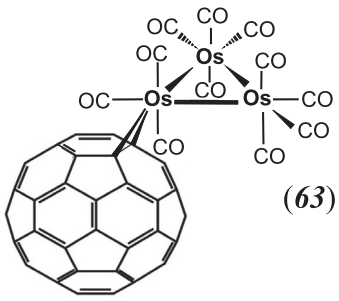

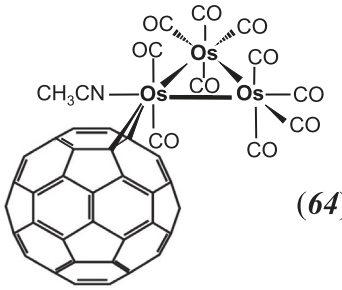

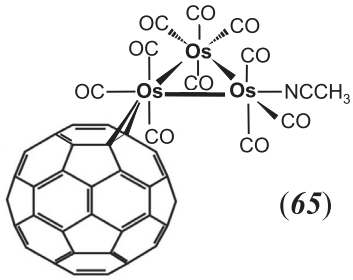

4.2. Complexes of fullerenes and transition metal clusters

Metal clusters can be also coordinated to the fullerenes moieties. Electrochemical properties of different triosmium cluster complexes of C_{60} were studied [85]. In these complexes, only one osmium atom is bonded to the fullerene center in η^2-fashion, as seen in structures (***63***) - (***65***) [86]. In the negative potential range, three fullerene moiety reduction waves were recorded. The first reduction step is negatively shifted in comparison to the potentials of pristine fullerene mono-anion formation, similar to the behavior of η^2-fullerene complexes with only one metal atom coordinated to the carbon sphere. The formation of the doubly negatively charged anion of the complex (***63***) is observed at a less negative potential with respect to the second reduction step of pristine C_{60}. The potential difference is equal to 100 mV. An even stronger shift of the reduction potential in the same direction (ca. 250 mV) was observed for the third fullerene cage reduction process. The electron accepting nature of the carbon monoxide ligands is responsible for such behavior. The π-back bonding interaction between the *d* orbitals of the osmium atom and the π* orbitals of the carbon monoxide ligands results in a shift of the extra negative charge from the fullerene moiety to the metal center. Therefore, negatively charged fullerene moieties coordinated to the osmium atom are more easily reduced in comparison to free fullerene anions. This effect can be significantly reduced by replacing CO ligand with electron-donating phosphine ligands (Table 4). For the second reduction step, a cathodic potential shift was observed for $(\eta^2\text{-}C_{60})Os_3(CO)_{10}PPh_3$ and $(\eta^2\text{-}C_{60})Os_3(CO)_9(PPh_3)_2$ in comparison to pristine C_{60}. The magnitude of this shift depends on the number of triphenylphosphine ligands coordinated to the osmium atoms (Table 4). The transfer of the second and third electron onto the η^2-C_{60} complexes of osmium cluster was also followed by the complex decomposition leading to the osmium cluster and fullerene anion formation [86].

Similar electrochemical properties were reported for μ_3-η^2:η^2:η^2-C_{60} complexes of the three-atom osmium cluster (***66***) – (***68***) [87]. Similar to the η^2-C_{60} complexes of osmium cluster, the formal potentials for the fullerene-centered reduction processes were affected by electron transfer from the carbon cage to the metal center during σ bond formation, electron π-back donation between fullerene moiety and three osmium atoms, and the

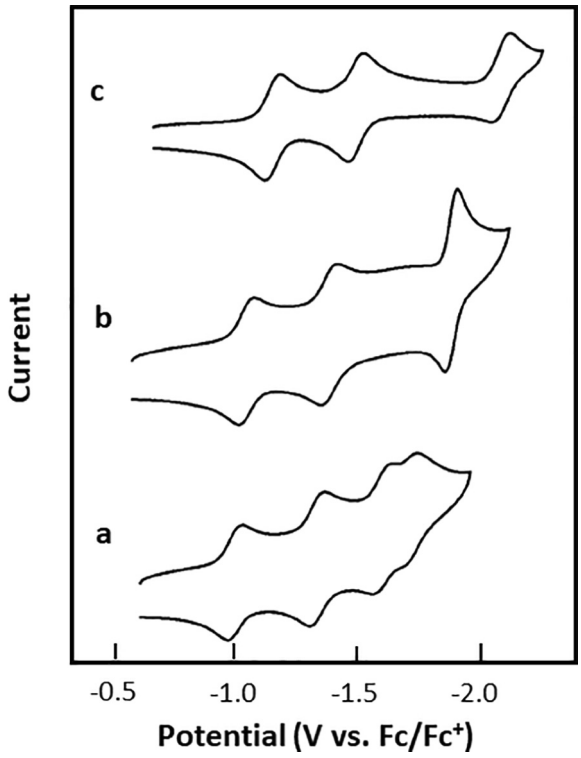

Fig. 22. Cyclic voltammograms of (a) $(\mu_3\text{-}\eta^2\text{:}\eta^2\text{:}\eta^2\text{-}C_{60})Os_3(CO)_7(PMe_3)_2$ (***68***), (b) $(\mu_3\text{-}\eta^2\text{:}\eta^2\text{:}\eta^2\text{-}C_{60})Os_3(CO)_{8\text{-}}(PMe_3)$ (***67***), and (c) $(\mu_3\text{-}\eta^2\text{:}\eta^2\text{:}\eta^2\text{-}C_{60})Os_3(CO)_9$ (***66***) in dry deoxygenated 1,2-dichlorobenzene containing 0.1 M $[(n\text{-}Bu)_4N]ClO_4$ at 50 mV s^{-1} Reproduced with permission from Ref. [87]. Copyright © 1998, American Chemical Society.

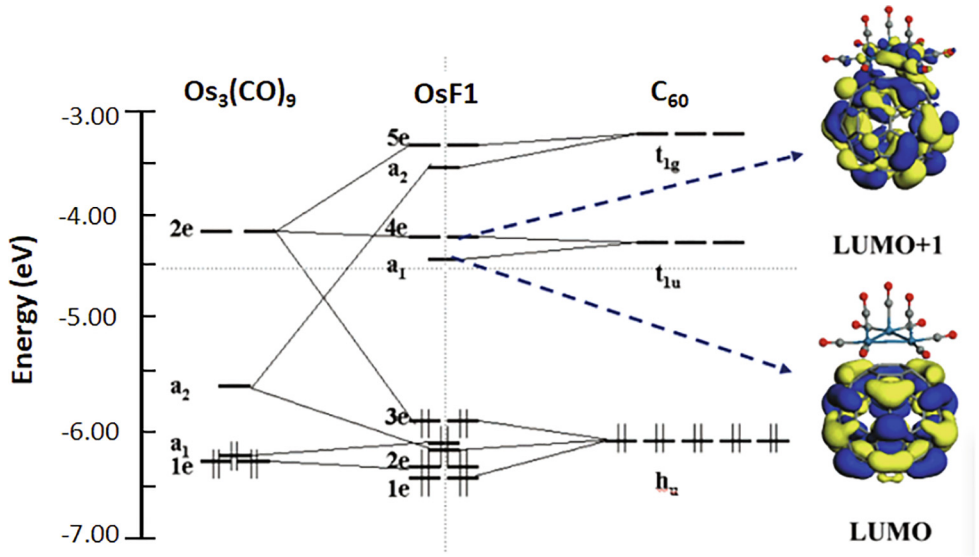

Fig. 23. Molecular orbital diagrams for $(\mu_3\text{-}\eta^2,\eta^2,\eta^2\text{-}C_{60})Os_3(CO)_9$ and LUMO and LUMO + 1 for $(\mu_3\text{-}\eta^2,\eta^2,\eta^2\text{-}C_{60})Os_3(CO)_9$. Reproduced with permission from Ref. [88]. Copyright © 2004, American Chemical Society.

electron accepting properties of the ligands coordinated to the metallic centers. The voltammetric behavior of $\mu_3\text{-}\eta^2\text{:}\eta^2\text{:}\eta^2\text{-}C_{60}$ complexes of the triosmium cluster is shown in Fig. 22 and redox potential values are collected in Table 4. Bonding of the metallic cluster to the fullerene moiety through three metal atoms significantly influences complex stability upon reduction. The voltammograms presented in Fig. 22 show that osmium-fullerene bonds are not cleaved during electron transfer processes within the potential range examined.

product of the electrode reaction. There is also good agreement between the experimentally obtained reduction potentials for the $\mu_3\text{-}\eta^2\text{:}\eta^2\text{:}\eta^2\text{-}C_{60}$ complexes [86] of triosmium cluster and those calculated from the theoretically predicted electronic structure [88]. In both cases, the sequence of reduction potential changes with an increase in the number of electron exchanged is the same. Solvation effects are responsible for the shift of the theoretically calculated reduction potentials toward more negative values.

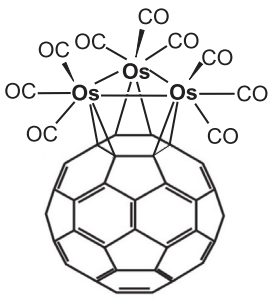

(66)

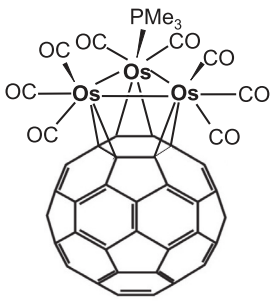

(67)

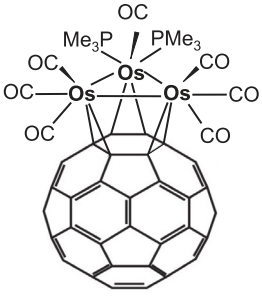

(68)

Theoretical calculations using density functional theory (DFT) were used to explain the electrochemical properties of the $\mu_3\text{-}\eta^2\text{:}\eta^2\text{:}\eta^2\text{-}C_{60}$ complexes of the triosmium cluster [88]. In Fig. 23, the molecular orbital diagram, and LUMO and LUMO + 1 for $(\mu_3\text{-}\eta^2\text{:}\eta^2\text{:}\eta^2\text{-}C_{60})Os_3(CO)_9$ are shown. The LUMO, which is responsible for transfer of the first two electron, is localized on the fullerene. However, the LUMO + 1 involved in the transfer of the third electron is delocalized over both the C_{60} cage and the osmium cluster. Theoretical calculations show that geometry of the complex is almost unaffected by the first and second reduction process. However, the third reduction process is accompanied by significant changes in the structure due to the increasing charge density on the triosmium cluster center. The coordination of the one of osmium atoms changes from η^2 to η^1 mode and the $(\mu_3\text{-}\eta^1\text{:}\eta^2\text{:}\eta^2\text{-}C_{60})Os_3(CO)_9^{3-}$ ion is formed as a

The $\mu_3\text{-}\eta^2\text{:}\eta^2\text{:}\eta^2\text{-}C_{60}$ complexes of triosmium cluster were also covalently immobilized on indium doped tin oxide (ITO) or gold electrodes [89]. The immobilization of $\mu_3\text{-}\eta^2\text{:}\eta^2\text{:}\eta^2\text{-}C_{60}$ complexes of triosmium cluster on ITO is schematically shown in Fig. 24a. The films that are formed on the ITO electrode exhibited electrochemical activity in the negative potential range. Voltammograms revealed three, well-resolved reduction waves corresponding to 1:1:2 ratio of electron exchange. Similar electrochemical behavior was reported for $(\mu_3\text{-}\eta^2\text{:}\eta^2\text{:}\eta^2\text{-}C_{60})\ Os_3(CO)_8(PMe_3)$ in solution [88]. The almost ideal electrochemical response is due to the structural homogeneity of the $\mu_3\text{-}\eta^2\text{:}\eta^2\text{:}\eta^2\text{-}C_{60}$ triosmium cluster layer. The redox potentials of the complex immobilized at the electrode surface are slightly shifted to negative potentials in comparison to those of the complex (***66***) in solution. Much less reversible voltammetric behavior was observed for $(\mu_3\text{-}\eta^2\text{:}\eta^2\text{:}\eta^2\text{-}C_{60})Os_3(\text{-}$

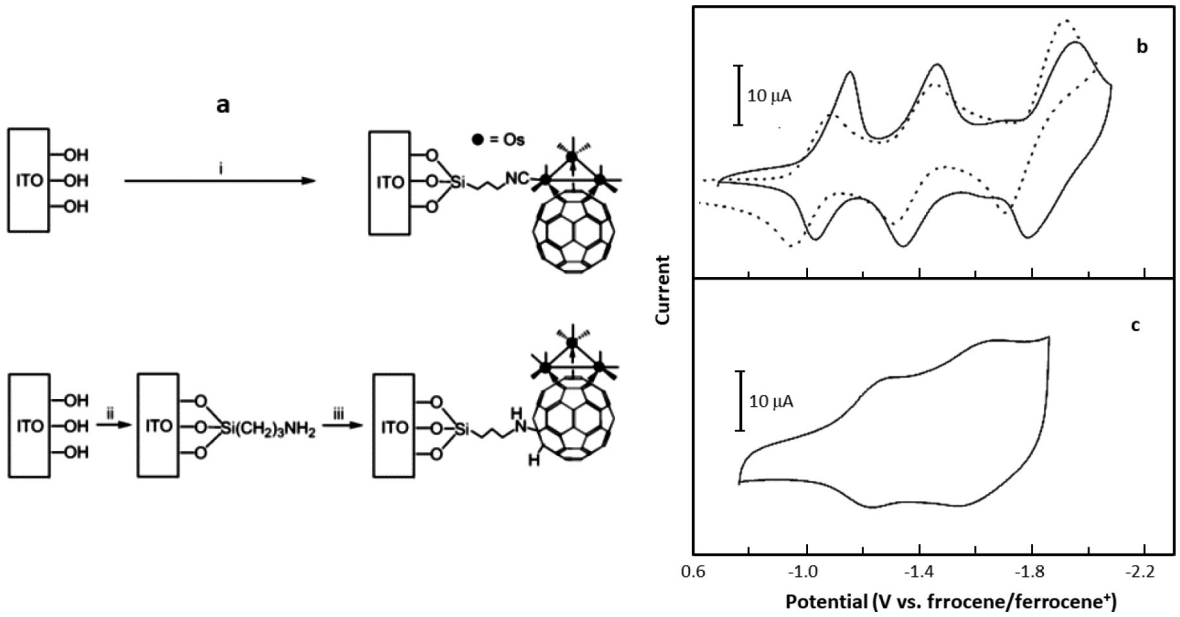

Fig. 24. (a) Schematic illustration of the μ_3-η^2:η^2:η^2-C_{60} complexes of triosmium cluster immobilization at the ITO electrode. Reagents and conditions: (*i,*) $(EtO)_3Si(CH_2)_3(CO)_8Os_3(\mu_3\text{-}\eta^2\text{:}\eta^2\text{:}\eta^2\text{-}C_{60})$, chlorobenzene, RT, 3 days; (*ii,*) $(EtO)_3Si(CH_2)_3NH_2$, chlorobenzene, RT, 2 days; (iii) $(CO)_9Os_3(\mu_3\text{-}\eta^2\text{:}\eta^2\text{:}\eta^2\text{-}C_{60})$, chlorobenzene, RT, 3 days. (b) Cyclic voltammograms of $ITO/O_3Si(CH_2)_3(CO)_8Os_3(\mu_3\text{-}\eta^2\text{:}\eta^2\text{:}\eta^2\text{-}C_{60})$, and $ITO/O_3Si(CH_2)_3NH(CO)_9Os_3(\mu_3\text{-}\eta^2\text{:}\eta^2\text{:}\eta^2\text{-}C_{60})$. (c) Cyclic voltammogram of $(CO)_9Os_3(\mu_3\text{-}\eta^2\text{:}\eta^2\text{:}\eta^2\text{-}C_{60})$ in CH_2Cl_2 with 0.1 M $[(n\text{-}Bu)_4N]PF_6$ as an electrolyte. Scan rate = 0.5 V s^{-1}. Reproduced with permission from Ref. [89]. Copyright © 2002, Royal Society of Chemistry.

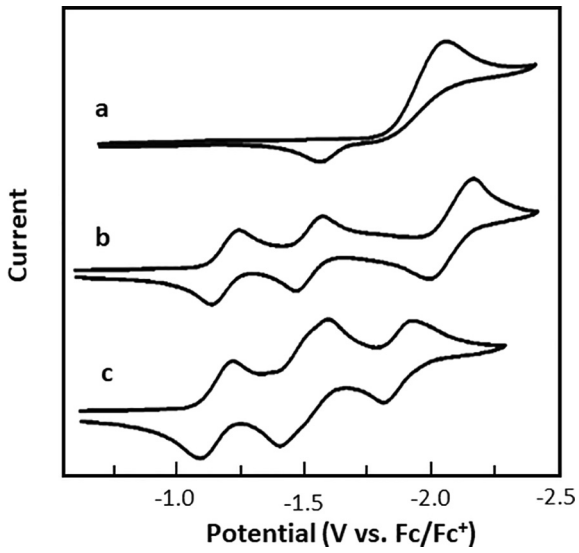

Fig. 25. Cyclic voltammograms of triiridium cluster (a) (***73***) and its μ^3-η^2:η^2:η^2-C60 complexes (b) (***71***) and (c) (***72***) in chlorobenzene containing 0.1 M $[(n\text{-}Bu)_4N]ClO_4$. The concentrations of compounds were ca. 0.3 mM and scan rate was 50 mV s^{-1}. Reproduced with permission from Ref. [91]. Copyright © 2006, American Chemical Society.

$(CO)_9$ immobilized through the fullerene moiety to the electrode surface as seen in Fig. 24b. Additionally, a significant cathodic shift of the reduction potential was observed. This poorly defined electrochemical response can be related to the bonding of the complex through different reaction sites of fullerene cage and, therefore, the resulting inhomogeneity of the layer [89].

A significant influence of the electron delocalization over the metallic cluster was also reported for negatively charged ions of the μ_3-η^2:η^2:η^2-C_{60} trirhenium hydrido cluster complexes (***69***) and (***70***) [90]. The potentials for reduction of the complexes are shifted toward less negative potentials in comparison to the potentials for pristine C_{60} reduction. The magnitude of this shift increases with an increase in the charge located on the complex (Table 4). It was postulated [90] that for multi-charged anions, excess negative charge is delocalized over fullerene cage and the metal cluster. Trirhenium hydrido cluster complexes also exhibit stable voltammetric behavior upon reduction. A comparison of the results presented in Table 4 reveals that the trirhenium centers display a more facile electronic communication between fullerene and metal cluster moiety than the triosmium centers.

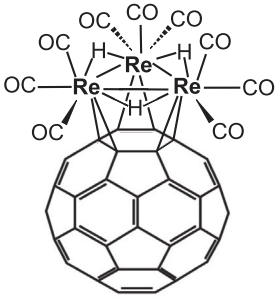

(***69***)

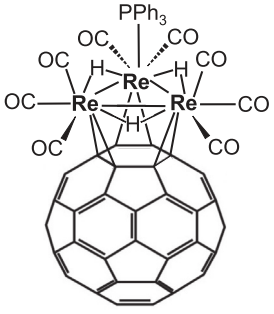

(***70***)

The electrochemical properties of fullerene complexes of tetrairidium clusters (***71***) and (***72***) were also examined [91]. The redox behavior of complex (***71***) resembles the behavior observed for the μ^3-η^2:η^2:η^2-C_{60} trirhenium hydrido cluster complex (**69**) [90]. In the potential range of the third voltammetric reduction peak, two signals corresponding to the transfer of the third and fourth electrons overlap (Fig. 25) due to the significant shift of the fourth electron reduction potential toward less negative potential values. Such behavior is related to the large contribution of metal orbitals to the LUMO + 1 (Fig. 26a), which is responsible for transfer of third and fourth electron. The third electron is highly delocalized over the fullerene cage and metal cluster. Park and co-workers calculated that for the −2/-3 redox step 63% of the charge is located on the tetrairidium center within the complex [91]. The lower density of charge located on the fullerene moiety makes further reduction of the carbon cage easier and explains the large anodic shift for the −3/-4 redox process. The contribution of metal cluster-based orbitals in the reduction process is even more pronounced for the diphosphine-coordinated C_{60}-tetrairidium complex (Fig. 26b) [91]. In this case, the third reduction peak is shifted by 370 mV toward less negative potentials in comparison to the third step of pristine fullerene reduction. Here, the orbitals of the metal cluster contribute significantly to both to the LUMO and the LUMO + 1 as seen in Fig. 26b. Additionally, the difference in the LUMO and LUMO + 1 energies is relatively small. Therefore, the LUMO + 1 is involved in second reduction step and excess of negative charge is delocalized over the fullerene and the tetrairidium moieties. As a consequence, the electron transfer processes occur at less negative potentials in comparison to the corresponding C_{60} reduction steps.

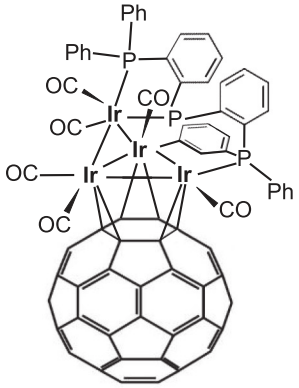

(*71*)

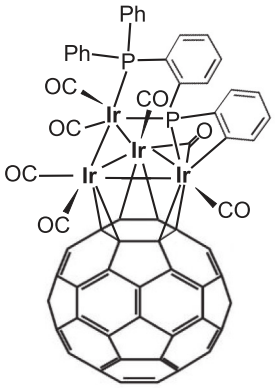

(*72*)

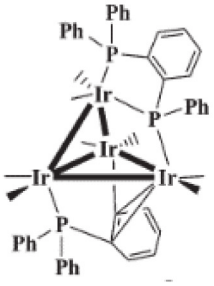

(*73*)

In the case of the carbidopentaruthenium μ_3-η^2:η^2-C_{60} complexes (***74***) – (***76***) (Fig. 27), the reduction of ruthenium clusters occurs in the potential range of fullerene cage reduction [92,93]. In the voltammograms presented in Fig. 28, irreversible two-electron, metal-centered and quasi-reversible one-electron fullerene-centered reduction peaks are observed. The formal potentials of these processes are collected in Table 4. In the case of (μ_3-η^2:η^2:η^2-C_{60})$Ru_3C(CO)_{11}(PPh_3)$ (***74***) and (μ^3-η^2:η^2:η^2-C_{60})$PtRu_5C(CO)_{11}$(μ-η^1:η^1-dppe) (***75***), the first reduction process is related to the two-electron reduction of metal cluster. The potential of this process is shifted toward less negative potentials with respect to the reduction potentials of their C_{60}-free analogs, $Ru_3C(CO)_{14}(PPh_3)$ and $PtRu_5C(CO)_{14}$(μ-η^1:η^1-dppe). The negative charge of the reduced complex causes a large shift of the fullerene cage reduction potential by *ca.* 350 mV toward more negative values as seen in Table 4.

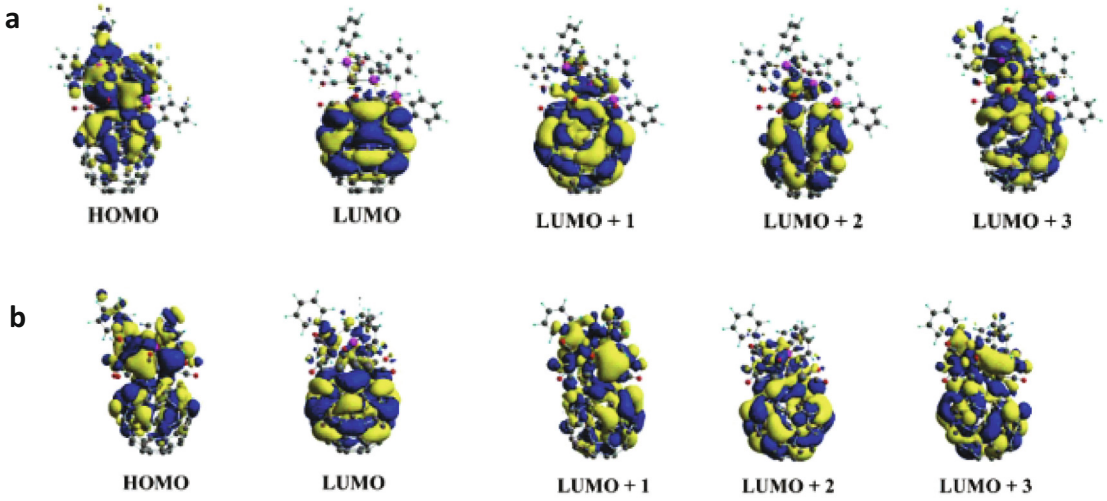

Fig. 26. MO diagrams for μ^3-η^2:η^2:η^2-C_{60} tetrairidium cluster complexes (a) (***71***) and (b) (***72***). Reproduced with permission from Ref. [91]. Copyright © 2006, American Chemical Society.

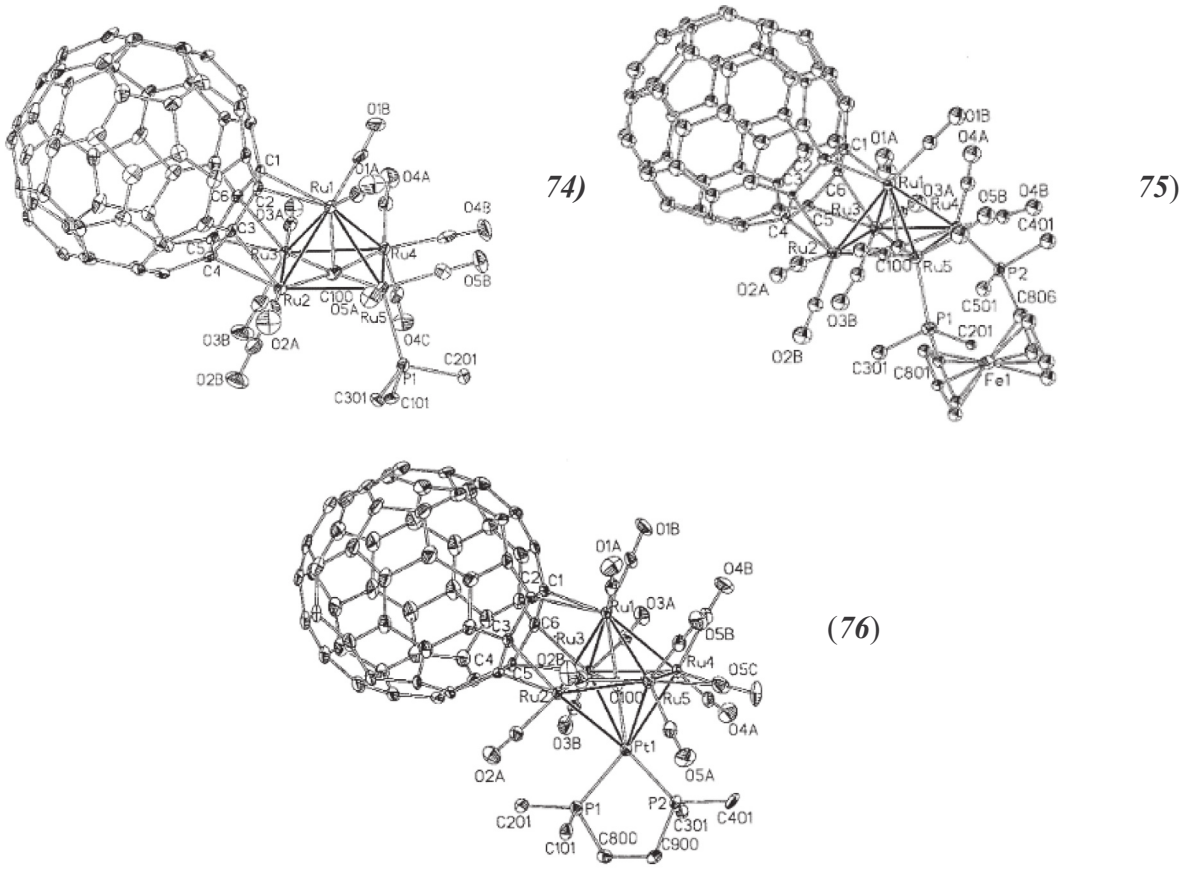

Fig. 27. Molecular geometry of $(\mu_3\text{-}\eta^2\text{:}\eta^2\text{:}\eta^2\text{-}C_{60})Ru_5C(CO)_{11}(PPh_3)$ (***74***), (b) $(\mu_3\text{-}\eta^2\text{:}\eta^2\text{:}\eta^2\text{-}C_{60})Ru_5C(CO)_{10}$(dppf) (***75***), and (c) $(\mu^3\text{-}\eta^2\text{:}\eta^2\text{:}\eta^2\text{-}C_{60})PtRu_5C(CO)_{11}(\mu\text{-}\eta^1\text{:}\eta^1$-dppe) (***76***) where dppf = 1,1′-bis(diphenylphosphino)ferrocene and dppe = 1,2-bis(diphenylphosphino)ethane. Reproduced with permission from Ref. [93]. Copyright © 1998, American Chemical Society.

Park and co-workers also investigated the electrochemical properties of $(\mu^3\text{-}\eta^2\text{:}\eta^2\text{:}\eta^2\text{-}C_{60})$ hexarhodium cluster complexes, $(\mu^3\text{-}\eta^2\text{:}\eta^2\text{:}\eta^2\text{-}C_{60})Rh_6(CO)_7(dppm)_2(CNR)_2$ (***77***) and $(\mu^3\text{-}\eta^2\text{:}\eta^2\text{:}\eta^2\text{-}C_{60})Rh_6(CO)_5(dppm)_2(CNR)$ (***78***) [94], where dppm is (1,2-bis(diphenylphosphino)methane) and R = $CH_2C_6H_5$. Crystal structures of both $(\mu^3\text{-}\eta^2\text{:}\eta^2\text{:}\eta^2\text{-}C_{60})$ hexarhodium cluster complexes are shown in Fig. 29. These complexes reveal similar voltammetric behavior as shown in Fig. 30. The voltammograms exhibit four reversible reduction peaks within the potential window of the solvent. In the third reduction process, two electrons are exchanged in a single reduction step. In the third two-electron reduction step, electrons are transferred to the metal cluster. Subsequently, they are delocalized over entire complex with predominant occupation of the fullerene cage. These conclusions are supported by the results of DFT calculations. The LUMO and LUMO + 1 involved in the exchange of four electrons are localized mainly on the fullerene cage. Reduction processes for the $(\mu^3\text{-}\eta^2\text{:}\eta^2\text{:}\eta^2\text{-}C_{60})$ hexarhodium cluster complex are shifted toward more negative potentials in comparison to the corresponding potentials of pristine fullerene reduction (Table 4) due to the presence of strongly electron-donating dppm and $C_6H_5CH_2CN$ ligands. These complexes also demonstrate considerable stability upon reduction Fig. 30.

The metal clusters can also act as bridging groups that connect two fullerene moieties. Because of the involvement of metal clusters in the charge delocalization, they provide electronic communication between the carbon cages in these fullerene dimers. The electrochemical properties of bis-fullerene complexes of metal clusters are summarized in Table 5. For every complex, electronic communication between the fullerenes and through the metal centers is observed. This effect is manifested by the sequence of pairwise voltammetric peaks corresponding to the one-electron fullerene-centered reduction processes.

In the case of the tetrairidium cluster bis-fullerene complex, $Ir_4(CO)_3(\mu_4\text{-}CH)(PMe_2)(CNCH_2C_6H_5)(\mu\text{-}\eta^2,\eta^2\text{-}C_{60})(\mu_4\text{-}\eta^1,\eta^1,\eta^2,\eta^2\text{-}C_{60})$ (***79***), the two carbon cages are differently coordinated to the metal cluster, [91,95]. The crystal structure of this fullerene dimer is shown in Fig. 31. The cyclic voltammogram of this complex exhibited six separated, reversible, one-electron peaks grouped into three pairs in the available potential window (Fig. 32a). The first redox peak in each pair is related to the electron transfer on the fullerene cage bounded to the metal center in $\mu\text{-}\eta^2,\eta^2$-fashion. The next electron is transferred at more negative potentials because of coulombic repulsion from the negative charge located on the neighboring fullerene and the negative charge delocalization over fullerene and metal cluster. The second effect dominates in the tuning of the electronic interaction between fullerene moieties. The separation between potentials within the redox pair increases with the increase number of transferred electrons. Theoretical studies of $Ir_4(CO)_3(\mu_4\text{-}CH)(PMe_2)(CNCH_2C_6H_5)(\mu\text{-}\eta^2,\eta^2\text{-}C_{60})(\mu_4\text{-}\eta^1,\eta^1,\eta^2,\eta^2\text{-}C_{60})$ allowed an explanation of the electrochemical properties of this complex (Fig. 32b) [91]. The LUMO is dominated by the C_{60} moiety where the first electron is located during the complex reduction process. The LUMO contributions from the two C_{60} units alternate from LUMO to LUMO + 3, which explains

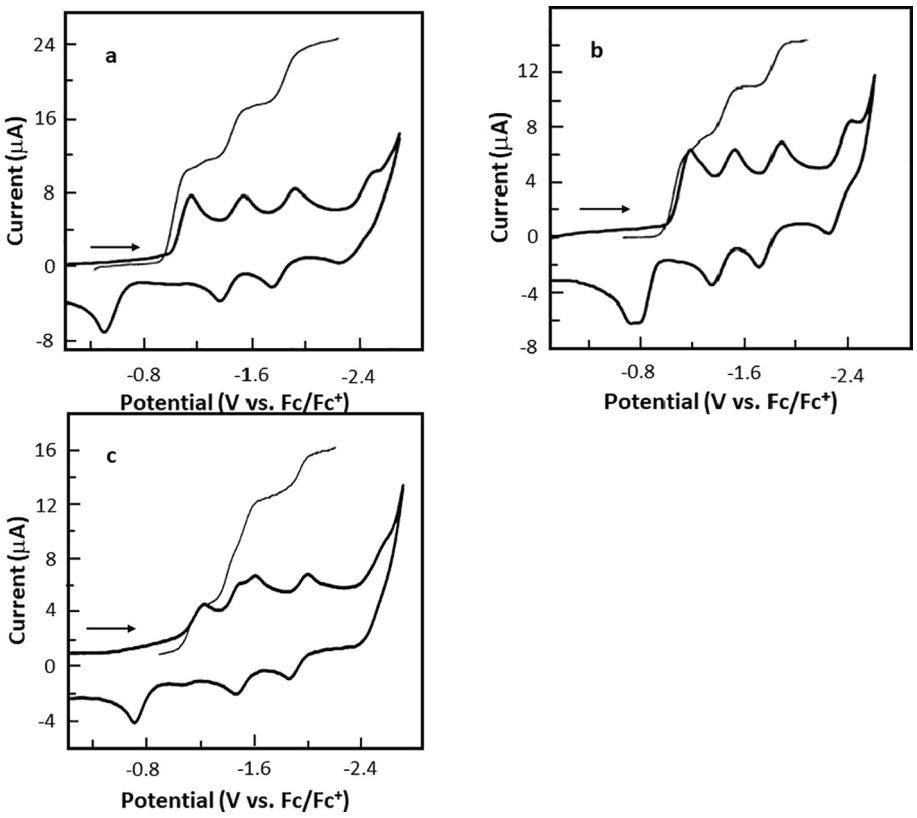

Fig. 28. Voltammograms of (a) $(\mu_3\text{-}\eta^2\text{:}\eta^2\text{:}\eta^2\text{-}C_{60})Ru_5C(CO)_{11}(PPh_3)$ (***74***), (b) $(\mu^3\text{-}\eta^2\text{:}\eta^2\text{:}\eta^2\text{-}C_{60})PtRu_5C(CO)_{11}(\mu\text{-}\eta^1\text{:}\eta^1\text{-dppe})$ (***76***), and (c) $(\mu_3\text{-}\eta^2\text{:}\eta^2\text{:}\eta^2\text{-}C_{60})Ru_5C(CO)_{10}$(dppf) (***75***) in 1,2-dichloroben-zene containing 0.1 M $[(n\text{-}Bu)_4N]BF_4$. Bold line: cyclic voltammograms at scan rate = 100 mV s^{-1}. Thin line: rotating disk electrode voltammograms at scan rate = 50 mV s^{-1} and rotation rate = 400 rpm. Arrow indicates initial scan direction. Reproduced with permission from Ref. [92]. Copyright © 2002, American Chemical Society.

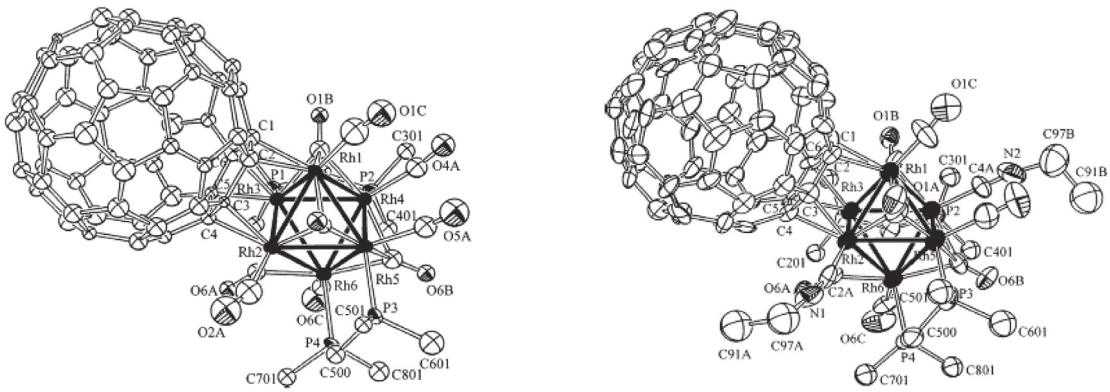

(*77*) (*78*)

Fig. 29. Molecular geometry of $(\mu^3\text{-}\eta^2\text{:}\eta^2\text{:}\eta^2\text{-}C_{60})Rh_6(CO)_7$-$(dppm)_2(CNR)_2$ (***77***) and $(\mu^3\text{-}\eta^2\text{:}\eta^2\text{:}\eta^2\text{-}C_{60})Rh_6(CO)_5(dppm)_2(CNR)$ (***78***). Phenyl groups except for the ipso carbons are removed for clarity. Reproduced with permission from Ref. [94]. Copyright © 2004, American Chemical Society.

the alternating electron addition to the two fullerene cages in the six successive reductions. The metal cluster contribution to the LUMO is lower in comparison to the one reported for the monofullerene complexes of these metal clusters [91] but it cannot be neglected. This metal cluster contribution increases with an increase of negative charge located on the fullerene moieties leading to electronic communication between fullerene units increasing and increase of potential separation within the redox pairs.

Extremely large splittings of the reduction potentials within the first, second and third consecutive redox pairs were observed for the bis-fullerene-hexarhodium sandwich complex, $Rh_6(CO)_5$(-dppm)$_2(CNCH_2C_6H_5)(\mu_3\text{-}\eta^2,\eta^2,\eta^2\text{-}C_{60})_2$ (***80***) [94]. The crystal structure of this complex and its electrochemical properties are shown in Fig. 33 and the values of redox potential corresponding to the electron transfer steps are collected in Table 5. Similar to other bis-fullerene complexes, each reduction peak corresponds to the transfer of one-electron onto a fullerene cage. All three pairs

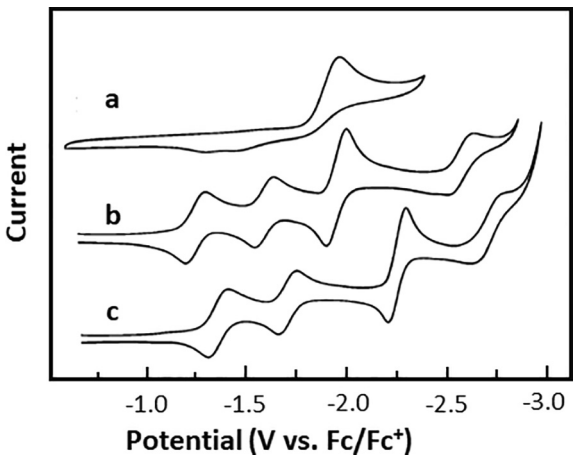

Fig. 30. Cyclic voltammograms of (a) $Rh_6(CO)_{12}(dppm)_2$, (b) (μ^3-η^2:η^2:η^2-C_{60})$Rh_6(CO)_7$-$(dppm)_2(CNR)_2$ (***77***), and (c) (μ^3-η^2:η^2:η^2-C_{60})$Rh_6(CO)_5(dppm)_2(CNR)$ (***78***) in chlorobenzene containing 0.1 M [(*n*-Bu)$_4$N]ClO_4 at scan rate of 10 mV s^{-1}. The concentrations of compounds were ca. 0.3 mM. Reproduced with permission from Ref. [94]. Copyright © 2004, American Chemical Society.

of redox peaks are shifted toward more negative potentials in comparison to the potentials of pristine fullerene reduction processes. In contrast to the redox behavior of the monofullerene complex of this hexarhodium cluster (Fig. 30), two-electron reduction processes involving the rhodium cluster are not observed due the coordination of the cluster to two C_{60} centers, which reduces the cluster electron affinity [94]. Theoretical calculations also show a significant contribution of the metal center to the unoccupied molecular orbitals that allows electronic communication between the fullerene moieties.

In conclusion, the fullerene cages in the complexes of C_{60} with transition metal clusters retain their redox properties. In general, these complexes are reduced at potentials more negative than the potentials for the corresponding steps for C_{60} reduction, particularly when the metal centers are additionally coordinated by electron-donating groups. Upon reduction, the cluster complexes of C_{60} are more stable in comparison to the monoatomic complexes of C_{60} due to the multisite bonding of the metal clusters to the fullerene. Metal clusters that bridge fullerene centers in bis-fullerene complexes allow electronic communication between carbon cages during reduction of the complexes. Coulombic repulsion from the negative charge located on the neighboring fullerene units and the negative charge delocalization over the fullerene and the metal cluster are responsible for this effect. Similar behavior was reported for fullerene dimers in which fullerene cages are bridged with non-metallic linkers, such as $C_{60}OC_{60}$ [96], $(C_{59}N)_2$ [97], C_{60}-$SiPh_2C_{60}$ [98], $C_{60}GePh_2C_{60}$ [99], and $C_{60}(CH_2)_2C_{60}$ [100]. However, the redox potential separation between subsequent electron transfers is much lower in these non-metal linked dimers in comparison to the bis-fullerene complexes connected by metal clusters. Therefore, stronger electronic communication between fullerene moieties and metal clusters enhances electronic interaction between fullerene moieties.

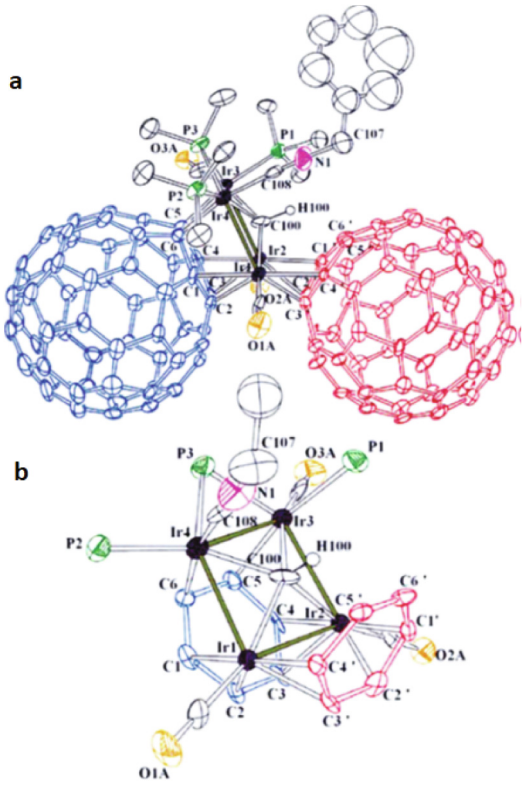

(79)

Fig. 31. (a) Molecular geometry for $Ir_4(CO)_3(\mu_4\text{-}CH)(PMe_2)(CNCH_2C_6H_5)(\mu\text{-}\eta^2,\eta^2\text{-}C_{60})(\mu_4\text{-}\eta^1,\eta^1,\eta^2,\eta^2\text{-}C_{60})$ (***79***) and (b) expanded view of ligated C_6 rings of the two C_{60} ligands. Reproduced with permission from Ref. [91]. Copyright © 2006, American Chemical Society.

4.3. Complexes with η^5-fullerene coordination to the metal center

The transition metal η^5-fullerene complexes of type (η^5-$C_{60}R_5$)ML_n, where R is organic group, such as methyl, ethyl or phenyl, M represents transition metal and L is ligand [101,102], belong to a new class of organometallic compounds with a variety of interesting physico-chemical properties, such as ability to form liquid crystalline materials [103] and light-induced charge separation [104]. These complexes are formed by the reaction of penta-alkylated [60]fullerene anions that are prepared as shown in Scheme 1 with transition metal complexes [105–107], metal-mediated C–H bond activation of penta-alkylated [60]fullerene [108,109], hydrometalation of [60]fullerene [110,111], and by reaction of fullerene halides with anionic metal complexes or low-valent metal complexes [112]. These reactions leading to the (η^5-$C_{60}R_5$)ML_n formation are shown in Scheme 5 [112]. In these complexes, the penta-alkylated [60]fullerene center exists as an negatively charged

Table 5
Comparison of redox potentials of C_{60} and bisfullerene complexes of metal clusters in chlorobenzene.

Compound	Redox potential in V vs. Fc/Fc^+						
	R_1	R_2	R_3	R_4	R_5	R_6	Ref.
C_{60}	−1.06		−1.43		−1.91		[91]
(***79***)	−1.25	−1.32	−1.66	−1.82	−2.35	−2.58	[91]
(***80***)	−1.19	−1.38	−1.62	−1.86	−2.12	−2.41	[94]

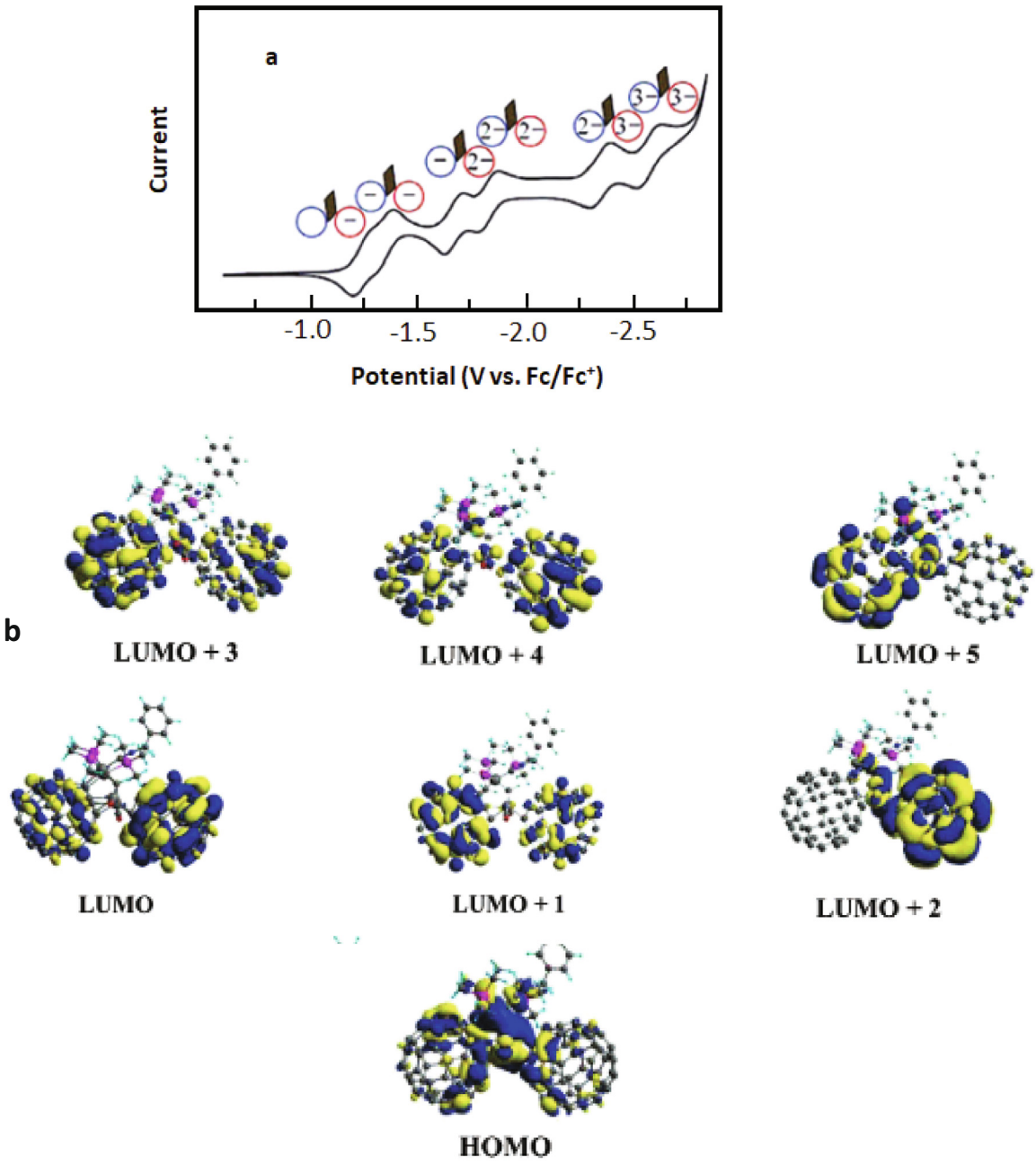

Fig. 32. (a) Cyclic voltammogram of 0.3 mM $Ir_4(CO)_3(\mu_4\text{-}CH)(PMe_2)(CNCH_2C_6H_5)(\mu\text{-}\eta^2,\eta^2\text{-}C_{60})(\mu_4\text{-}\eta^1,\eta^1,\eta^2,\eta^2\text{-}C_{60})$ (***79***) in chlorobenzene containing $[(n\text{-}Bu)_4N]ClO_4$ as a supporting electrolyte at scan rate of 10 mV s^{-1} and (b) MO diagrams for this fullerene dimer. Reproduced with permission from Ref. [91]. Copyright © 2006, American Chemical Society.

ligand that contains a cyclopentadienyl moiety homoconjugated with the 50 π-electrons of the fullerene cage.

The electrochemical properties of a variety of $(\eta^5\text{-}C_{60}R_5)ML_n$ complexes have been investigated by Nakamura and co-workers [112–115]. Fig. 34 shows the electrochemical behavior of $[\eta^5\text{-}C_{60}(CH_3)_5]Ir(CO)_2$ (***81***) in tetrahydrofuran (THF) [113]. At negative potentials, three reduction steps assigned to the reduction of the fullerene are observed. Similar behavior was observed for η^5-type fullerene complexes of other transition metals, such as $[\eta^5\text{-}C_{60}(CH_3)_5]Rh(CO)_2$ (***82***) [114], $[\eta^5\text{-}C_{60}(CH_3)_5]RuCl(CO)_2$ (***83***), $[\eta^5\text{-}C_{60}(CH_3)_5]RuCl(CO)(t\text{-}BuNC)$ (***84***) $[\eta^5\text{-}C_{60}(CH_3)_5]RuCH_3(CO)_2$ (***85***) [115]. Values of the formal potentials reported for various $(\eta^5\text{-}C_{60}R_5)ML_n$ complexes are summarized in Table 6. The metal-dependent change of the complex redox behavior in the fullerene moiety can be controlled by the nature of the metal and the ligands coordinated to the metallic center. However, the limited number of complexes studied does not allow more detailed conclusions to be made. The negative range of complex stability depends on the potential of metal ion reduction. For example, $[\eta^5\text{-}C_{60}(CH_3)_5]Ir(CO)_2$ is stable in the potential range of first three reduction steps of fullerene moiety [113]. The Rh (I) analog decomposed at potentials more negative than the

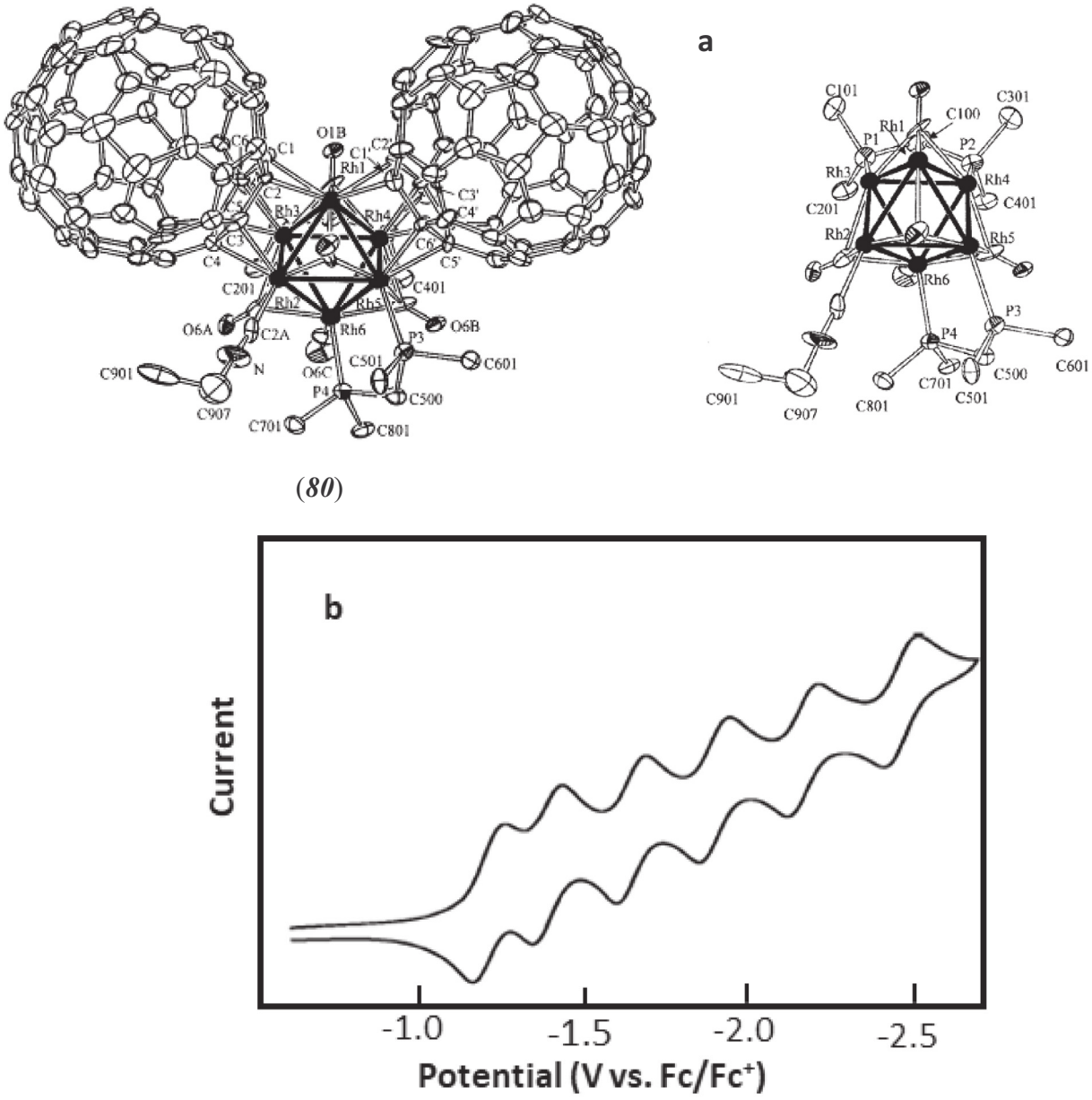

Fig. 33. (a) Molecular geometry of $Rh_6(CO)_5(dppm)_2(CNCH_2C_6H_5)(\mu_3\text{-}\eta^2,\eta^2,\eta^2\text{-}C_{60})_2$ (***80***) and expanded view of the cluster core. Phenyl groups except ipso carbons are removed for clarity. (b) Cyclic voltammogram of 0.3 mM $Rh_6(CO)_5(dppm)_2(CNCH_2C_6H_5)(\mu_3\text{-}\eta^2,\eta^2,\eta^2\text{-}C_{60})_2$ in chlorobenzene containing 0.1 M $(n\text{-}Bu)_4NClO_4$ as a supporting electrolyte at scan rate of 10 mV s^{-1}. Reproduced with permission from Ref. [94]. Copyright © 2004, American Chemical Society.

potentials of the second fullerene moiety reduction step at which the metal center is irreversibly reduced [114]. A decrease of the reduction currents recorded under square-wave voltammetry conditions was also observed for $(\eta^5\text{-}C_{60}Bn_2PhH_2)Re(CO)_3$ (***86***) complex, where Bn is a benzyl group [116]. The authors of these studies attributed the decrease of the current to the decrease of the rate of heterogeneous electron exchange, rather than a chemical reaction following reduction. However, similar width of the peaks at the half of their height suggests that the complex decomposition is responsible for the reported square-wave voltammetric behavior. Nakamura and co-workers synthesized $(\eta^5\text{-}C_{60}R_5)M(\eta^3\text{-}CH_2CHCH_2)$ complexes, where M = Ni(II) (***87***) and (***88***), Pd(II) (***89***) and (***90***), and Pt(II) (***91***) and (***92***) and R = Me and Ph [117]. Steric protection by the bulky $C_{60}Me_5^-$ ligand allows the formation of heat-, water-, and air-stable π-alkyl complexes of Group 8 transition metals. The electrochemical properties of the Pd(II) and Pt(II) complexes were investigated [117]. The results of voltammetric studies revealed that the electron located on the fullerene moiety is delocalized over the carbon cage and can be transferred to the metal center through the cyclopentadienide moiety. As a consequence, the metal–$C_{60}R_5$ bond is cleaved, leading to the formation of a free metal complex and the $C_{60}R_5^{n-}$ anion. The current corresponding to $C_{60}R_5^{n-}$ oxidation can be detected on the voltammetric anodic scan [117]. The stability of these complexes during reduction depends on the organic group surrounding cyclopentadienide ring. Thus, the $(\eta^5\text{-}C_{60}Ph_5)$-Pd bound is more stable than the $(\eta^5\text{-}C_{60}Me_5)$-Pd [117].

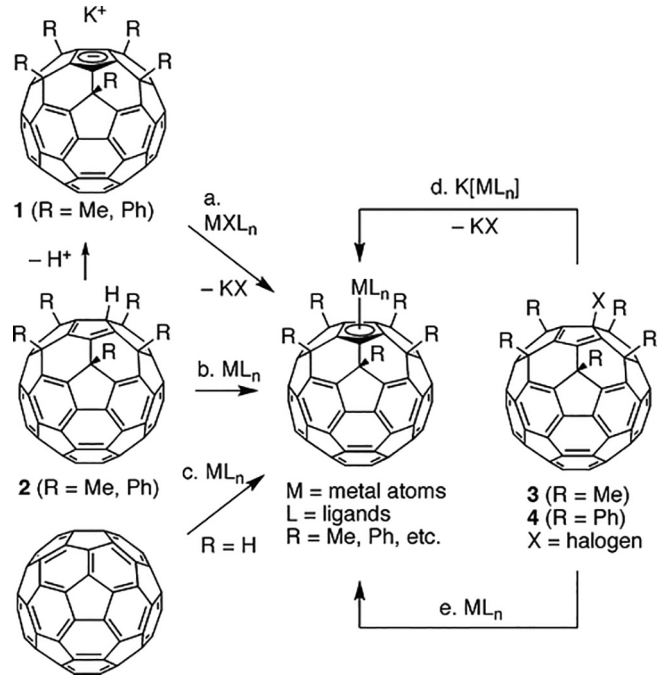

Scheme 5. Means of formation of (η^5-$C_{60}R_5$)ML_n (R = alkyl or aryl,M = metal ion, L = ligand) [112].

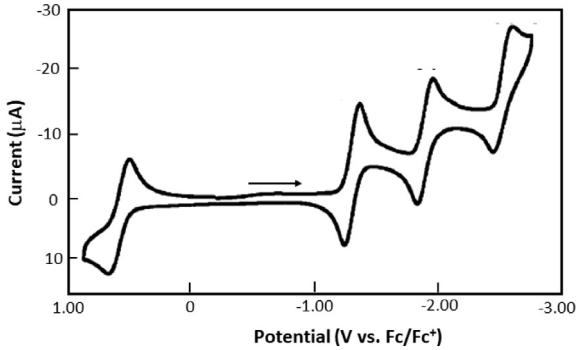

Fig. 35. Cyclic voltammogram of (η^5-C_{60}{C_6H_4-(OCO-C_6H_3-$(OR)_2$–3,4)-4})Fe(η^5-C_5H_5) (***93***) at 25 °C in a THF solution containing [(*n*-Bu)$_4$N]ClO_4 as a supporting electrolyte (scan rate 100 mV/s). Reproduced with permission from Ref. [118]. Copyright © 2006, American Chemical Society.

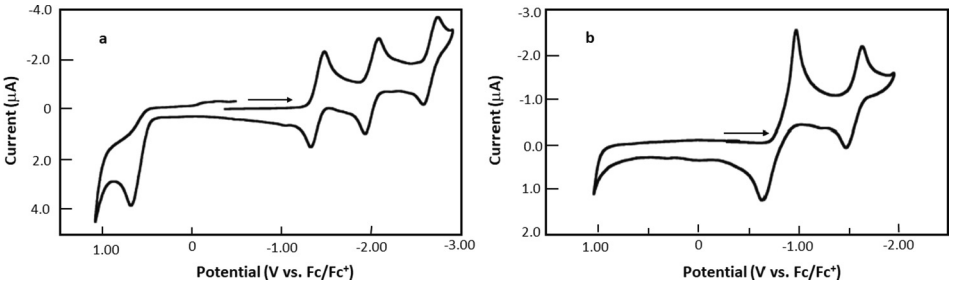

Fig. 34. Cyclic voltammograms for (a) [η^5-$C_{60}(CH_3)_5$]$Ir(CO)_2$ (***81***) and (b) [η^5-$C_{60}(CH_3)_5$]$Ir(CO)I_2$ at 25 °C in a THF solution containing [(*n*-Bu_4)N]ClO_4 as a supporting electrolyte at scan rate of 100 mV s^{-1}. Reproduced with permission from Ref. [113]. Copyright © 2005, American Chemical Society.

Table 6
Comparison of redox potentials of C_{60} and selected η^5-C_{60} complexes of transition metals.

Compound	Redox potential in V vs. Fc/Fc^+				
	O_1	R_1	R_2	R_3	Ref.
C_{60}[a]		−0.86	−1.44	−2.00	[70]
C_{60}[b]		−086	−1.48	−2.08	[75]
[η^5-$C_{60}(CH_3)_5$]$Ir(CO)_2$ (***81***)[a]	−0.34[c]	−1.39	−2.01	−2.66	[113]
[η^5-$C_{60}(CH_3)_5$]$Ir(CO)I_2$[a]		−0.81	−1.56		[113]
[η^5-$C_{60}(CH_3)_5$]$Rh(CO)_2$ (***82***)[a]	0.58[c]	−1.34	−1.94		[114]
[η^5-$C_{60}(CH_3)_5$]$RuCl(PEt)_3CO$ (***83***)[a]	0.85	−1.45			[115]
[η^5-$C_{60}(CH_3)_5$]$RuCl(CO)$(*t*-BuNC) (***84***)[a]		−1.53			[115]
[η^5-$C_{60}(CH_3)_5$]$RuCH_3(CO)_2$ (***85***)[a]		−1.34	−1.94		[115]
(η^5-$C_{60}Bn_2PhH_2$)$Re(CO)_3$ (***86***)[a]		−1.49	−1.92		[116]
(η^5-$C_{60}Bn_2PhH_2$)$Re(CO)_3$ (***86***)[b]	1.10	−1.43	−1.89		[116]
[η^5-$C_{60}(CH_3)_5$]$Pd(\eta^3$-$C_3H_5)$ (***89***)[a]		−1.40	−1.99		[117]
(η^5-$C_{60}Me_5$)Fe(η^5-C_5H_5) (***8***)[a]	0.22	−1.46			[35]
[(η^5-$C_{60}(RO)_2C_6H_3COOC_6H_4$]Fe($\eta^5$-$C_5H_5$) (***93***)[a]	0.50	−1.30	−1.88	−2.35	[118]
(η^5-$C_{60}PMe_5$)Ru(η^5-C_5H_5) (***94***)[a]	0.85	−1.43	−2.01		[119]
(η^5-$C_{60}Ar_5$)CoTTFCo(η^5-$C_{60}Ar_5$) (***95***)[a]	0.42 0.12	−1.07	−1.30	−1.68[d]	[121]

[a] in tetrahydrofuran Bn = benzyl
[b] in dichloromethane Ph = phenyl
[c] peak potential Ar = 4-*n*-BuC_6H_4
[d] two-electron process R = $C_{18}H_{37}$

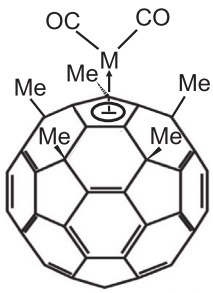

M = Ir (*81*)

M = Rh (*82*)

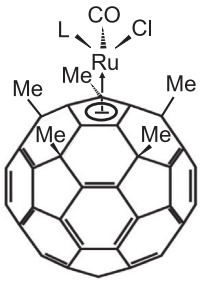

L = PEt_3 (*83*)

L = *t*-BuNC (*84*)

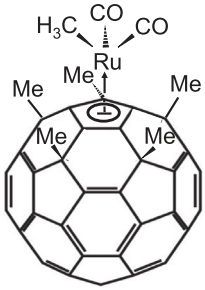

(*85*)

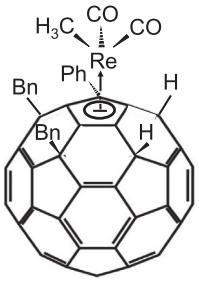

(*86*)

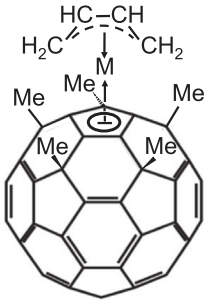

M = Ni (*87*)

M = Pd (*89*)

M = Pt (*91*)

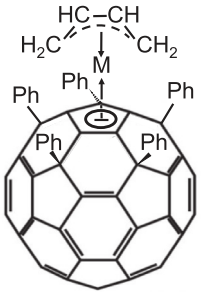

M = Ni (*88*)

M = Pd (*90*)

M = Pt (*91*)

At positive potentials, the low-valent η^5-type fullerene complexes can undergo metal-centered oxidation processes. For example, $[\eta^5\text{-}C_{60}(CH_3)_5]Ir(CO)_2$ exhibits a one-step, two-electron irreversible oxidation, which corresponds to the Ir(I)/Ir(III) redox process shown in Fig. 34 [113]. Similar behavior was observed for $[\eta^5\text{-}C_{60}(CH_3)_5]Rh(CO)_2$ [114]. $[\eta^5\text{-}C_{60}(CH_3)_5]Ir(CO)_2$ can be also chemically oxidized with iodine to form $[\{\eta^5\text{-}C_{60}(CH_3)_5]Ir(CO)I_2$ [113]. The voltammetric redox properties of this Ir(III) complex are shown in Fig. 34b. A two-electron reduction step at −0.9 V vs. Fc/Fc^+ is due to the Ir(III)/Ir(I) metal center reduction. The reversible behavior of this process indicates that reduction occurs without structural changes to the complex. The coordination of the iodide ligands with the metal center stabilizes the product of reduction. The second process, which is observed at −1.56 V, corresponds to the reduction of the fullerene moiety. The potential of this process is cathodically shifted by ca. 170 mV in comparison to the potential for reduction of $[\eta^5\text{-}C_{60}(CH_3)_5]Ir(CO)_2$ (Table 6).

Mixed fullerene-ferrocene mesogens (crystal structure of $(\eta^5\text{-}C_{60}Me_5)Fe(\eta^5\text{-}C_5H_5)$ (***8***) is shown in Fig. 6) show reversible multi-electron redox behavior both in negative and positive potential ranges as seen in Fig. 35 [118]. At positive potentials oxidation of the metal center is observed. Replacing of one cyclopentadienyl ligands in $Fe(Cp)_2$ with a $\eta^5\text{-}C_{60}Ph_5^-$ anion results in stabilization of the lower valence state of metal (Fe(II)). The oxidation potential for $(\eta^5\text{-}C_{60}\{C_6H_4\text{-}(OCO\text{-}C_6H_3\text{-}(OR)_2\text{–}3,4)\text{-}4\})Fe(\eta^5\text{-}C_5H_5)$, where R is octadecyl group (***93***) is *ca.* 500 mV more anodic than the formal potential of the $Fe(\eta^5\text{-}C_5H_5)_2/Fe(\eta^5\text{-}C_5H_5)_2^+$ redox couple [119]. Generally, the anodic shift of the metal-centered oxidation process is related to the electron-withdrawing nature of the fullerene ligands. Therefore, the change of fullerene moiety electronic structure by introduction of electron withdrawing or electron donating groups, or by modulation of π-conjugation in the fullerene moiety, influences the potential for metal-centered oxidation [119]. Upon reduction, $(\eta^5\text{-}C_{60}Ph_5)Fe(\eta^5\text{-}C_5H_5)$ exhibits one-electron reduction steps corresponding to the reduction of fullerene moiety [119].

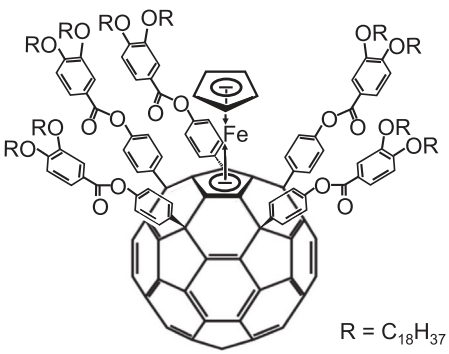

(*93*)

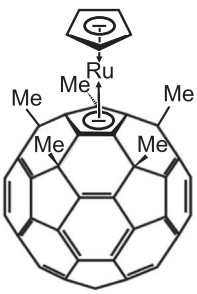

(*94*)

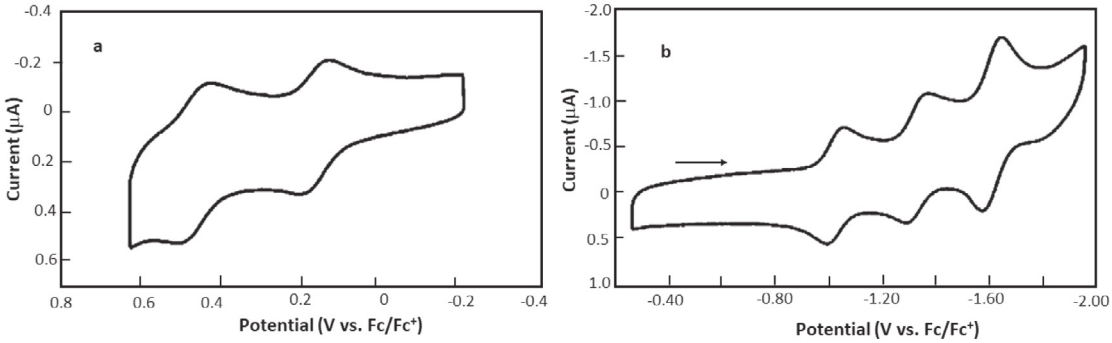

Fig. 36. Oxidation (a) and reduction (b) waves in the cyclic voltammograms of (η^5-$C_{60}Ar_5$)CoTTFCo(η^5-$C_{60}Ar_5$) (***95***) in CH_2Cl_2 containing $[(n\text{-}Bu)_4N]ClO_4$ as supporting electrolyte. Reproduced with permission from Ref. [121]. Copyright © 2009, American Chemical Society.

Similar electrochemical behavior was reported for (η^5-$C_{60}Me_5$)Ru(η^5-C_5H_5) (***94***) [120]. Two one-electron reduction steps at potentials comparable to those of the parent $C_{60}Me_5H$ indicated that electrons were added on the fullerene moiety. The oxidation process depends on the solvent. For example, a two-electron, irreversible oxidation is observed in benzonitrile. In dichloromethane, (η^5-$C_{60}Me_5$)Ru(η^5-C_5H_5) is oxidized in a reversible, one-electron step at more anodic potential in comparison to the potential for oxidation of the parent Ru(η^5-C_5H_5)$_2$ [120]. In contrast to buckyferrocene (***8***), the ruthenium analog exhibits more reversible behavior, particularly upon reduction.

Interesting electrochemical properties have been reported for a complex in which two cobalt-η^5-fullerene moieties were bridged with tetrathiafulvalene (TTF) tetrathiolate, to form an acceptor–a cceptor-donor–acceptor–acceptor array (***95***) [121]. The voltammetric behavior of this system is shown in Fig. 36. In the positive range, two one-electron oxidation steps at 0.12 and 0.42 V vs. Fc/Fc$^+$ are related to the processes centered at the TTF moiety and result in formation a radical cation and a dication, respectively. Two, one-electron reduction steps at −1.07 and −1.30 V vs. Fc/Fc$^+$ are related to the metal-centered, Co(III)/Co(II), charge transfer processes. The difference in reduction potentials of the Co(III) ions indicates that electronic communication occurs between these two redox centers. However, the processes of reduction of the two fullerene moieties occur at the same potential. As a result, a single two-electron reduction peak is observed at −1.68 V [121]. The potential for reduction of the two fullerene cages in complex (***95***), which results in formation of a doubly negatively charged η^5-fullerene ligand, is much more negative in comparison the respective process of monometallic complexes reported in Table 6. For the lowest oxidation potential (0.12 V) and the lowest reduction potential (-1.07 V), the remarkably small energy gap of 1.19 eV was calculated [121].

Polynuclear complexes in which metal ions are bound to the fullerene moiety in η^5-fashion exhibit an extended *d*-π-d conjugated system in which the metal atoms interact with each other.

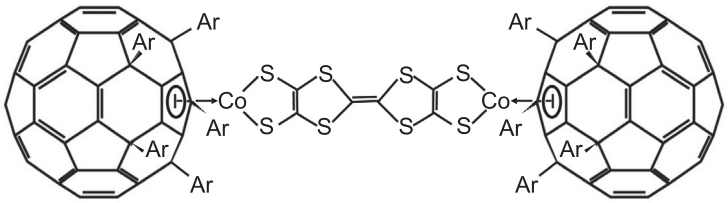

(***95***)

Double-decker buckyferrocenes of C_{60} (***96***) and (***97***) [122] and double- (***98***), and triple-decker (***99***) buckyruthenocenes of C_{70} [123] have been synthesized. Metal-centered oxidation steps are observed during the anodic scans. The number of these steps depends on the number of metal centers bonded to the fullerene as shown in Fig. 37. Strong conjugation between the metal *d* electrons and the π electrons of the fullerene allows effective electronic communication between metallocene moieties and is responsible for the large potential separation between their oxidation steps. As one can expect, reduction of the fullerene cage is observed in the negative potential range (Fig. 37). Due to the increase of negative charge on the fullerene cage produced by the attachment of metal centers, the potential for reduction of the fullerene cage shifts toward more negative values as the number of attached metallocene units increases as seen in Table 7.

4.4. Complexes with endohedral metallfulerenes coordinated to the transition metals

Since there are only a few examples of transition metal complexes that have been attached to endohedral fullerenes, there is also a very limited number of studies of the electrochemical behavior of these compounds. A study of (η^2-$Sc_3N@I_h$-C_{80})W(CO)$_3$($Ph_2PC_2H_4PPh_2$) (***13***), whose structure is shown in Fig. 10, reveals that attachment of the tungsten center to the cage results in three reductions at −1.50, −1.80 and −2.41 V (vs. Fc/Fc$^+$), in dichlorobenzene, whereas the pristine $Sc_3N@I_h$-C_{80} exhibits these three reductions at −1.26, −1.62 and −2.37 V [52]. Thus, as with empty cage

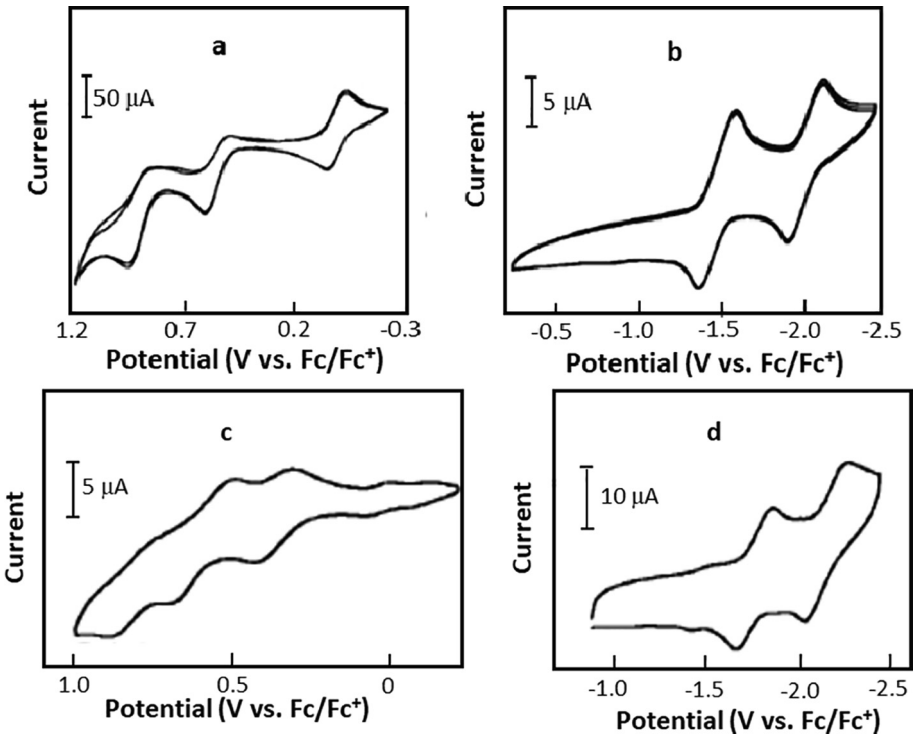

Fig. 37. Oxidation (*a* and *c*) and reduction (*b* and *d*) waves on the cyclic voltammogram of $[\eta^5{:}\eta^5\text{-}C_{70}(Bn_5)_2][Ru(\eta^5\text{-}C_5H_5)]_2$ (***98c***) (*a* and *b*) and $[\eta^5{:}\eta^5{:}\eta^5\text{-}C_{70}(Bn_5)_3][Ru(\eta^5\text{-}C_5Me_5)]_3$ (***99b***) (*c* and *d*) in CH_2Cl_2 containing 0.1 M $[(n\text{-}Bu)_4N][B\{C_6H_3\text{-}(CF_3)_2\text{–}3,5\}_4]$ (*a* and *c*) and in tetrahydrofuran containing 0.1 M $[(n\text{-}Bu)_4N]ClO_4$ as supporting electrolyte (*b* and *d*). Reproduced with permission from Ref. [123]. Copyright © 2009, Wiley-VCH Verlag.

fullerenes, the reduction of this endohedral fullerene is made more difficult by the attachment of an external metal complex. In solution (η^2-$Sc_3N@I_h$-C_{80})$W(CO)_3(Ph_2PC_2H_4PPh_2)$ undergoes four oxidations at −0.13, +0.22, + 0.56 and + 1.07 V [52]. The adduct is much more easily oxidized than the parent $Sc_3N@I_h$-C_{80}, which undergoes two, one-electron oxidation processes at + 0.59 and + 1.09 V [52].

A cyclic voltammetric study of the η^1–bound complex, η^1-($Y@C_{2v}(9)$-C_{82})$Re(CO)_5$, shows that attachment of the rhenium complex produces only minor alterations in the electrochemical behavior of this endohedral fullerene. Thus, η^1-($Y@C_{2v}(9)$-C_{82})$Re(CO)_5$ undergoes reversible reduction at −0.42, −1.42, and −2.29 V, whereas η^1-($Y@C_{2v}(9)$-C_{82}) is reduced at −0.36, −1.36 and −2.23 V [53]. Reversible oxidation for η^1-($Y@C_{2v}(9)$-C_{82})$Re(CO)_5$ occurs at + 0.05 V, while η^1-($Y@C_{2v}(9)$-C_{82}) is oxidized at + 0.11 V [53].

5. Electrochemistry of fullerene-based coordination polymers

The metal fullerene bonding in η^2-fashion allows formation of pearl necklace-like polymeric structures. These materials have been recently reviewed [9]. Therefore, this part of the review will be mainly focused on the basic electrochemical aspects of these polymers. In these macromolecular systems, the fullerene moieties are linked through metal atoms (Pd and Pt) or low valent metal complexes -$[Rh(O_2CCF_3)_4]$-, -$[Ni(PPh_3)_2]$-. The suggested structures of the 1-D polymeric chains are shown in Fig. 38. Coordination polymers of fullerenes and transition metal complexes can be chemically synthesized in solution [124–127] or through the electrochemical deposition at the electrode surface [128–131].

In the chemical synthesis, the low-valent transition metal complexes react with fullerenes to form coordination polymers. The most intensively studied *poly*-$C_{60}Pd_3$ polymer is precipitated from

Table 7
Redox potentials of C_{60} and η^5-C_{60} and η^5-C_{70} polynuclear complexes of iron.

Compound	Redox potential in V vs. Fc/Fc^+			
	E_{ox}	$R_{red}^{0/-1}$	$R_{red}^{-1/-2}$	Ref.
C_{60}		−0.86[c]	−1.44[c]	[70]
$[\eta^5{:}\eta^5\text{-}C_{60}(Me_5)_2][Fe(\eta^5\text{-}C_5H_5)]_2$ (***96***)	+0.06 + 0.17[a]	−1.46[c]		[122]
$[\eta^5{:}\eta^5\text{-}C_{60}Me_5Ph_5][Fe(\eta^5\text{-}C_5H_5)]_2$ (***97***)	+0.08 + 0.36[a]	−2.24[c]	−2.63[c]	[122]
$[\eta^5{:}\eta^5\text{-}C_{70}(Bn_5)_2][Ru(\eta^5\text{-}C_5H_5)]_2$ (***98c***)	+0.88 + 0.54[b]	−1.50[c]	−2.06[c]	[123]
$[\eta^5{:}\eta^5{:}\eta^5\text{-}C_{70}(Bn_5)_3][Ru(\eta^5\text{-}C_5Me_5)]_3$ (***99b***)	+0.85 + 0.65[b]	−1.77[c]	−2.19[c]	[123]

[a] in benzonitrile
[b] in dichloromethane
[c] in tetrahydrofuran

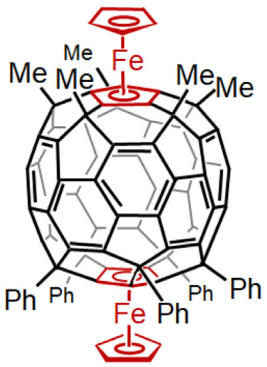

(96)

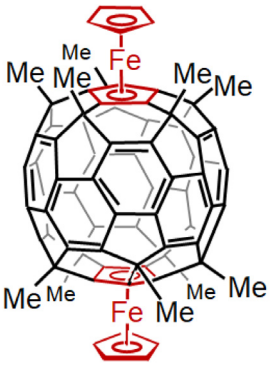

(97)

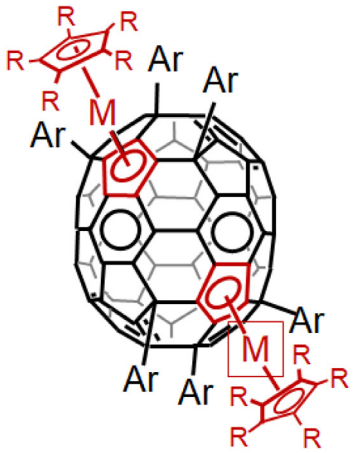

(98)

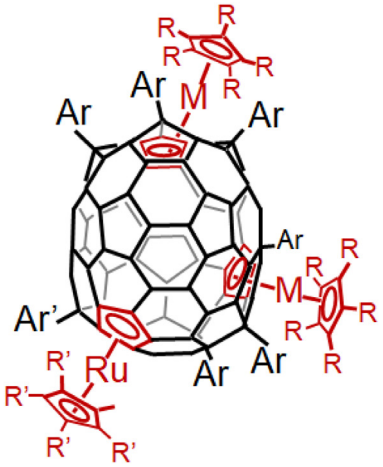

(99)

98a: M=Fe, R=CH_3, Ar= C_6H_4-(*tert*-C_4H_9)-*p*
98b: M=Ru, R=H, Ar= C_6H_4-CH_3-*p*
98c: M=Ru, R=CH_3, Ar= C_6H_4-CH_3-*p*

99a: M=Fe, R=CH_3, R'=H, Ar=Ar'=C_6H_4-(*tert*-C_4H_9)-*p*
99b: M=Ru, R=H, R'=H, Ar=Ar'=C_6H_4-CH_3-*p*
99c: M=Ru, R=H, R'=H, Ar=C_6H_4-CH_3-*p*, Ar'=Ph
99d: M=Ru, R=CH_3, R'=CH_3, Ar= C_6H_4-CH_3-*p*, Ar'=Ph

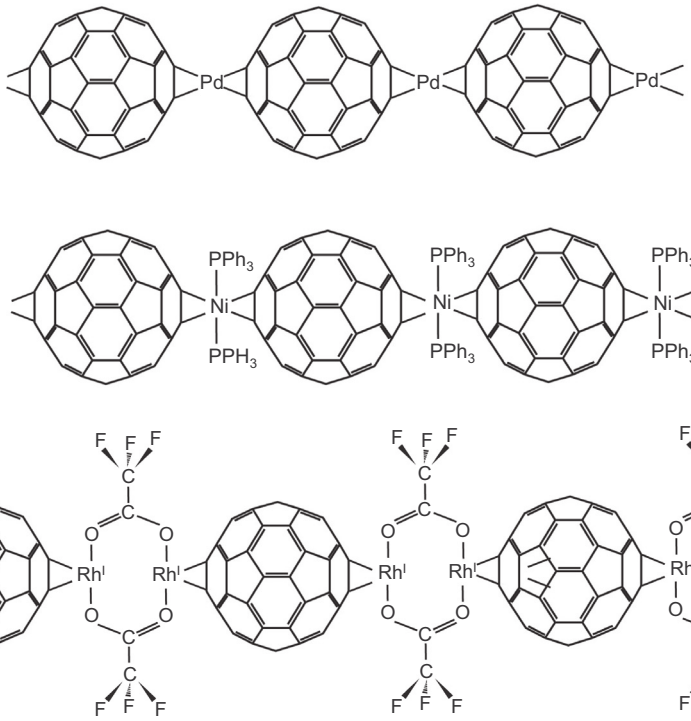

Fig. 38. Suggested1-D structures of selected η^2-fullerene coordination polymers.

the solution in form of large particles composed of small spherical nano- or micro particles (Fig. 39) [126]. The size of these spherical particles depends on the synthesis conditions (time of reaction, concentration of polymerization precursors, stirring conditions). The large polymeric particles can by decomposed to the stable colloidal solution of nanoparticles with ultra-waves [126].

In the electrochemical synthesis, a solution containing a transition metal complex, a fullerene, and supporting electrolyte is electrolyzed. The electrodeposition process of the coordination fullerene polymer can be described by reactions presented in Scheme 6 [132]. The intermediate [M–C_{60}] metal low-valent complex, which is formed at the electrode surface during metal complex reduction, initiates the growth of polymeric phase. The formation of nanoparticles of metallic phase can be also observed as a competitive process. The contribution of both reactions to the overall deposition process depends on the concentrations of polymerization precursors in the solution. Multicyclic voltammograms of *poly*-$C_{60}Pd_3$ and *poly*-$C_{70}Pd_3$ deposition are shown in Fig. 40 [130]. Similar voltammograms have been reported for other fullerene coordination polymers.

Fullerene coordination polymers are electrochemically active in negative potential range due to reduction of the fullerene moiety. The electrochemical properties of the coordination fullerene polymers depend on the structure of polymeric layer, which is determined by the polymerization conditions, particularly the ratio of polymerization precursors in solution [133]. The voltammetric properties of selected electrochemically formed coordination fullerene polymers are shown in Fig. 41. Two poorly separated reduction peaks are observed within the potential window studied. The polymer reduction process is accompanied by the transport of counter-ions of the supporting electrolyte from the solution into the polymeric phase. Therefore, the voltammetric response of the polymer is affected by the nature of cation of supporting electrolyte [134]. Additionally, during the reduction process, the polymeric chains are charged and the electrical double layer is formed at the polymer/solution interphase. The current corresponding to the charging of this double layer significantly contributes to the overall reduction current. Large polymer charging current (Faradaic and double layer charging current) makes these polymers useful as electroactive materials in charge storage devices [126,130,135]. Additional enhancement of the charge storage properties of the fullerene coordination polymers can be achieved by incorporation of these polymers into structure of carbon nanostructures, such as carbon nanotubes, carbon nano-onions or graphene [136–140].

The oxidation state of the fullerene conducting-polymer influences its electronic conductivity. The neutral polymer exhibits high resistance. The conductivity of the polymer increases upon reduction [141]. Theoretical calculation have shown [142] that isolated negative polarons are the preferred state for the reduced polymer and the polymer conductivity can be described by the electron hoping model [141].

Fullerene derivatives can be also incorporated into polymeric structure via η^2-type coordination with transition metal atoms or complexes [143–147]. Examples of coordination polymers of fullerene derivatives are shown below (***100***) – (***106***). Due to the presence of two different redox active centers, they can act as a multifunctional materials. Polymers of fullerenes with covalently attached ferrocene centers, (***100***) - (***102***), are electrochemically active and electronically conductive, both in negative and positive potential ranges (Fig. 42a) [143,144]. The reduction of the fullerene moieties is responsible for the conductivity at negative potentials. In the positive potential range, the conductivity of this polymer is related to the electron transfer between ferrocene moieties with different redox states (Fig. 42b). Materials with two different potential windows of conductivity are called as "double cables". Similar electrochemical behavior was reported for *poly*-$C_{60}Pd_3$ with zinc porphyrin redox center covalently attached to the fuller-

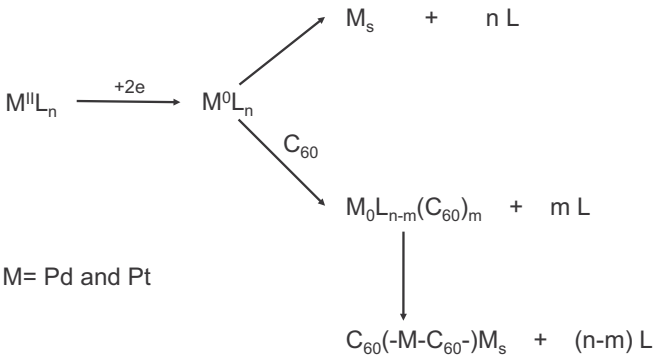

Scheme 6. Electrode processes in solution containing fullerene C_{60} and Pd(II) or Pt (II) complexes which results in formation coordination fullerene polymers.

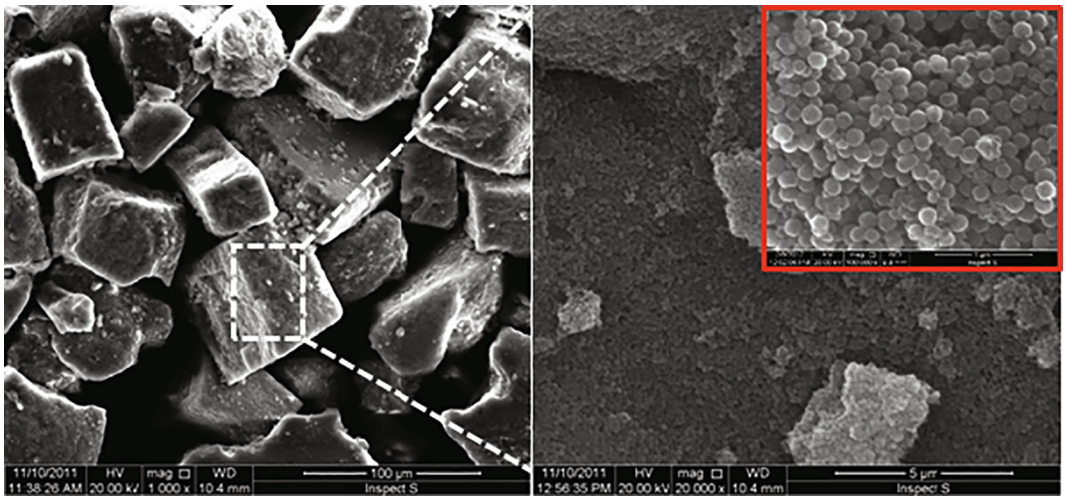

Fig. 39. Morphology of three-dimensional polymeric structure of *poly*-$C_{60}Pd_3$.). Reproduced with permission from Ref. [126]. Copyright © 2013, Elsevier.

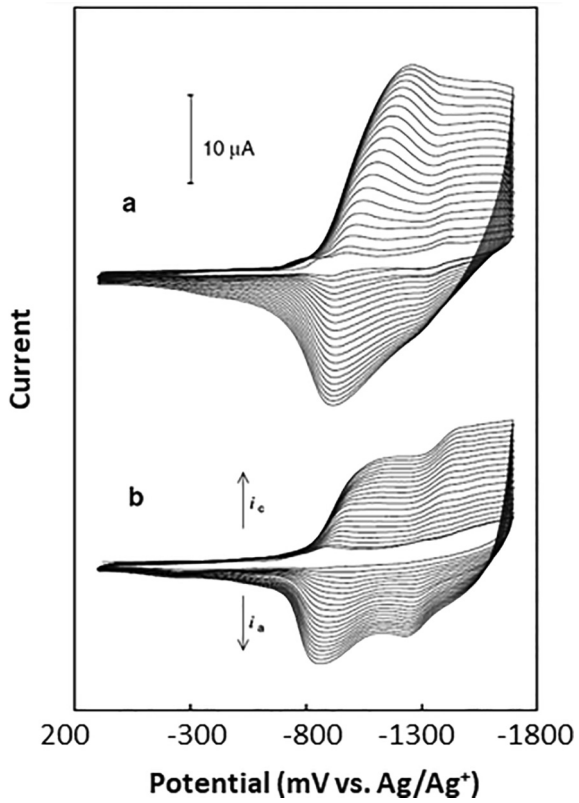

Fig. 40. Multicyclic voltammograms for (a) 0.25 mM C_{60} and 0.85 mM $Pd(acetate)_2$ and (b) 0.25 mM C_{70} and 0.85 mM $Pd(acetate)_2$ in acetonitrile/toluene (1:4, v/v) containing 0.1 M $[(n\text{-}Bu)_4N]ClO_4$ recorded at gold disk electrode. Sweep rate was 100 mV s^{-1}. Reproduced with permission from Ref. [130]. Copyright © 2007, Springer-Verlag.

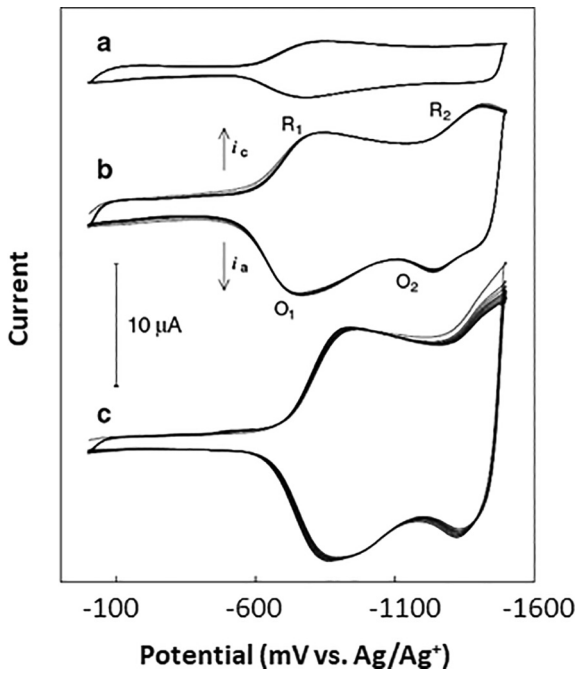

Fig. 41. Cyclic voltammograms of (a) *poly*-Pd_3C_{60} and (b and c) *poly*-Pd_3C_{70} films in acetonitrile containing 0.10 M $[(n\text{-}Bu)_4N]ClO_4$ (a and b) and 0.10 M $[(Et)_4N]ClO_4$ (c) recorded at Au (1.5 mm). Sweep rate was 100 mV s^{-1}. *Poly*-Pd_3C_{60} and *poly*-Pd_3C_{70} films were grown under cyclic voltammetry conditions in acetonitrile/toluene (1:4, v:v) containing 0.10 $[(n\text{-}Bu)_4N]ClO_4$, 0.25 mM C_{60} or C_{70}, and 0.85 mM $Pd(ac)_2$. Reproduced with permission from Ref. [130]. Copyright © 2008 Springer-Verlag.

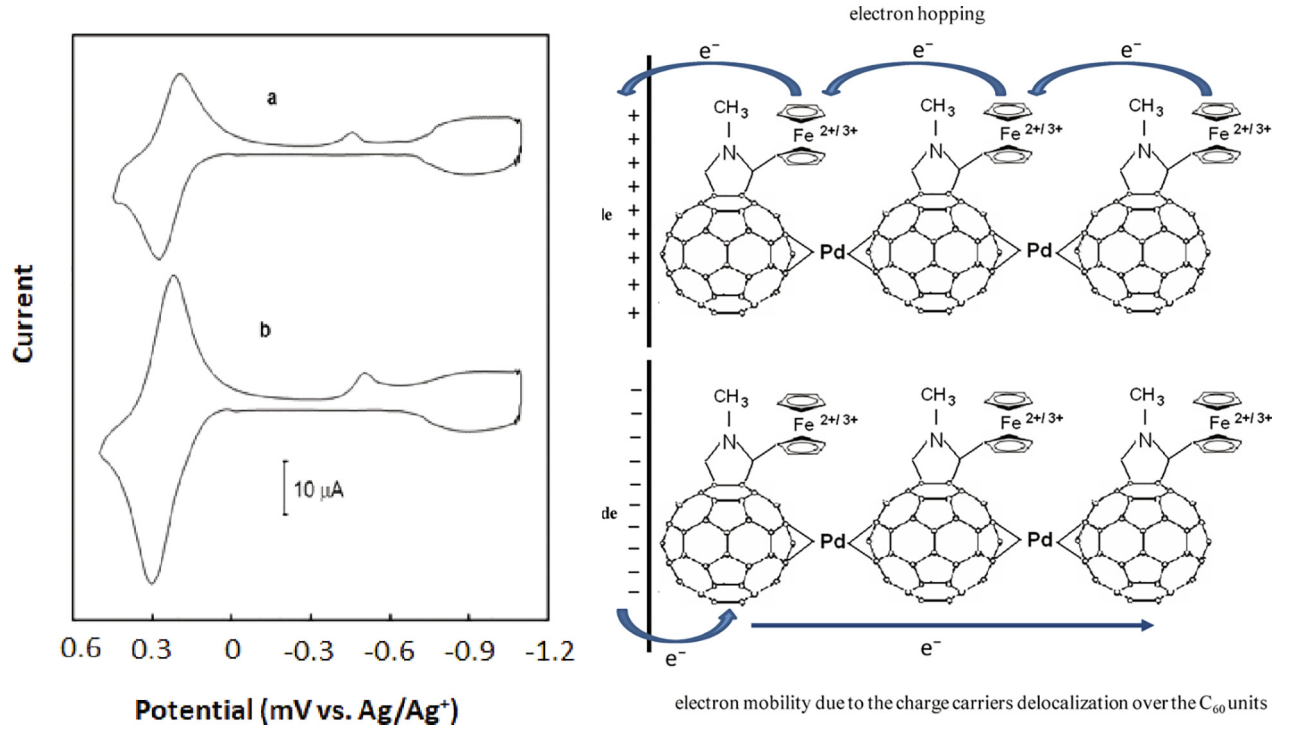

Fig. 42. (*a*) Cyclic voltammograms of (*1*) *poly*-Pd_3C_{60}-Fc (***100***) and (b) *poly*-Pd_3C_{60}-bis-Fc (***101***) in acetonitrile containing 0.1 M $[(n\text{-}Bu)_4N]ClO_4$ recorded at Au electrode. Sweep rate was 100 mV s^{-1}. Reproduced with permission from Ref. [144]. Copyright © 2011, Elsevier. (*b*) Schematic representation of electron transfer processes during *poly*-Pd_3C_{60}-Fc oxidation and reduction.

ene moieties (***103***) [145]. The coordination polymer of C_{60} with covalently attached crown ether units (***104***) can be used as sensors for alkali metal cations [146].

Recently, a new single layer graphene oxide hybrid polymeric material was fabricated [148]. In this system, the fullerene moieties covalently attached to the surface of graphene oxide layer were coordinated to palladium atoms in an η^2-fashion, similar to the fullerene coordination polymer, *poly*-$C_{60}Pd_3$. This material exhibits electrochemical activity in the negative potential region due to the fullerene cage reduction, with an overall electrochemical behavior resembling that of typical organic conducting polymers. The electronic interaction between the graphene oxide sheets and the covalently bonded fullerene cages facilitates the reduction of the fullerene moiety. Therefore, the potential for reduction of the graphene oxide hybrid polymeric material is shifted toward less negative potentials in comparison to *poly*-$C_{60}Pd_3$. The electron transfer between single-layer graphite oxide sheets through –C_{60}-Pd-C_{60}- units is also promoted [148].

6. Fullerenes with a metal complex redox couple covalently attached through a linker

Photoactive systems containing electron-donor and electron-acceptor centers were extensively studied due to their application in devices converting light into electronic current [11–13]. High electron capacity and low reorganization energy of fullerenes make these molecules particularly attractive as electron acceptors in photoactive systems. Structure of fullerenes offers possibility of multiple modification and macromolecular structure formation. On the other hand, transition metal complexes, such as porphyrin

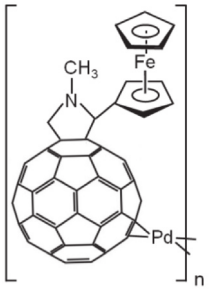

(***100***)

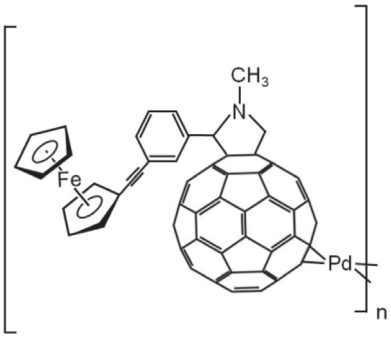

(***101***)

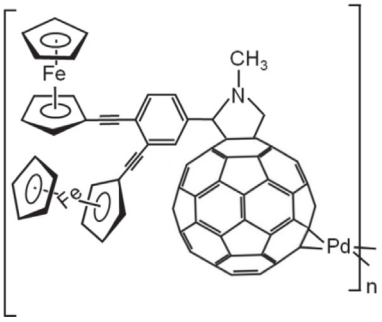

(***102***)

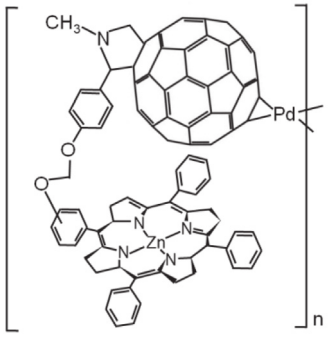

(***103***)

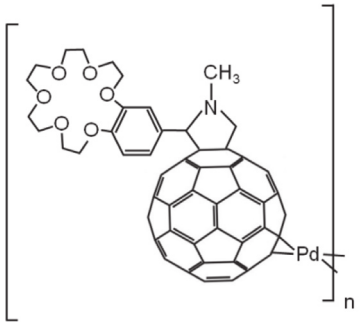

(***104***)

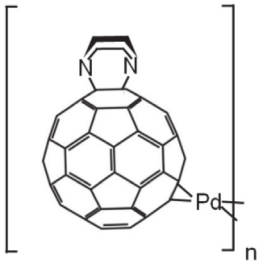

(***105***)

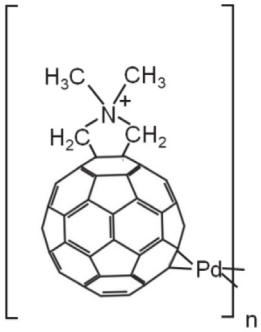

(***106***)

and polypyridyl complexes as well as metallocenes, are commonly used as electron donating moieties. The electronic interaction between the electron-donating and electron-accepting centers of the dyad also depends on the nature of linker between the two electroactive units. In this section, the electrochemical properties of photoactive systems composed of fullerenes and transition metal complexes will be summarized. Special attention will be focused the structural effects in the electrochemical properties of both electroactive systems.

6.1. Transition metal complexes of fullerenes with covalently attached polypyridyl units

The complexes of transition metal and fullerene derivatives with pyridine and polypyridine units are particularly interesting from both the electrochemical and photophysical point of view. Modulation of the electronic coupling between C_{60} electron-acceptor and metallopolypyridine units that exhibit electron-donating properties can result in more efficient charge-transfer processes. The attachment of fullerenes to the metal-binding domains of polypyridine groups can also leads to the formation of macromolecular multifunctional assembly.

Several polypyridine ligands, such as 2,2′-bipyridine (bpy) [149–152], 2,2′:6′,6″-terpyridine (tpy) [153,154], 1,10-*ortho*-phenanthroline (phen) [155–157], 3-(2-pyridyl)pyrazoline [158], 3,6-di(2-pyridyl)pyridazine [159], and others [160] have been attached to the fullerene units through different spacers. For example, bipyridyl and terpyridyl units can be directly attached to the nitrogen atoms of the fulleropyrolidines (***107***) and (***108***). These compounds can serve as bidenate and tridenate ligands to coordinate transition metals. The electrochemical behavior $[Ru(bpy)_2(bpy\text{-}C_{60})](PF_6)_2$ (***107***), the ligand alone, and the $[Ru(bpy)_3]Cl_2$ complex are shown in Fig. 43 [152]. In the potential range examined, three reduction steps assigned to the reduction of fullerene moiety and two reduction steps associated with Ru-based reduction process are observed. The C_{60}-centered, one-electron reversible reduction processes are shifted positively by 30–50 mV in comparison to the values obtained for free ligand. On the other hand, a significant shift of the Ru-based reduction process toward more negative values was observed for the $[Ru(bpy)_2(bpy\text{-}C_{60})]^{2+}$ complex in comparison to the $[Ru(bpy)_3]^{2+}$. Similar behavior has been reported for $[Ru(tpy)_2(tpy\text{-}C_{60})](PF_6)_2$ (***108***) [152]. The electrochemical properties of both ruthenium complexes are summarized in Table 8. These results indicate electronic coupling between the metal center and the fullerene cage.

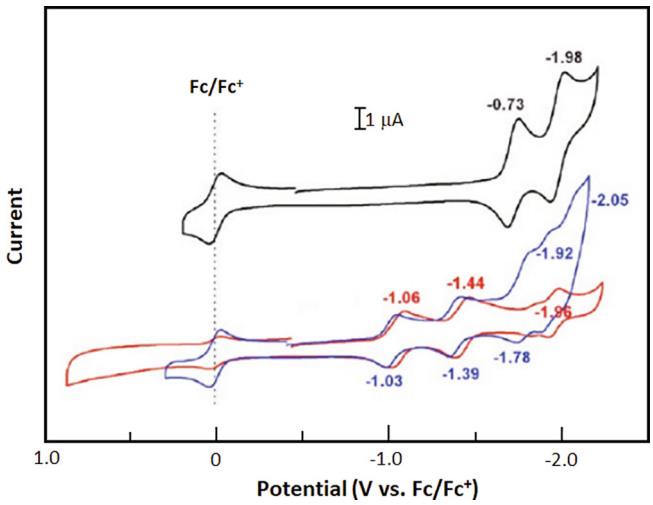

Fig. 43. Cyclic Voltammograms of $[Ru(bpy)_3]Cl_2$ (black), bpy-C_{60} (red) and $[Ru(bpy)_2(bpy\text{-}C_{60})](PF_6)_2$ (blue) in CH_2Cl_2 containing 0.1 M $[(n\text{-}Bu)_4N]PF_6$. Reproduced with permission from Ref. [152]. Copyright © 2009, Wiley-VCH Verlag.

Polypyridine moieties were also connected to fullerene cages through various rigid or flexible spacers. Such architectures provide opportunities to modulate the redox properties of the assembly. The dyads and triads in which oligopyridine (bpy and tpy) metal-binding domains are separated from the fullerene moiety by the polyethyleneoxy spacers (***110*** and ***111***) were synthesized [153]. The anodic shift in the range of 30 to 80 mV was observed for fullerene-based reduction processes in comparison to the corresponding free ligands (Table 8). However, the presence of the fullerene units shows almost no influence on the Ru(II)/Ru(III) oxidation process even when two fullerene centers are bound to the bipyridyl units as seen in compound (***112***).

Electrochemical properties of the ruthenium(II) complex (***113***) and rhenium(I) complex (***114***) with a crown-linked methanofullerene ligands were also intensively investigated [161]. The complex votammetric behavior of these compounds shown in Fig. 44 is due to the presence of three electroactive centers: the metal ion, the bpy ligand, and the fullerenopyrolidine moiety. A comparison of voltammograms obtained for these complexes with the voltammetric response of reference compounds allowed the assignment

Table 8
Redox potentials of C_{60}-bipyridine and C_{60}-terpyridine complexes of Ru(II) in dichloromethane.

Compound	Redox potential in V vs. Fc/Fc^+						
	E_{ox}[a]	R_1[b]	R_2[b]	R_3[c]	R_4[c]	R_5[b]	Ref.
bpy-C_{60}		−1.06	−1.44		–	−1.96	[152]
$Ru(bpy)_3^{2+}$	0.94			−1.73	−1.98		[152]
$[Ru(bpy)_2(bpyC_{60})]^{2+}$	0.69	−1.03	−1.39	−1.78	−1.92	−2.05	[152]
tpy-C_{60}		−1.07	−1.46			−1.99	[152]
$Ru(tpy)_2^{2+}$	0.86			−1.66	−1.96		[152]
$[Ru(tpy)(tpyC_{60})]^{2+}$ (***108***)	0.59	−1.04	−1.43	−1.76	−2.02		[152]
(***109***)	0.95	−1.00	−1.40			−1.83	[153]
(***110***)	0.80	−1.02	−1.43			−1.91	[153]
(***111***)	0.82	−1.03	−1.42			−1.80	[153]
(***112***)	0.93	−1.10	−1.48			−1.92	[153]

[a] metal-centered redox process
[b] fullerene moiety reduction processes
[c] ligand-involved redox processes

of the redox processes to the voltammetric signals presented in Fig. 44. These processes are summarized in Table 9 for both (***113***) and (***114***) [161]. For compound (***113***) the energy for the Ru^{III}-C_{60}^{-} charge-separation process is close to 1.8 eV. This is a very promising value for the possibility of light-induced formation of a charge separated state. For the Re(I) complex (***114***), the band gap energy is much higher (2.3 eV) because of the significant anodic potential shift of Re(I) oxidation process.

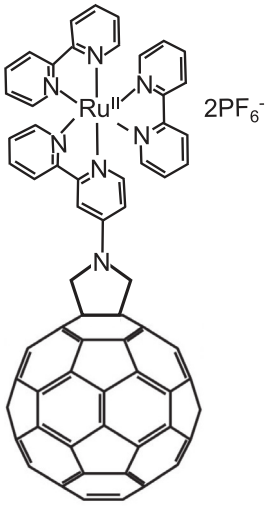

(*107*)

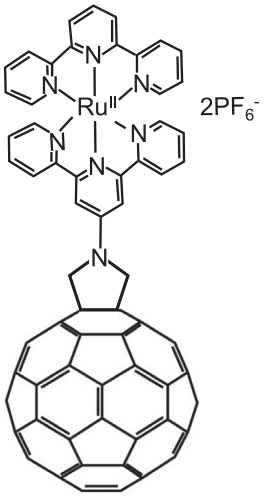

(*108*)

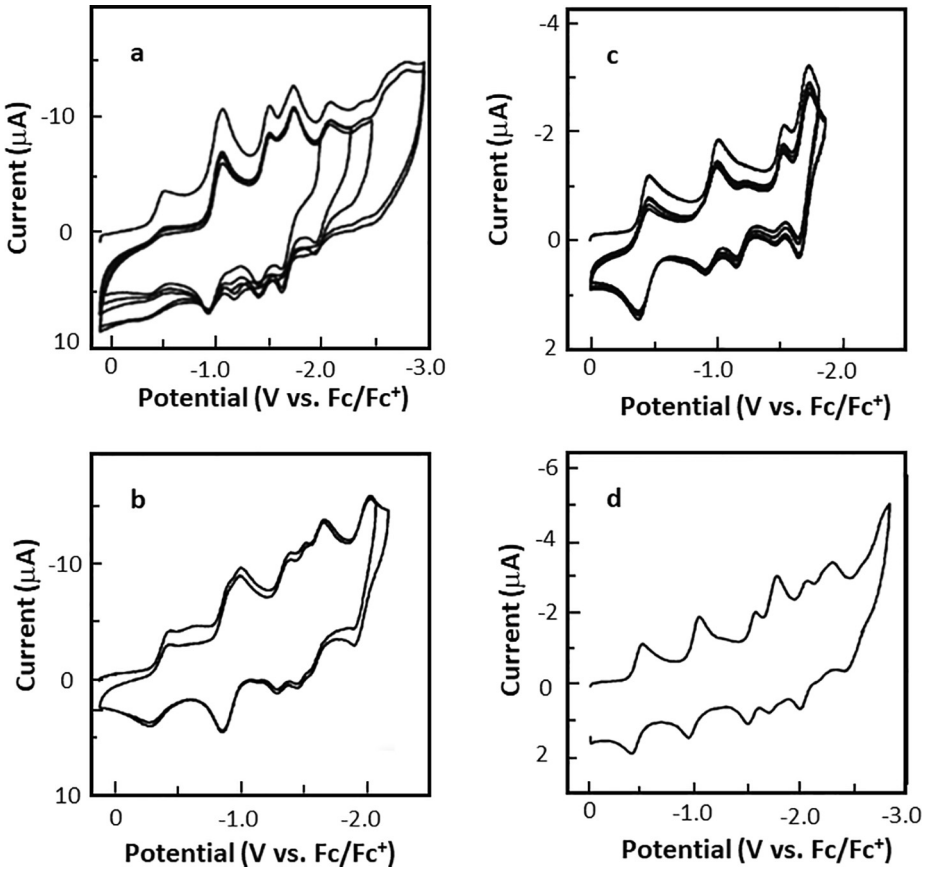

Fig. 44. CV curves of a 0.5 mM (***113***) (a and b), and 0.3 mM (***114***) (c and d) in THF containing 0.05 M $[(n\text{-}Bu)_4N]PF_6$ THF; scan rate: (a and c) 0.1 V s^{-1}; T = 25∘C; (b and d) 0.5 V s^{-1}; T = − 55∘C. Working electrode: platinum wire. Reproduced with permission from Ref. [161].

Crown-like linkers were also used to form pseudo-octahedral Ru (II), Ir(III), and Fe(II) complexes of terpyridine-fullerene (***115***) [162]. Metal-centered oxidation processes have been reported for the octahedral, six-fold fullerene complexes of Ru(II) and Fe(II) at potentials very close to the potentials for oxidation of $[Ru(tpy)_2]^{2+}$ and $[Fe(tpy)_2]^{2+}$, respectively. Oxidation of Ir(III) to Ir(IV) in the Ir (III) analog (***115***) has not been observed. For all complexes, two *tpy*- centered reduction potentials have been reported. Surprisingly, no electrochemical processes related to the [60]fullerene-involved charge transfer processes have been observed [162].

the biruthenium complex (***117***) is particularly interesting. In the positive potential range, two one-electron oxidation processes of Ru(II) redox center are observed at 1.52 and 1.70 V vs. saturated calomel electrode (SCE). The large potential shift demonstrates a strong interaction between the two metal centers. The electrochemical activity of the 2,3-bipyridyn-2-yl-quinoxaline bridging ligand, the four bpy units, and fullerene cage are responsible for the complex voltammetric behavior at negative potentials.

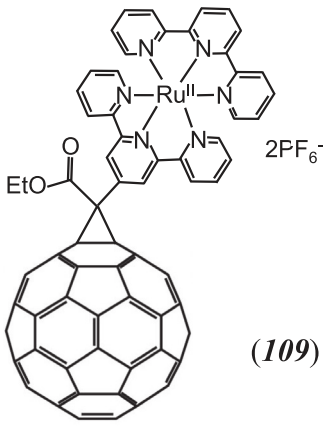

(***109***)

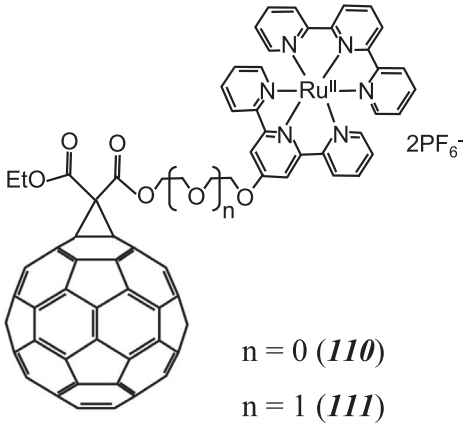

n = 0 (***110***)

n = 1 (***111***)

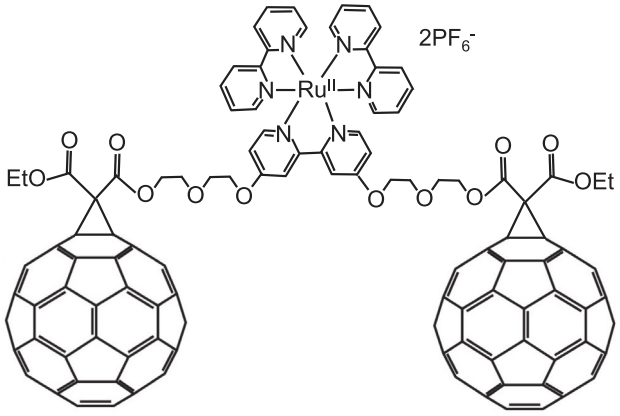

(***112***)

The electrochemical properties of mono (***116***) and bimetallic (***117***) ruthenium complexes with bipyridine units bonded through androstane skeleton to the fulleropyrrolidine have been also reported as seen in Fig. 45 [163]. The redox behavior of

In order to investigate the influence of the linker structure and its length on the communication between the electron-donating ruthenium bis-(terpyridine) and the electron-accepting fullerene unit, a series of terpyridine methanofullerene and pyrrolidino-

Table 9
Redox potentials of Ru(II) (***113***) and Re(I) (***114***) complexes with a crown-linked methanofullerene ligands in tetrahydrofuran[161].

Compound	Redox potential in V vs. SCE		
	Ru-centrated oxidation	Ligand-centered reduction	Fullerene-centered reduction
(***113***)	1.45	−0.90–1.32–1.46–1.83. −2.05–2.67	−0.38–0.95–1.62–2.28
(***114***)	1.90	−0.88–1.34–1.55–1.96	−0.36–0.92–1.61–2.20

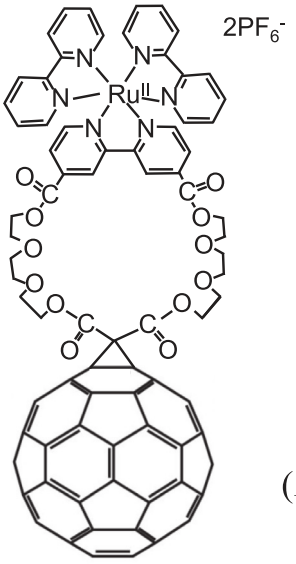

(*113*)

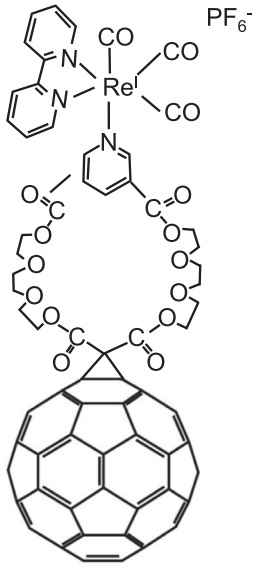

(*114*)

fullerene dyads linked *via* short *p*-phenylene or longer *p*-phenyleneethynylenephenylene units (***118***) – (***121***) was studied [164]. The rigid structure and π conjugation of these linkers provide pathways for efficient charge transfer. However, voltammetric experiments do not provided any evidence that both redox centers electronically communicate in the ground state [164].

In addition to the Ru(II) complexes, which have been the most extensively studied, the electrochemical properties of Cu(I) complexes bounded to the fullerene cages through phenanthroline units (***122***) have been reported [165]. For such structures, excellent photostability, long-lived luminescent excited states and energy adsorption throughout the wide UV/Vis spectral range can be expected, making them particularly useful for solar cell devices [166,167]. In the positive potential range, a Cu-centered oxidation process is observed. Surprisingly, a significant positive potential shift of 0.865 V (vs. SCE) for the Cu(I)/Cu(II) redox process is

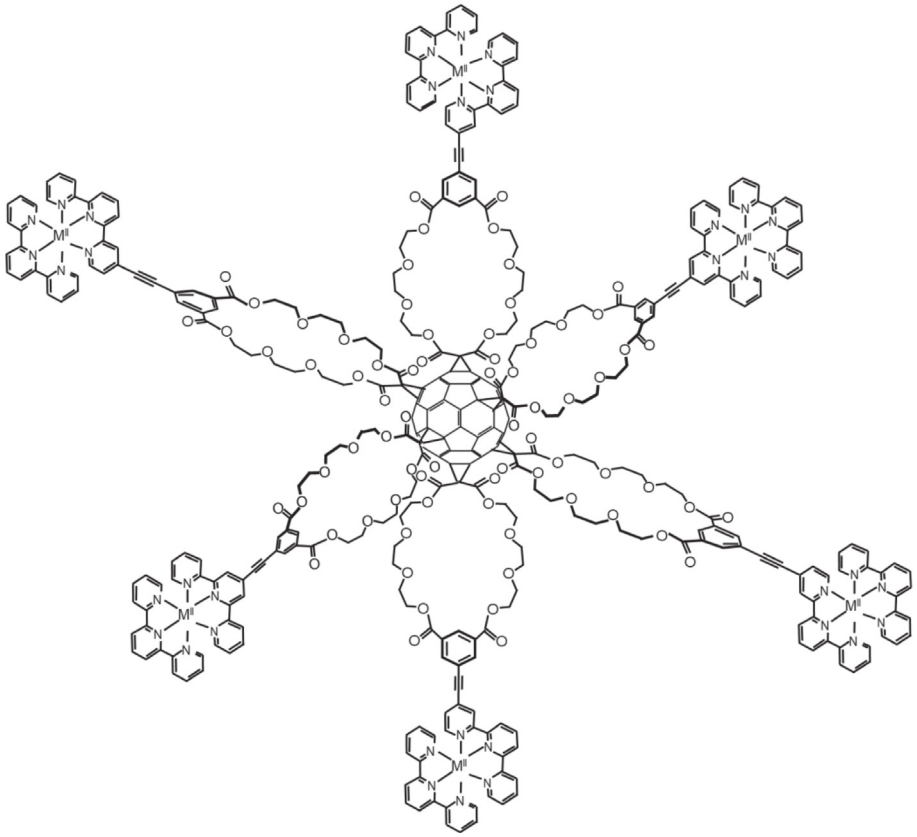

(*115*)

observed for the fullerene containing complex (***122***) in comparison to the reference complex (***123***). The potential for oxidation of (***123***) is 0.565 V [165]. At negative potentials, redox processes related to the reduction of the fullerene moieties have been observed. These processes appear at potentials typical for potentials of C_{60} mono-adduct reduction.

Copper(I) ions have been also used to form a new class of [2] catenanes containing Zn(II)-porphyrin and [60]fullerene triads (***124***) [168]. The electrochemical properties of these complexes and reference compounds (***125***) – (***127***) have been investigated [168]. The values of the redox potentials of these complexes are summarized in Table 10. The presence of fullerene units in the complexes does not influence electrochemical properties of the Cu(I)/Cu(II) oxidation process in contrast to the data reported by Armaroli and co-workers [165] for complexes bounded to the fullerene cages through phenanthroline units (***122***). A small shift of about 60 mV to more positive potentials for the one-electron oxidation process of the Zn(II)-porphyrin moiety is observed in comparison to the reference compound. At negative potentials, the processes related to the fullerene cage oxidation are almost unaffected by the presence of both Cu(I)-phenantoline and Zn(II)-porphyrin redox centers.

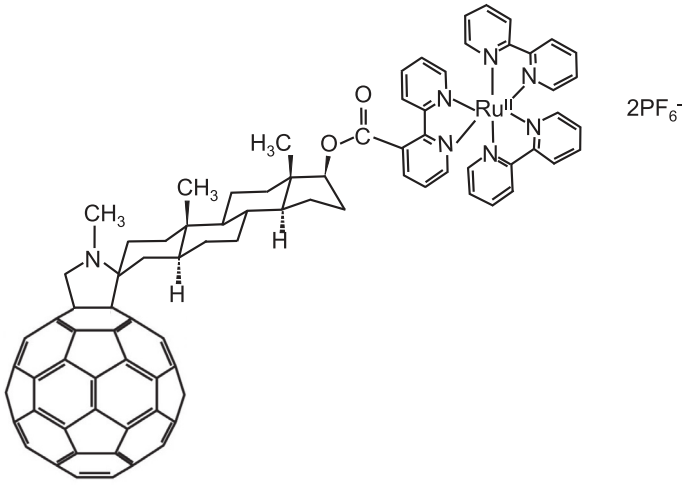

(***116***)

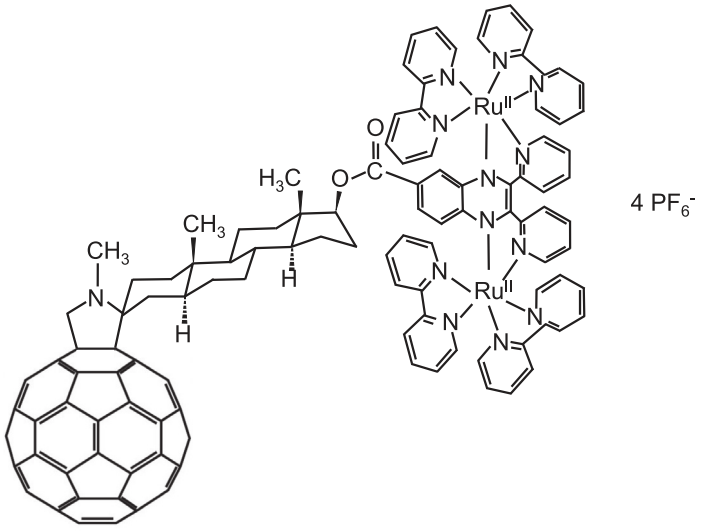

(***117***)

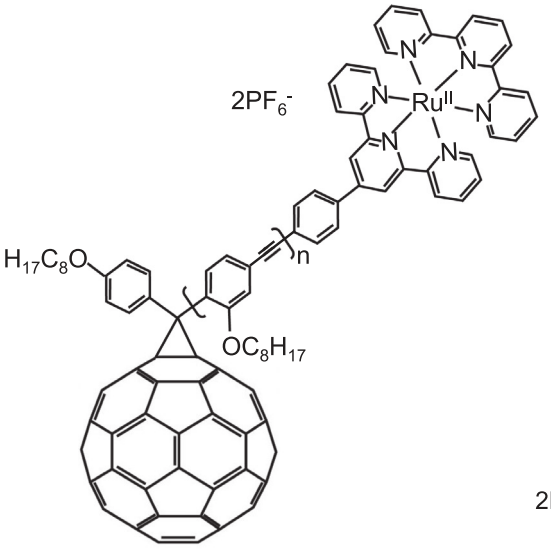

n = 1 (***118a***)

n = 2 (***118b***)

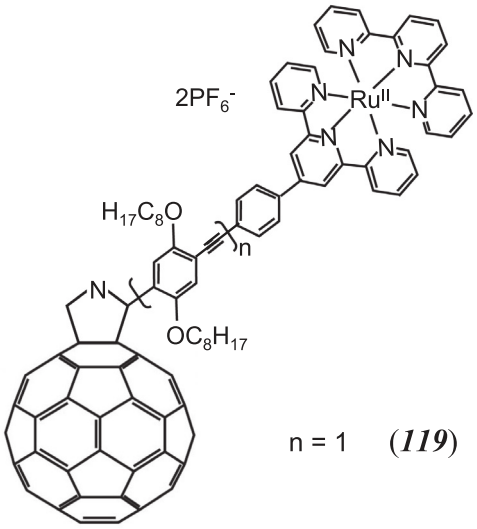

n = 1 (***119***) n = 2 (***120***)

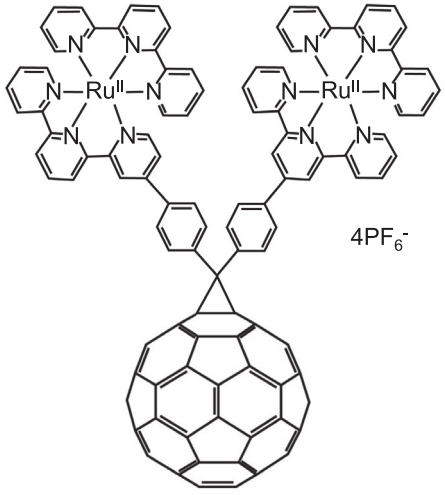

(***121***)

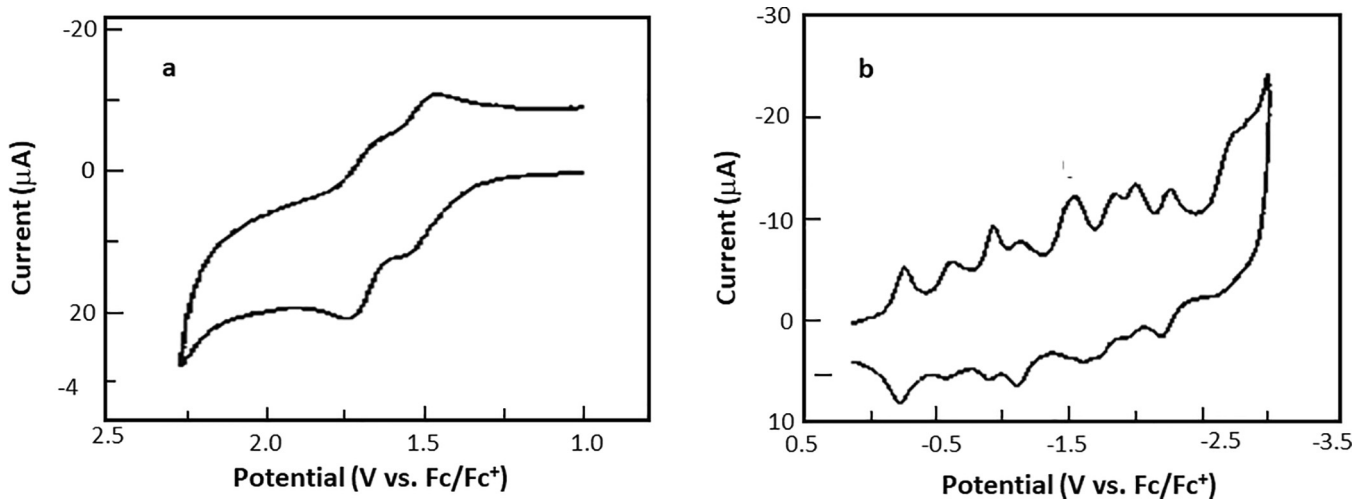

Fig. 45. Cyclic voltammogram recorded at Pt electrode of (a) 0.5 mM (***117***) (a) in CH_3CN containing 0.05 M $[(n\text{-}Bu)_4N]PF_6$ and (b) < 0.2 mM (***117***) in THF 0.05 M $[(n\text{-}Bu)_4N]PF_6$. T = 25 °C, v = 0.5 V s^{-1}. Reproduced with permission from Ref. [163]. Copyright © 2001, Wiley-VCH Verlag.

Silver(I) ions were used as a bonding center to form dimeric complexes of C_{60}-phenanthroline derivatives (***128***) [156]. The presence of the phenanthroline moiety shifts the reduction potential of the fullerene cage toward more negative values in comparison to the pristine [60]fullerene. This effect is additionally enhanced by the presence of silver ions. The fullerene dimeric complex is stable upon reduction within the first three reduction steps. Surprisingly, no reduction of silver(I) has been observed within studied potential range.

Fullerene moieties have been connected through linkers containing Ru(II)-bpy (***129***) and Re(I)-bpy (***130***) units to form C_{60} dimers. The cyclic voltammograms of these complexes exhibit

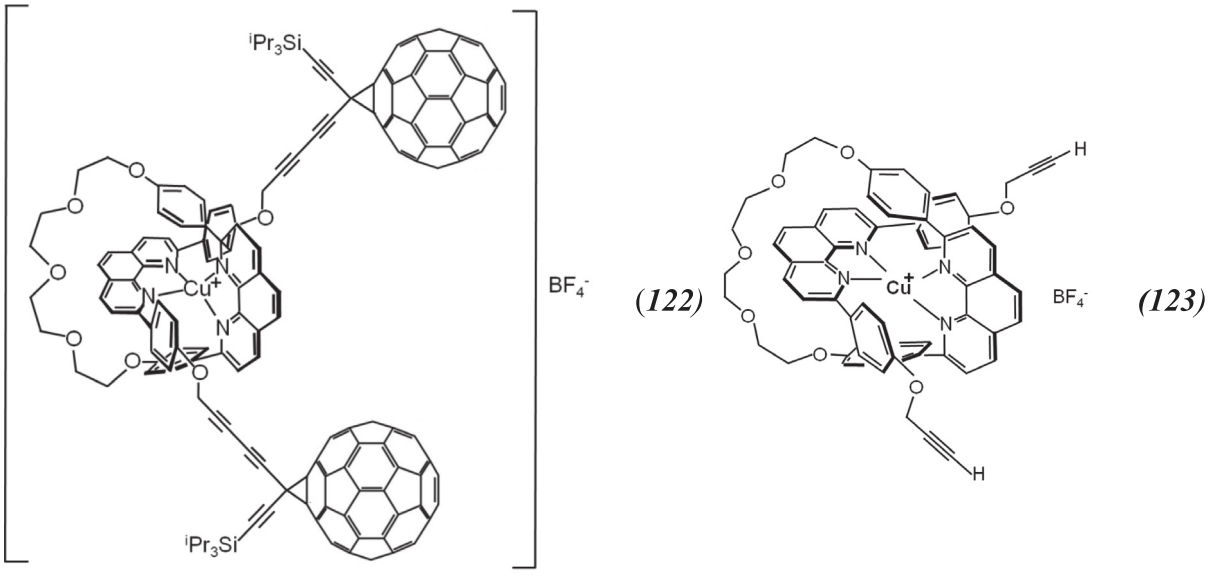

Table 10
Redox potentials of Zn(II)-porphyrin and [60]fullerene triad (***124***) and reference compounds (***125***) – (***127***) in *o*-dichlorobenzene [168]

Compound	Redox potential in V vs. Fc/Fc^+							
	Oxidation		Reduction					
	Cu^+/Cu^{2+}	ZnP/ZnP^+	$C_{60}^{0/-}$	$C_{60}^{-/2-}$	$C_{60}^{2-/3-}$	$C_{60}^{3-/4-}$	ZnP/ZnP^-	Cu^+/Cu
(***124***)	0.18	0.18	−1.12	−1.48	−1.96		−1.92	−2.30
(***125***)	0.16							−2.30
(***126***)	0.20	0.20					−1.92	−2.30
(***127***)	0.16		−1.12	−1.48	−1.96	−2.54		−2.30

quasi-reversible, likely bpy-centered oxidation process and complex electrochemical behavior in the negative potential range [169]. These long linkers connecting fullerene moieties do not allow for effective electronic interaction between the two C_{60} cages.

Donor-chromophore-acceptor triads containing Pt(II)-bipyridyl moiety (chromphore) separating fullerene-acceptor part and *N*-(4-ethynylphenyl)cabazole (***131***) and *N*-(4-ethynylphenyl)3,7-di-*tert*-butylcabazole (***132***) [170], phenothiazine (***133***) [171] and 3,7-di-*tert*-butylphenothiazine (***134***) [171] units as electron donors have been synthesized. A comparison of the redox properties of these triads and reference compounds are shown in Table 11.

The HOMO and LUMO of complex (***131***) are shown in Fig. 46a. The HOMO orbitals, which are located on the phenothiazine moieties, are involved in two-electron reversible oxidation process as shown in Fig. 46b [171]. The potential of this process is unaffected by the presence of the fullerene units. The first and second reduction processes are related to reduction of the fullerene cage. The formal redox potential of this process is shifted toward less cathodic potentials in comparison to reduction potentials of reference compound (Table 11). The LUMO is entirely located on the fullerene moiety. At more negative potentials, reduction of bipyridine ligand occurs, followed by the transfer of the forth electron onto the fullerene moiety. In contrast to the fullerene-involved reduc-

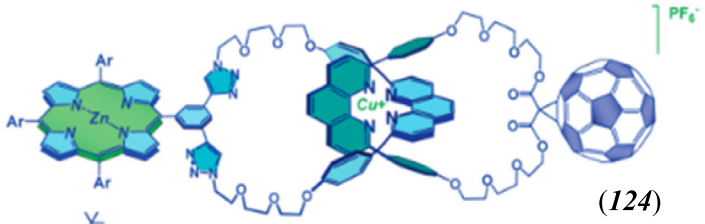

(***124***)

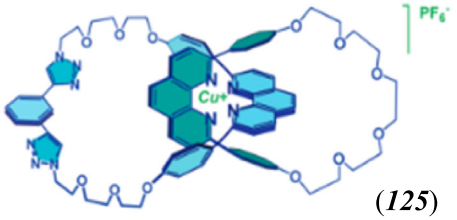

(***125***)

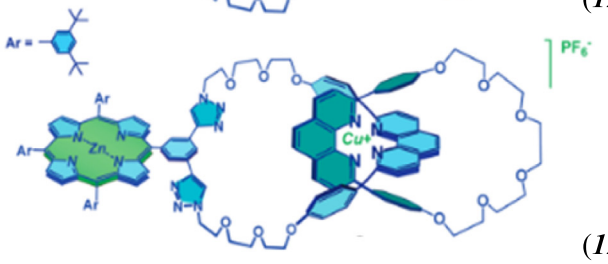

(***126***)

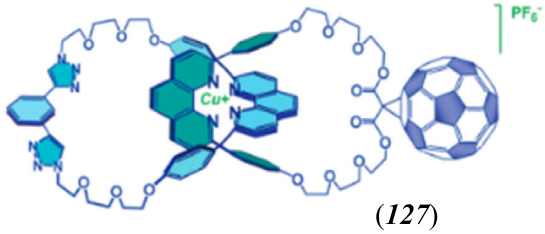

(***127***)

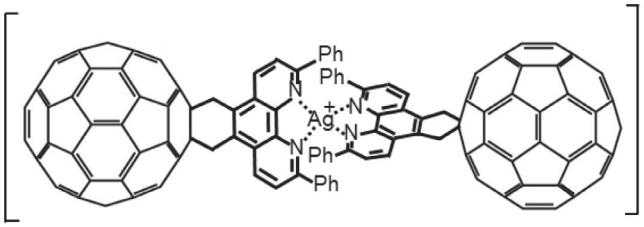

(***128***)

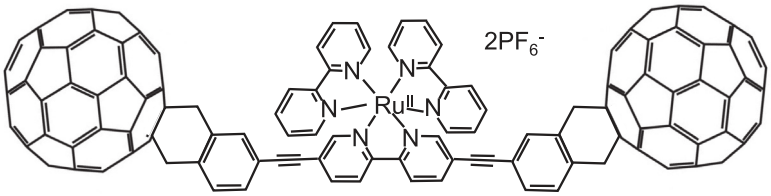

(***129***)

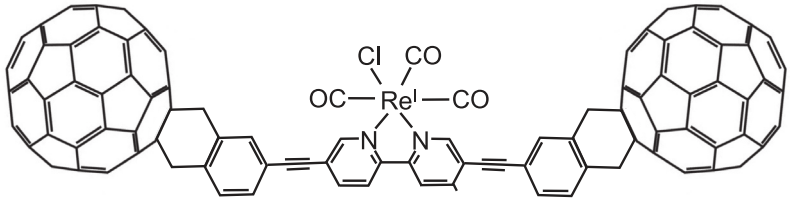

(***130***)

tion processes, the reduction of the bipyridine ligand is shifted cathodically in comparison to the reference compound (see Table 11). The free energies for charge separation and charge recombination were determined on the base of electrochemical data. In dichloromethane, both triads undergo very fast, photo-induced, charge separation process within few hundreds femtoseconds leading to the formation of $(Cbz)_2^+$-Pt(bpy)-C_{60}^- charge separation state which recombine to C_{60}* excited triplet state, and finally decays to ground state in 22–28 microseconds [170].

Complexation of Cu(I) ions with 1,10-phenanthroline units bounded to the [60]fullerene cage through alkane chain were used to form dendrimers with a bis(1,10-phenanhroline)coper(I) core and peripheral fullerene cages (***135***–***137***) [157]. In these systems, the fullerene-functionalized dendrimeric branches surround and isolate the central $[Cu(phen)_2]^+$ core. The electrochemical properties of dendrimers with different numbers of surrounding [60]fullerene moieties and reference compounds are summarized in Table 12. The first fullerene-centered reduction step is electrochemically reversible. The presence of the Cu(I) ion does not influence the potential of this process. Transfer of the second electron on the fullerene moiety is irreversible and followed by the chemical reaction [157]. The peripheral [60]fullerene units behave as independent redox centers in dendrimers. The dendrimer oxidation process related to the Cu(I)/Cu(II) redox couple is observed only for dendrimer containing four [60]fullerene units surrounding

Table 11
Redox properties of triads composed of fullerene-carbazole and fullerene-phenothiazine separated by Pt(II)-bipirydyl moiety in dichloromethane.

Compound	Electron donor	Redox potentials in V vs. Fc/Fc^+				Ref.
		Oxidation	Reduction			
		Donor/Donor^{2+}	$C_{60}^{0/-/2-}$	C_{60}^-	Pt(bpy)$^{0/-}$	
(***131***)	*N*-(4-ethynylphenyl) carbazole	0.88	−1.07	−1.46	−1.80	[170]
(***132***)	*N*-(4-ethynylphenyl)-3,6-di-*tert*-butyl-carbazole	0.88	−1.07	−1.46	−1.80	[170]
(***133***)	*N*-(4-ethynylphenyl) phenothiazine	0.31	−1.07	−1,45	−1.80	[171]
(***134***)	*N*-(4-ethynylphenyl)-3,6-di-*tert*-butyl-phenothiazine	0.13	−1.07–1.45		−1.80	[171]

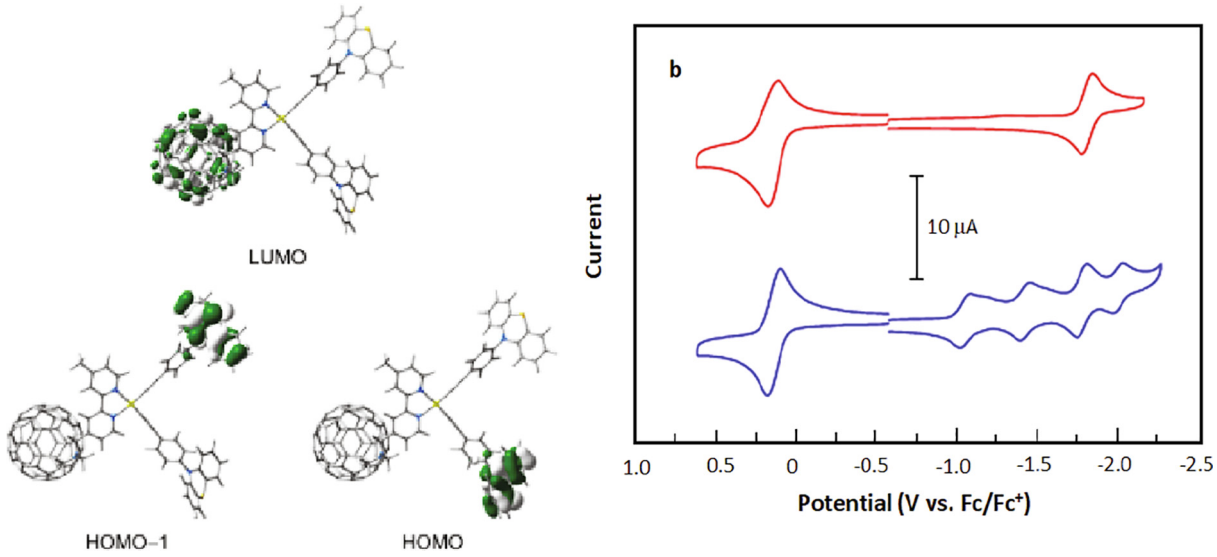

Fig. 46. (a) Spatial plots (isovalue = 0.03) of selected molecular orbitals of $(PTZ)_2$-Pt(bpy)-C_{60} (***131***) obtained from PBE0/CPCM calculation. (b) Cyclic voltammograms of (*t*-BuPTZ)$_2$-Pt(bpy) (top) and(*t*-BuPTZ)$_2$-Pt(bpy)-C_{60} (***132***) (bottom) in CH_2Cl_2 containing 0.10 M $[(n\text{-}Bu)_4N]PF_6$ at 298 K. Reproduced with permission from Ref. [171]. Copyright © 2014, American Chemical Society.

Table 12
Redox properties of bis(1,10-phenanhroline)coper(I) core with peripheral fullerene cages dendrimers and reference compounds in dichloromethane [157].

Compound	Redox potentials in V vs. Fc/Fc^+		
	Reduction		Oxidation
	$C_{60}^{0/-}$	$C_{60}^{-/2}$	$Cu^+/Cu2^+$
G1$CO_2{}^t$Bu	−1.07	−1.45[a]	+1.2
G2$CO_2{}^t$Bu	−1.07	−1.45[a]	+1.1
G3$CO_2{}^t$Bu	−1.08	−1.45[a]	+1.1
CuG0		−2.20	+0.60
CuG1	−1.08	−1.39[a]	+0.60
CuG2	−1.08	−1.43[a]	not observed
CuG3	−1.07	−1.40[a]	not observed

[a] peak potential of voltammetric irreversible process at 0.1 V s^{-1}.

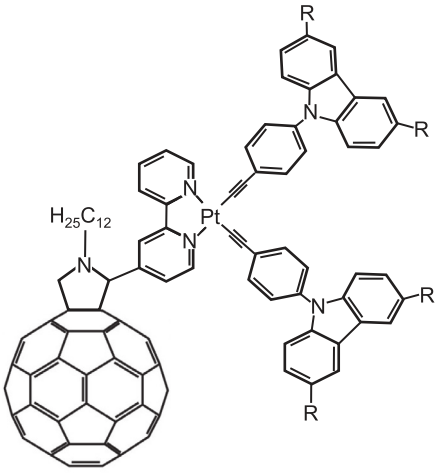

M = H (***131***)

M = *t*-Bt (***132***)

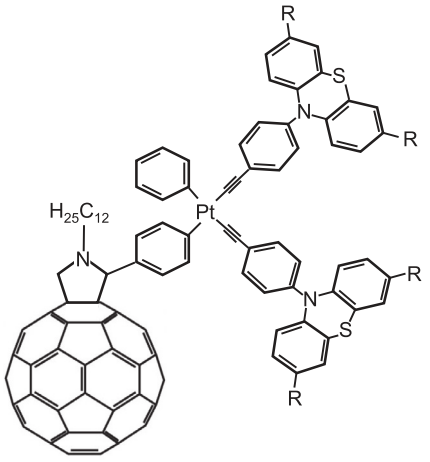

M = H (***133***)

M = *t*-Bt (***134***)

metal center (***135***). This process is irreversible and the current density is much smaller than the theoretical value predicted from the ratio of C_{60} to Cu(I) redox center. Such behavior indicates that the large peripheral fullerene units inhibit the redox processes involving the copper(I) center. The metal centers in dendrimers with larger numbers of bulky [60]fullerene units, compounds (***136***) and (***137***), are so effectively isolated that Cu(I) redox center is totally inaccessible for electrons from the electrode, thus preventing dendrimer electrooxidation [157].

The electrochemical properties of well-defined fullerene and tris(bipyridine)ruthenium(II) dual end terminated macromolecular systems (***138***) were also investigated [172]. Because of the long distance between the two electroactive centers, no electronic interaction occurs between them in this system. The peak related to the metal-centered Ru(II)/Ru(III) oxidation process is observed at positive potentials (1.34 V vs. Ag/Ag^+). The pattern of the voltammogram in the cathodic region is more complex. Four reduction steps corresponding to reduction of the fullerene moiety were observed, but these waves were shifted toward more cathodic potentials when compared to that of pristine C_{60}. Additionally, two reduction peaks attributed to the first and second steps of Ru $(bpy)_3^{2+}$ unit were reported [172].

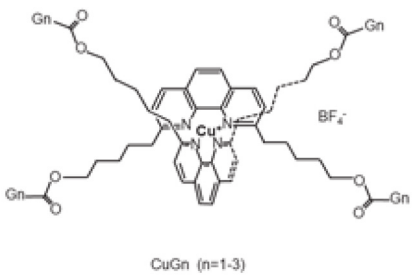

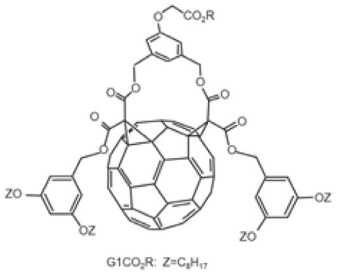

(*135*)

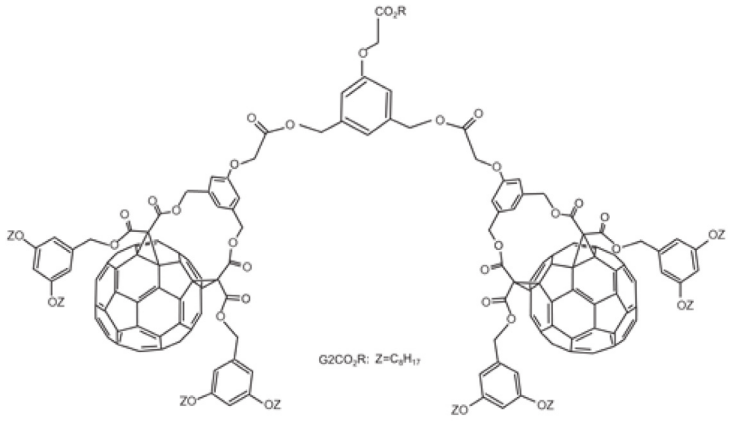

(*136*)

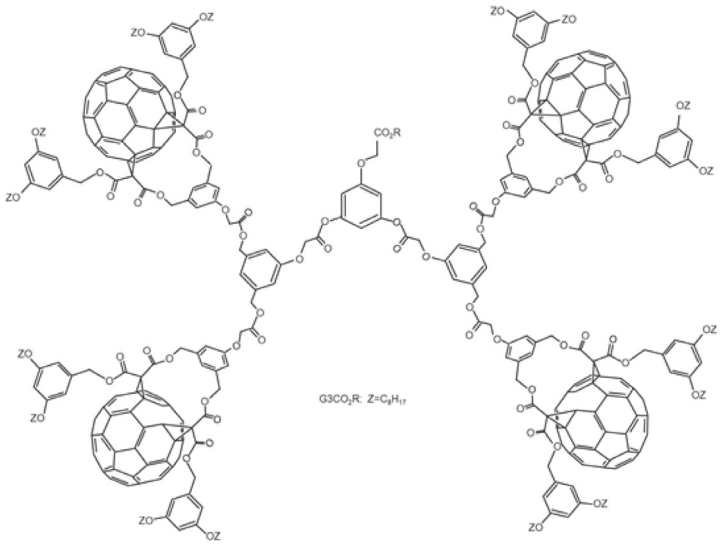

(*137*)

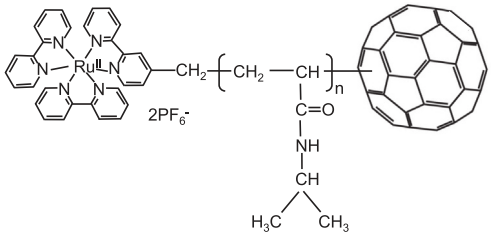

(*138*)

6.2. Fullerene with covalently attached metallocene units

Metalloocenes exhibit relatively good electron-donating properties. They can be also reversibly oxidized with only minimal structural changes when an electron is released from them. The ferrocenyl-C_{60} dyads are usual formed by covalent attachment of ferrocenyl groups to a fulleropyrolidine [144,173–178]. The saturation of a double bound in the C_{60} portion of these compounds results in the shift of the redox potential toward more negative potentials. The ferrocenyl moiety acts as electron-donor. This effect is very weak and only a small shift in ferrocene moiety is observed. A separation of fullerene cage from the ferrocene center reduces this interaction. Table 13 summarizes the electrochemical properties of selected fullerpyrrolidines with ferrocene covalently attached to the pyrrolidine ring through linkers with different length (***139***) – (***142***) [173]. The formal redox potentials are compared to these obtained for [60]fulleropyrolidine. All fullerene-centered redox processes are cathodically shifted in respect to the redox processes of the pristine fullerene. The potential shift changes from *ca.* 110 mV for the first fullerene moiety reduction process up to 380 mV for the fifth electron transfer step. Weak electronic interactions between the fullerene and the ferrocene redox centers are observed only for C_{60} derivatives in which the ferrocenyl groups are directly bonded to the pyrrolidine ring. However, even in this case this effect is very weak. The presence of an electron-attracting carbonyl group in (***140***) derivatives prevents any electronic communication between fullerene and ferrocene unit centers [173].

Table 13
Redox properties of ferrocenlpyrrolodino[C_{60}]fullerene dyads in 3:1 toluene–acetonitrile solutions 0.1 M [(*n*-Bu)$_4$N]ClO_4 at −45 °C [173].

Compound	Redox potentials in V vs. ferrocene/ferrocene$^+$					
	Reduction					Oxidation
	$C_{60}^{0/-}$	$C_{60}^{-/-2}$	$C_{60}^{-2/-3}$	$C_{60}^{-3/-4}$	$C_{60}^{-4/-5}$	Fc/Fc^+
N-metylpyrrolidino-C_{60}	−1.05	−1.44	−2.01	−2.42	−3.12	
(***139***)	−1.08	−1.47	−2.03	−2.44	−3.14	+0.05
(***140***)	−1.00	−1.38	−1.95	−2.36	−3.05	+0.16
(***141***)	−0.99	−1.40	−1.91	−2.32	−3.00	0.0
(***142***)	−1.00	−1.39	−1.97	−2.37	−3.05	0.0

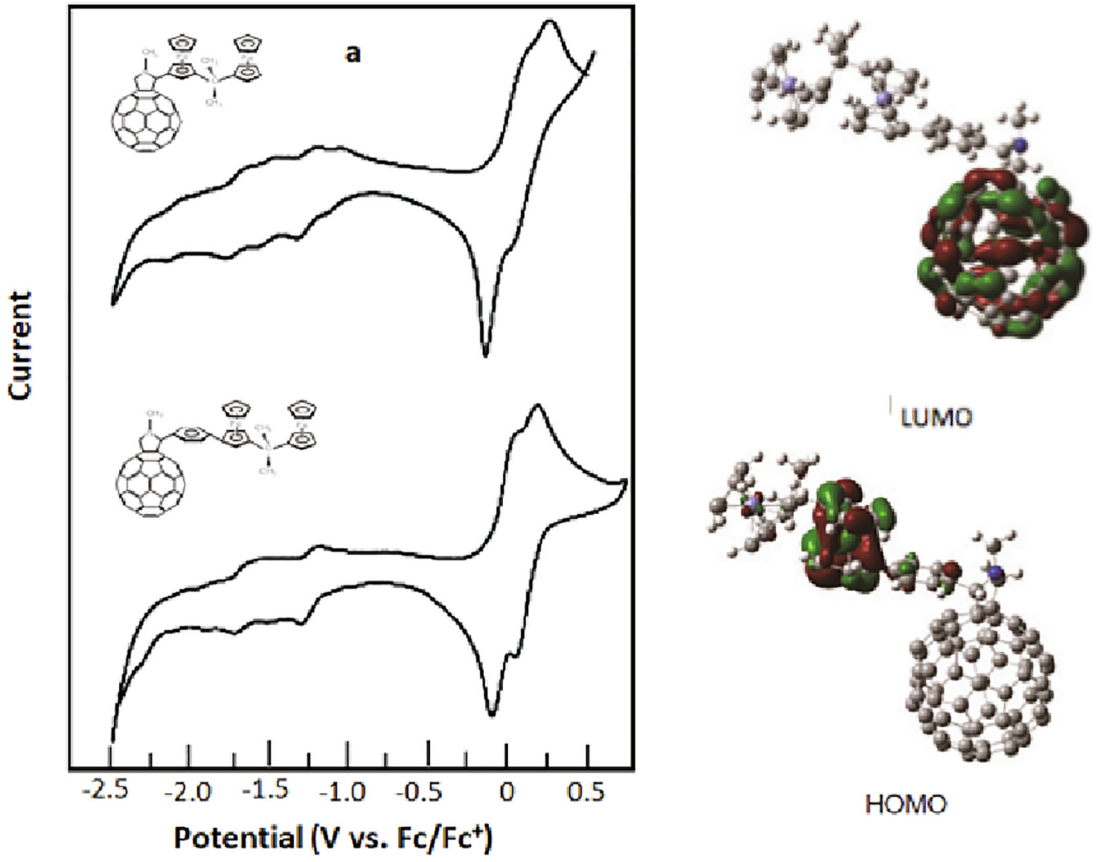

Fig. 47. (a) Cyclic voltammograms of C_{60}-diFc (***145***) and C_{60}-ph-diFc (***144***). Reproduced with permission from Ref. [177]. Copyright © 2017, Elsevier. (b) HOMO and LUMO of C_{60}-ph-diFc (***144***). Reproduced with permission from Ref. [178]. Copyright © 2017, CSIRO Publishing.

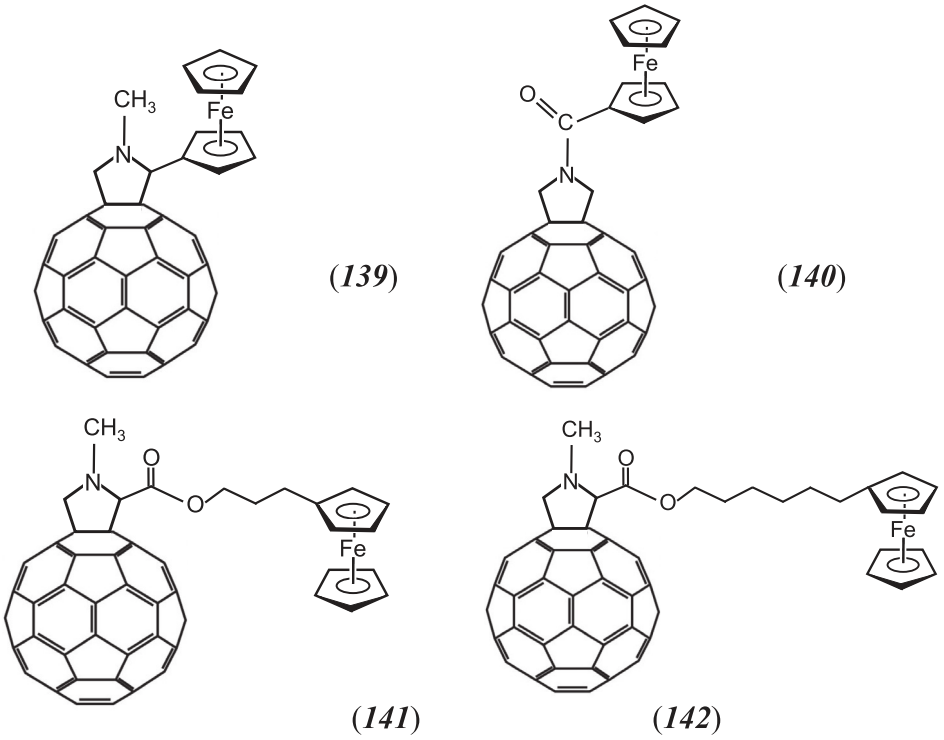

Biferrocenes formed by two ferrocene units bridged by different linkers show significant delocalization of electron density, which depends of the structure of linkers. Biferrocene derivatives exhibit neutral, mono-cationic and di-cationic redox states. The mono-cationic state can show mixed valence character [179]. These complexes can be bonded to the fullerene cages to form C_{60}-biferrocene triads (***143***) [144,174], (***144***) and ***145*** [177,178] and (***146***) [176]. During oxidation of biferrocene derivatives (***143***) and (***146)*** one two-electron step is observed. The observation that both ferrocene moieties are oxidized at the same potential indicates the absence of coupling of the two ferrocene centers through the bridging units. The electronic interaction between ferrocenyl centers were reported for *N*-methyl-2-(ferrocenyl)(phenyl)full-eropyrrolidine (***144***) and *N*-methyl-2-(diferrocenylpropane)fulleropyrrolidine (***145***) [177,178]. Cyclic voltammograms of these compounds are shown in Fig. 47. Two poorly separated oxidation steps correspond to the one-electron ferrocene-centered redox processes. In the negative potential range, reduction of fullerene moiety is observed. These experimental results are confirmed by the theoretical calculations. The HOMO is located at ferrocenyl units and C_{60} moiety mainly contribute to LUMO [178]. It was also reported that the

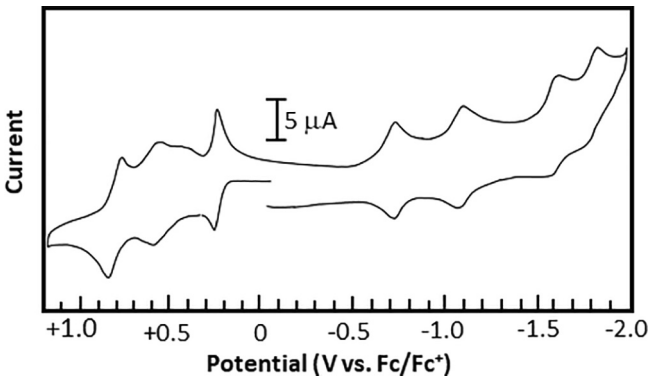

Fig. 48. Cyclic voltammogram recorded at a platinum electrode for a CH_2Cl_2 solution containing 0.2 M $[(n\text{-}Bu)_4N]PF_6$ and 0.7 mM and (***146***). Scan rate = 0.2 V s^{-1}, T = -10 °C. Reproduced with permission from Ref. [179]. Copyright © 1999, American Chemical Society.

Table 14
Redox properties of selected bi-ferrocene derivatives of [C_{60}]fullerene in 3:1 toluene-acetonitrile solutions containing 0.1 M $[(n\text{-}Bu)_4N]PF_6$.

Compound	Redox potentials in V vs. ferrocene/ferrocene$^+$					
	Reduction			Oxidation		Ref.
	$C_{60}^{0/-}$	$C_{60}^{-/-2}$	$C_{60}^{-2/-3}$	Fc/Fc$^+$		
(***143***)[a]	−1.086	−1.516	−1.672	+0.103[b]		[144]
(***144***)	−1.245	−1.671	−1.872	−0.042	+0.114	[177]
(***145***)	−1.250	−1.692	−2.088	−0.030	+0.150	[178]

[a] 4:1 toluene–acetonitrile solutions containing 0.1 M $(n\text{-}Bu)_4NClO_4$.
[b] two-electron oxidation of two ferrocene redox centers

energy of the HOMO is slightly lower and the energy of the LUMO is higher for triad (***144***) in comparison to the compound that contains a bi-ferrocene moiety bonded directly to the pyrrolidine ring (***145***) [177]. The oxidation peaks of the ferrocenyl group are shifted toward less positive potentials with respect to the ferrocene/ferrocene$^+$ redox couple. However, this potential shift is lower than that observed for 2,2-biferrocenylpropane indicating that grafting of C_{60} onto the bi-ferrocene leads to a reduction in the electron density on the ferrocene units and, consequently, in weaker electronic communication between the two ferrocene units. On the other hand, the fullerene-centered reduction processes, which are observed at negative potentials, are shifted toward more negative potentials with respect to the redox potentials of pristine C_{60}. The electrochemical properties of bi-ferrocene derivatives of C_{60} are summarized in Table 14. The interaction between the bi-ferrocene moiety and the fullerene cage is slightly weaker in compound (***144***) due to the partial delocalization of electron density over the phenyl ring.

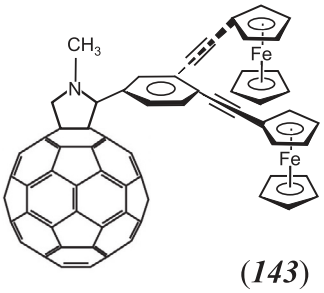

(***143***)

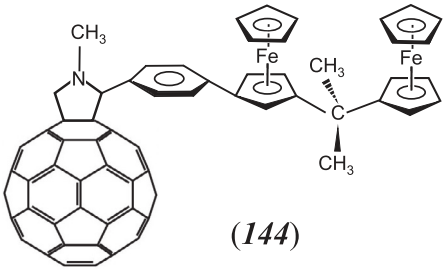

(***144***)

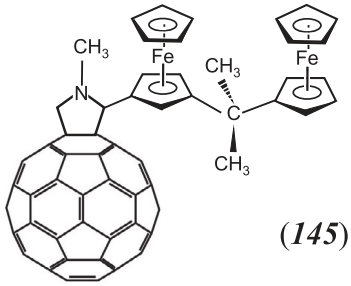

(***145***)

A complex electrochemical behavior was reported for dyad composed of tetraferrocenyl[5]cumulene unit and C_{60} fullerene (***146***) [179]. The voltammetric behavior of this compound is shown in Fig. 48. There are three electroactive moieties within this compound. The cumulene chain is oxidized at ca. 0.82 V vs. SCE and reduced at ca. −1.56 V vs. SCE. In both processes, two electrons are exchanged. The three fullerene reduction steps are shifted toward more negative potentials with respect to the redox potentials for pristine C_{60}. The voltammetric currents recorded in potential range from 0.1 to 0.7 V vs. SCE are probably related electron exchange processes of the bi-ferrocene moiety. According to the authors of these studies, only the two-electron oxidation peak at ca. 0.25 V is responsible for oxidation of one ferrocenyl unit of each bi-ferrocene moiety [179]. However, two other oxidation steps, which are observed at more positive potentials, can be related to the stepwise one-electron oxidation of the remaining ferrocenyl units.

Separation of the ferrocene units by longer carbon chains limits their electronic communication. Therefore, the voltammogram recorded for the bi-ferrocene derivative of C_{60} (***146***) exhibits only one, two-electron oxidation step for both ferrocene redox centers [176]. In the case of bi-ferrocene derivative of fulleropyrolidine (***143***), two ferrocene units are also oxidized independently in one, two-electron oxidation step [144].

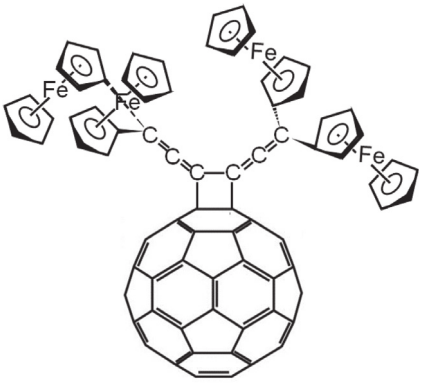

(***146***)

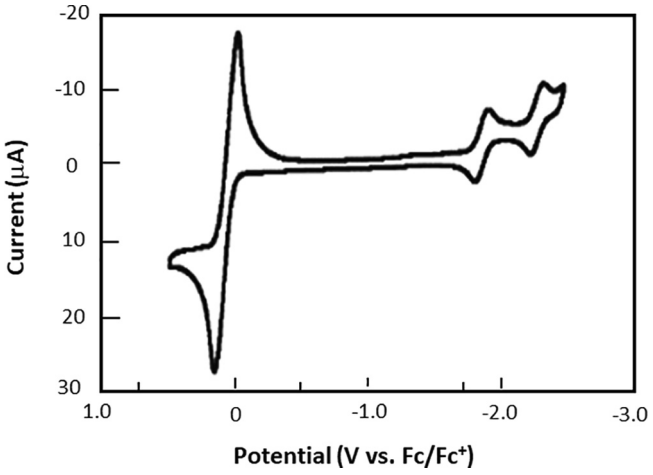

Fig. 49. Electrochemical properties of (***147***) in THF solution containing 0.1 M [(n-Bu)$_4$N]ClO$_4$ as supporting electrolyte. Reproduced with permission from Ref. [180]. Copyright © 2010, American Chemical Society.

An interesting ferrocene derivative of C_{60} (***147***) was synthesized by Matsuo and co-workers [180]. The ten aryl groups bonded to the opposite sites of the fullerene moiety create a large, rigid, hand-drum-shaped dendritic structure. This conjugated system consists of five ferrocenyl groups covalently attached to the top of the C_{60} to act as an electron donor along with a hoop-shaped benzoic acceptor. The voltammogram of this compound exhibited a reversible five-electron oxidation peak (Fig. 49) indicating the absence of interaction between the ferrocenyl groups through the space. The potential of this peak is slightly shifted by ca. 80 mV toward positive potentials against the ferrocene/ferrocenium redox couple. At negative potentials, two, one-electron reduction peaks of the 40 π-electron cyclophenancene system is observed at less negative potentials in comparison to the reduction potentials of reference dendrimer which does not contain electron-withdrawing ferrocene moieties [180].

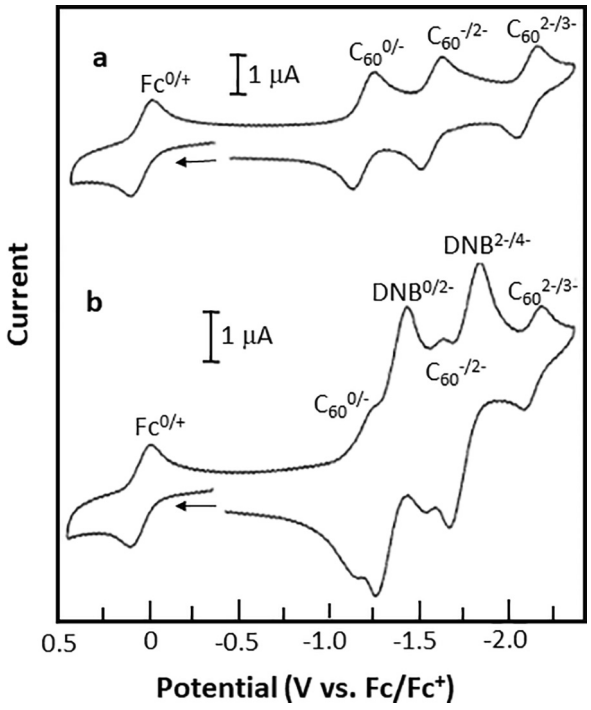

Fig. 50. Cyclic voltammograms of (a) 2-(ferrocenyl)fulleropyrrolidine and (b) N-(3′,5′-dinitrobenzoyl)-2-(ferrocenyl)fulleropyrrolidine (***152***) at Pt disc electrode in *o*-dichlorobenzene containing 0.1 M $[(n\text{-}Bu)_4N]ClO_4$,. Scan rate = 100 mV^{-1}. Reproduced with permission from Ref. [175]. Copyright © 2002, American Chemical Society.

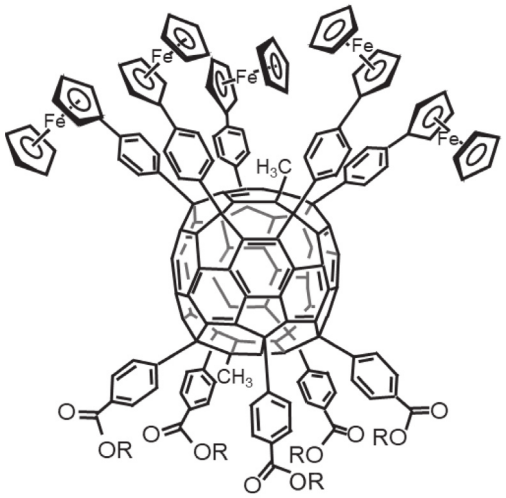

(***147***)

Heteronuclear transition metal fullerene complexes, *mer*-$M(CO)_3(dppf)(\eta^2\text{-}C_{60})$ where dppf = 1,1′-bis(diphenylphosphino)ferrocene and M = Mo (***148***) and W (***149***) were synthesized and their electrochemical properties investigated [181]. The $\eta^2\text{-}C_{70}$ analog was also investigated [181]. Three fullerene-centered reduction steps at potentials of ca. 200 mV more negative with respect of corresponding processes of C_{60} were reported for these compounds. The reduction potentials of ferrocene-containing bimetallic complexes were comparable to the reduction potentials of reference complexes that do not contain ferrocene moiety. Similar to these complexes, the bimetallic compounds also decompose during reduction. The rate of this following chemical reaction is much higher for $W(CO)_3(dppf)(\eta^2\text{-}C_{60})$ (***149***) than for molybdenum analog. The two-electron oxidation process that involves the metal center coordinated, which is observed at positive potentials, is also

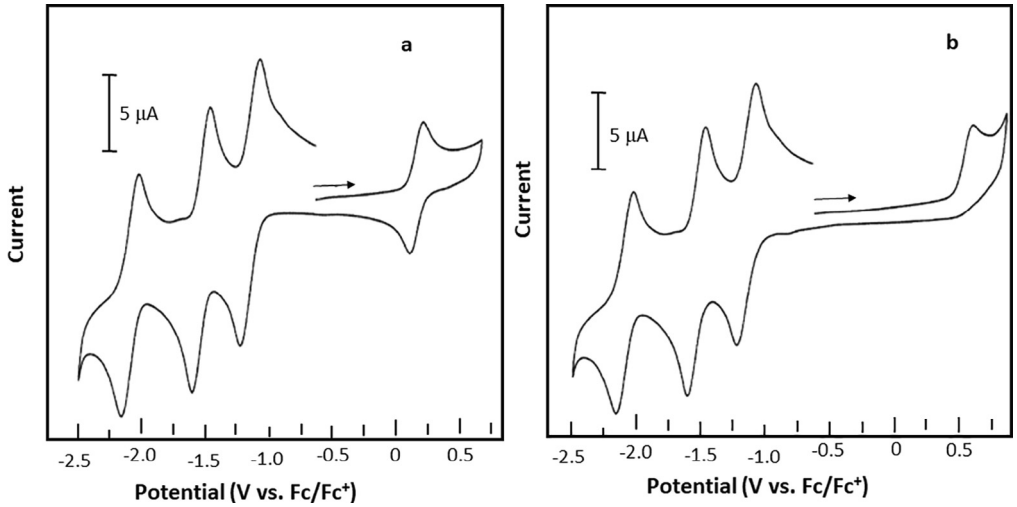

Fig. 51. Cyclic voltammogram of 0.2 mM solution of (a) Et-(***153***) and (b) Et-(***154***) in *o*-dichlorobenzene containing 0.2 M $[(n\text{-}Bu)_4N]BF_4$ at 293 K. Reproduced with permission from Ref. [184]. Copyright © 2013, Royal Society of Chemistry.

followed by cleavage of the metal-ferrocene bond. Similar electrochemical behavior was reported for the Pd/Fe bimetallic η^2-C_{60} complex, Pd(dppf)(η^2-C_{60}) (***150***) [182].

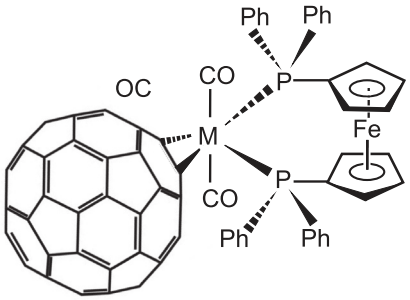

M = Mo (***148***)

M = W (***149***)

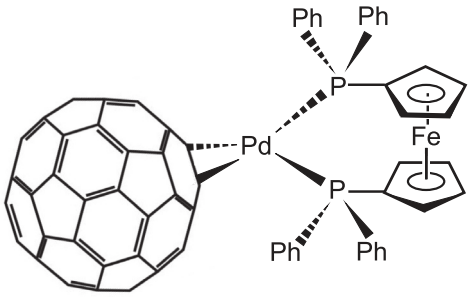

(***150***)

The electrochemical properties of C_{60}-coper(I) phenanthroline/-ferrocene hybrid (***151***) were also studied [183]. The electronic properties of the fullerene moiety are not affected by the presence of copper(I) phenanthroline/ferrocene redox centers. A small electronic interaction between copper(I) phenanthroline center and the fullerene moiety results in a shift of the oxidation potential of the ferrocene portion toward more positive values by *ca.* 110 mV. This compound may adopt folded conformation in which fullerene and ferrocene moieties approach each other more closely [183].

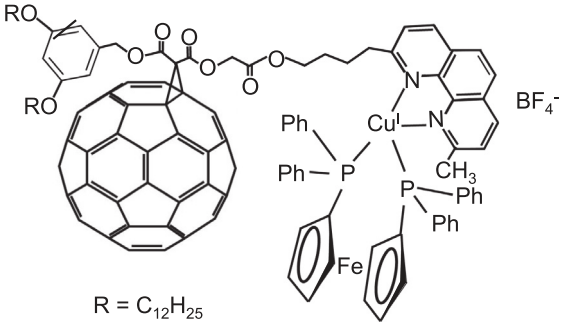

(***151***)

A triad (***152***) with a ferrocenyl group and an dinitrobenzene redox center attached covalently to the pyrrolidine ring of [60]fulleropyrolidine exhibits multiple redox processes involving the three redox active entities [175]. The HOMO responsible for the oxidation process is localized on the ferrocene unit. The electrode processes observed in the negative potential range correspond to the one-electron reduction of the fullerene portion and two dinitrobenzene-involved two-electron reduction processes as seen in Fig. 50. The sequence of these processes corresponds to the energy diagram of LUMOs [175]. However, there is not any significant electronic interaction between the different redox entities.

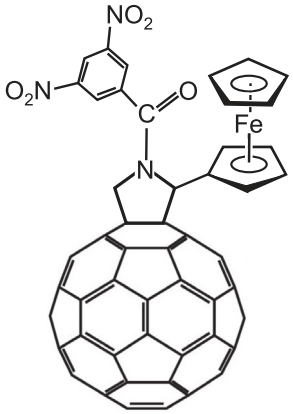

(***152***)

Ferrocene and ruthencene units were used to bridge fulleropyrolidine moieties to form the dimeric compounds (***153***) and (***154***) [184]. Reversible one-electron oxidation occurred for the ferrocene compound while irreversible one-electron oxidation was observed for the ruthenocene compound as seen in Fig. 51. At negative potentials, only one peak (corresponding to the exchange of two electrons) for each step of reduction of the fullerene moiety was recorded. Therefore, both C_{60} units in triads (***153***) and (***154***) are reduced simultaneously indicating no electronic communication between the carbon cages through the metallocene bridging center or through space [184].

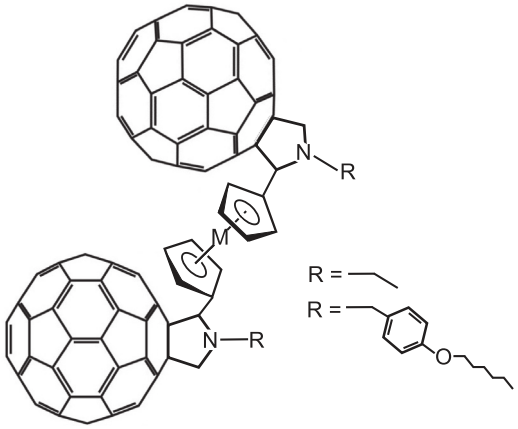

M = Fe (*153*)

M = Ru (*154*)

A weak communication between fullerene cages was observed for the dimer composed of the tetrairon cluster, $(C_5H_5)_2Fe_4(CO)_4(C_5H_4CHO)_2$, which bridged two fullerene units (***155***) [185]. In Fig. 52, the electrochemical properties of this compound are compared to the electrochemical behavior of monofullerene-tetrairon cluster adduct (***156***) and $(C_5H_5)_2Fe_4(CO)_4(C_5H_4CHO)$ as a reference compound. In the case of compound (***156***), the first and second fullerene-involved reduction steps are shifted toward less cathodic potentials with respect to that reported for pristine C_{60}. This compound is a rare example of a ferrocene derivative of C_{60} that exhibits an anodic shift of the reduction potential of the fullerene cage. The third reduction step, which corresponds to reduction of the Fe_4 cluster, as well as following fullerene cage reduction process proceed more difficultly than these observed for $(C_5H_5)_2Fe_4(CO)_4(C_5H_4CHO)$ and C_{60}, respectively. This behavior is due to the negative charge

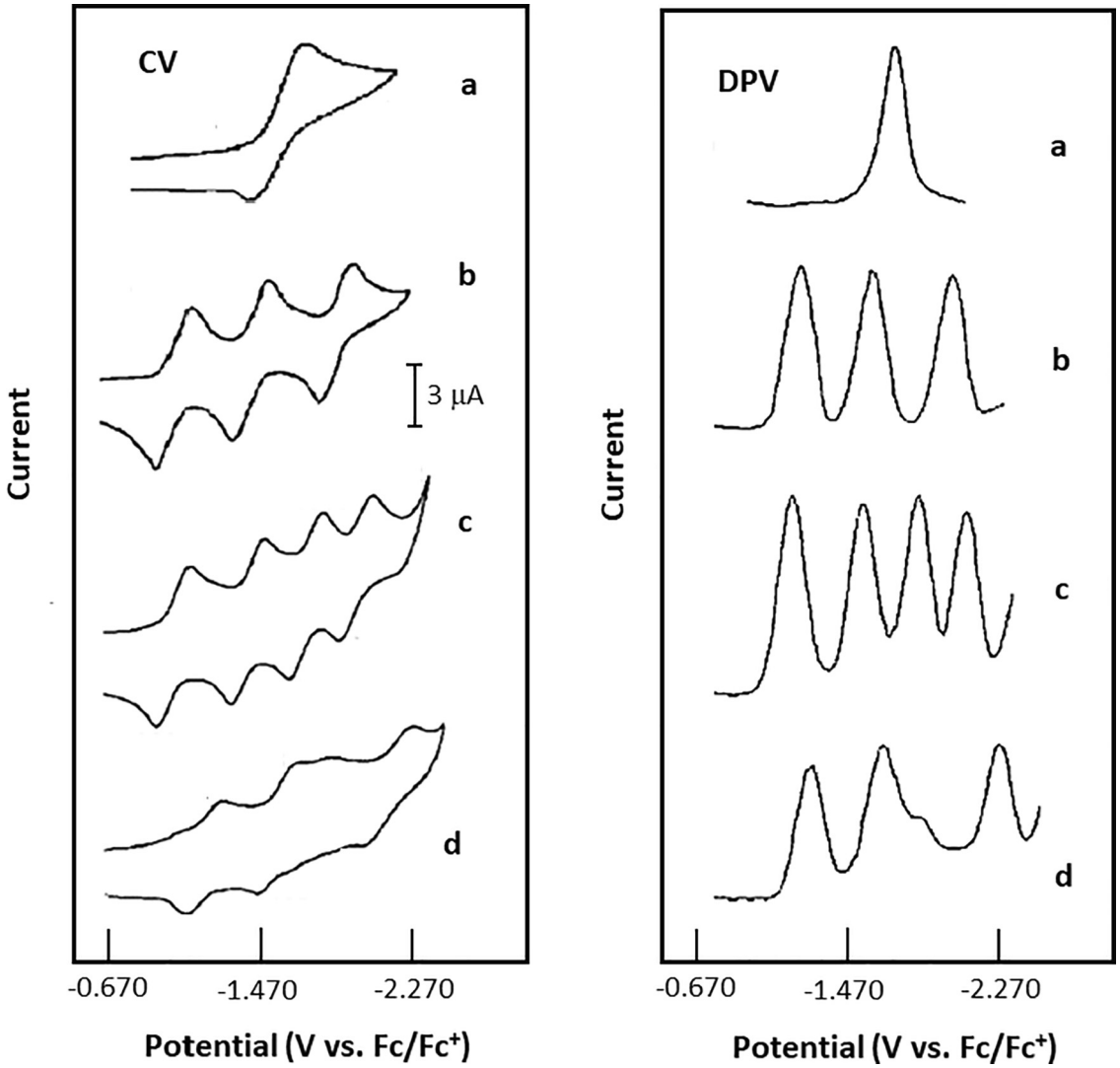

Fig. 52. Cyclic voltammograms and differential pulse voltammograms in *o*-dichlorobenzene–benzonitrile (5:1, v/v) containing 1 mM $Cp_3Fe_4(CO)_4(C_5H_4CHO$ (a), C_{60} (b), (***155***) (c) and (***156***) (d), and 0.2 M $[(n\text{-}Bu)_4N]PF_6$ as supporting electrolyte. Reproduced with permission from Ref. [185]. Copyright © 2013, Royal Society of Chemistry.

accumulated on the neighboring moieties. In the case of triad (***155***), the first two fullerene-centered reduction steps are spit into two voltammetric signals indicating electronic communication occurs between the fullerene moieties. Due to the large negative charge of the reduced fullerene units, a large shift of ca. 0.55 V is observed for the process of Fe_4 cluster reduction.

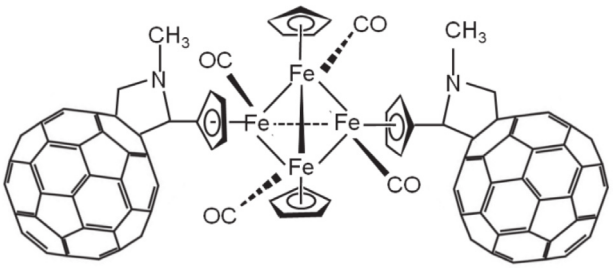

(***155***)

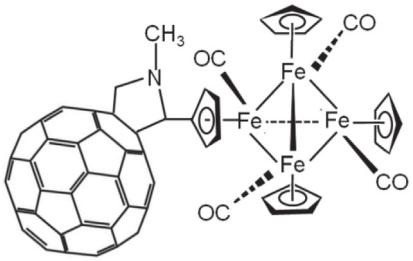

(***156***)

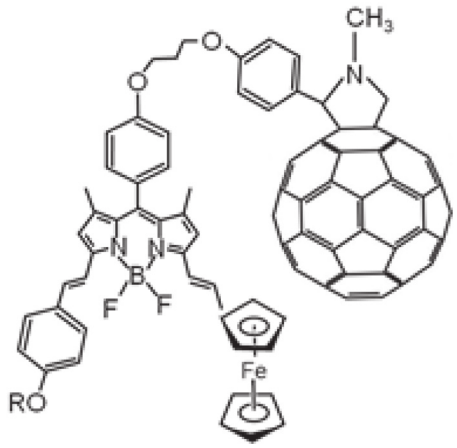

(***157***)

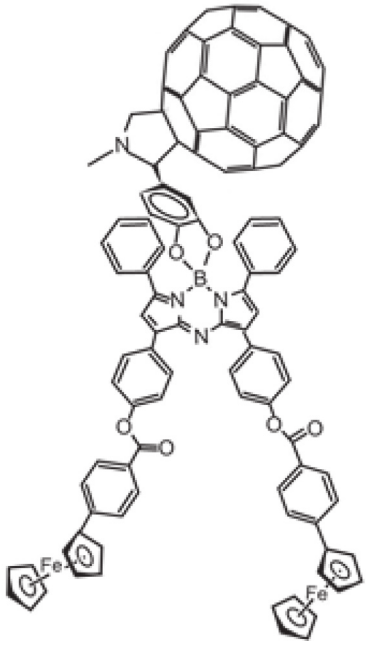

(***158***)

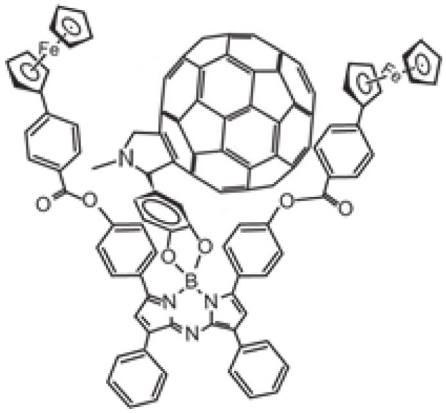

(***159***)

Electrochemical studies were performed to establish the energy levels in ferrocene-DSBDP-C_{60} (DSBDP = distyryl boron-dipyrromethene) triads (***157***) [186] and bisferrocene-ADP-C_{60} (ADP = BF_2-chelated-azadipyrromethane) tetrads (***158***) and (***159***) [187]. The formal potentials of the redox processes observed for these donor–acceptor systems are collected in Table 15. These results indicate the electron-donating properties of the ferrocene units and the electron-accepting nature of C_{60}, DSBDP and ADP moieties. Generally, there is not strong electronic communication between redox centers of these compounds. A weak influence of fullerene electron density on the electrochemical properties of the ferrocenyl groups in tetrad (***159***) was observed. The potential for reduction of the ferrocene moieties in this compound is ca. 50 mV less anodic in comparison to the reduction potential of ferrocenyl groups in tetrad (***158***).

6.3. Fullerene – Porphyrin and fullerene-phthalocyanine system

Fullerene–metalloporphyrin mixed systems have recently become an active area of research due to their ability for the photocurrent generation [18–20,188–190]. There are a large variety of fullerene-porphyrin systems including large dendrimer architectures. In these systems, the porphyrin core acts as a light-harvesting antenna and electron donor, while the fullerene plays the part of an electron acceptor to form a charge-separated state. Supramolecular systems composed of fullerenes covalently bonded to metalloporphyrins have been also investigated to mimic photosynthetic systems [191–194]. For all these applications, knowledge about electrochemical properties of the fullerene–metallopor phyrin dyad is essential.

6.3.1. Fullerene–metalloporphyrin complexes with an axial ligation of the metal center

Pyridine exhibits coordination properties toward a wide variety of metal porphyrins via axial ligation [195,196]. The electrochemical properties of two basic pyridine derivatives of [60]fullerene, in which pyridine is covalently bonded to the fulleropyrolidine moiety through the nitrogen atom of the pyrrolidine ring (***160***) and via insulating sp^3 carbon atom of this ring (***161***) are summarized in Table 16 [197]. The values of the formal potentials of first three one-electron reduction steps of the fullerene moiety are compared to the electrochemical properties of reference compounds, *N*-methylfulleropyrolidine and pristine C_{60}. As can be expected, the electron-withdrawing properties of pyridine result in a small shift of the reduction potentials for both compounds toward less negative values in comparison to the redox potential of the reference compound, *N*-methylfulleropyrolidine. The axial ligation of the zinc tetraphenylporphyrin to the fullerene center results in formation of dyads (***162***) and (***163***), which exhibit additional electrochemical activity both in positive and negative potential ranges (Table 16). The location of the complexing pyridine center with respect to the fullerene cage affects the electrochemical behavior of zinc porphyrin moiety. The potential of the first one-electron oxidation of zinc tetraphenylporphyrin shifts cathodically by 120 and 80 mV after complexation with (***160***) and (***161***), respectively [197]. Additionally, a positive shift by 40 mV for the first C_{60} cage reduction potential was observed for dyad (***162***). These results indicate weak electronic communication between the metal center of the porphyrin and the fullerene cage in compound (***162***).

A variety of metalloporphyrin-fullerene donor–acceptor dyads was investigated by D'Souza and co-workers [198–200]. The effects of the linker nature and the metalloporphyrin structure on the photochemical and electrochemical properties of dyads were particularly extensively examined. The structures of some of the metalloporphyrin complexes and fullerene C_{60} derivatives used for dyad formation *via* axial coordination are shown below. In all these cases, the HOMO is located on the metalloporphyrin and the nitrogen containing center of the fullerene derivative coordinated to the metal ion, while the fullerene cage is involved in the LUMO as shown in Fig. 53a. Consequently, the first dyad reduction process is always related to reduction of the fullerene cage, while the porphyrin portion is involved in the oxidation process. In Fig. 53b, the voltammetric behavior of a series of zinc tetraphenylporphyrins (***164***)- (***168***) coordinated to the imidazole-appended fulleropyrolidine (***169***) is shown [199]. For comparison, the electrochemical properties of uncoordinated zinc tetraphenylporphyrin and the fulleropyrolidine derivative (***161***) are presented. The increase of the number of electronegative halogen atoms on the *meso*-aryl substituents makes oxidation of the porphyrin moiety more difficult, while the reduction process becomes easier. There are

Table 15
Redox potentials of bisferrocene-ADP-C_{60} complexes in benzonitrile containing 0.1 M $[(n\text{-Bu})_4N]ClO_4$.

Compound			Redox potential in V vs. Ag/AgCl			
	ADP^+/ADP	Fc^+/Fc	$DSBDP/DSPDP^-$	C_{60}/C_{60}^-	C_{60}/C_{60}^-	Ref.
			ADP/ADP^-		ADP^-/ADP^{2-}	
(***157***)		0.50	−1.00	−0.58		[186]
(***158***)	1.14	0.49	−0.37	−0.63	−1.02	[187]
(***159***)	1.12	0.44	−0.36	−0.64	−1.04	[187]

Table 16
Redox properties of pyridine derivatives of [60]fullerene and their complexes with zinc tetraphenylporphyrin (ZnTPP) in CH_2Cl_2 solution containing 0.1 M $[(n\text{-Bu})_4N]PF_6$ [197].

Compound	Redox potentials in V vs. Fc/Fc^+							
	Reduction					Oxidation		
	$C_{60}^{0/-}$	$C_{60}^{-/-2}$	$C_{60}^{2-/-3}$	$ZnTPP^{0/-2}$	$ZnTPP^{-2/-4}$	$ZnTPP^{0/+}$	$ZnTPP^{+/3+}$	$ZnTPP^{3+/5+}$
(***160***)	−1.06	−1.44	−1.96					
(***161***)	−1.07	−1.45	−1.98					
ZnTPP				−1.78	−2.16	+0.02	+0.37	+0.68
(***162***)	−1.03	−1.39	−1.95	−1.84		+0.03	+0.27	+0.69
(***163***)	−1.07	−1.44	−1.98	−1.81	−2.18	+0.04	+0.30	+0.71

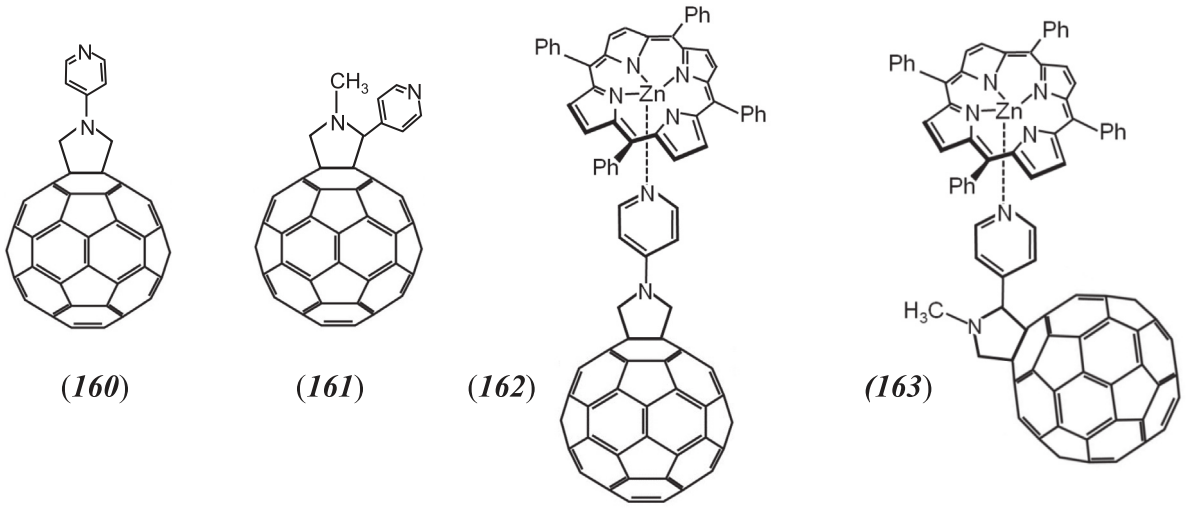

substantial differences in the electrochemical properties of zinc tetraphenylporphyrins in negative potential rang due to the axial coordination. A significant cathodic shift of the reduction potential of the metalloporphyrin portion is observed. A weak effect, a shift of up to 50 mV toward more anodic potentials, of axial coordination on the redox potential of the imidazole-centered oxidation process was also recorded. A larger anodic shift of the porphyrin oxidation potential of 100 mV was reported for the dyad composed of magnesium tetraphenylporphyrin and fulleropyrolidine appended with an imidazole coordinating ligand [201]. The first reduction of the fullerene does not reveal any significant changes. In general, the absence of any significant electronic interaction between fullerene and the metalloporphyrin moiety in the ground state was reported for other studied dyads [199,200].

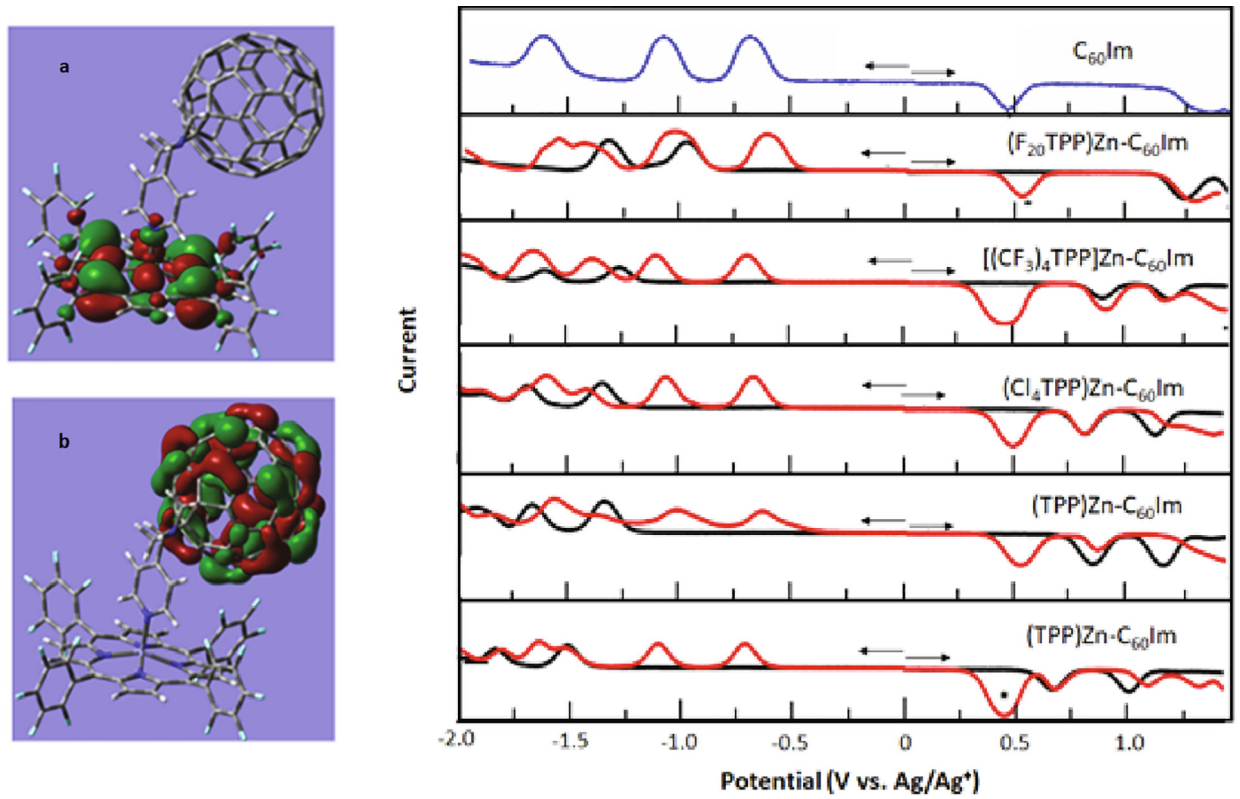

Fig. 53. The frontier HOMO (a) and LUMO (b) of (F20TPP)Zn ← C_{60}Py. Differential pulse voltammograms corresponding to both oxidation and reduction processes of pristine (P)Zn (black line) and (P)Zn ← ImC_{60} dyads (red line) in dichloromethane containing 0.1 M [(*n*-Bu)$_4$N]ClO_4, (P)Zn = (F_{20}TPP)Zn, ($(CF_3)_4$TPP)Zn, (F_4TPP)Zn, (Cl_4TPP)Zn, or (TPP)Zn). DPV of C_{60}Im is shown on the top (blue line) for comparison. Scan rate, 5 mV/s; pulse width, 0.25 s; pulse height, 0.025 V. Potential versus Ag/Ag^+. The * represents oxidation of ferrocene, which was used as an internal standard. Reproduced with permission from Ref. [199]. Copyright © 2014, American Chemical Society.

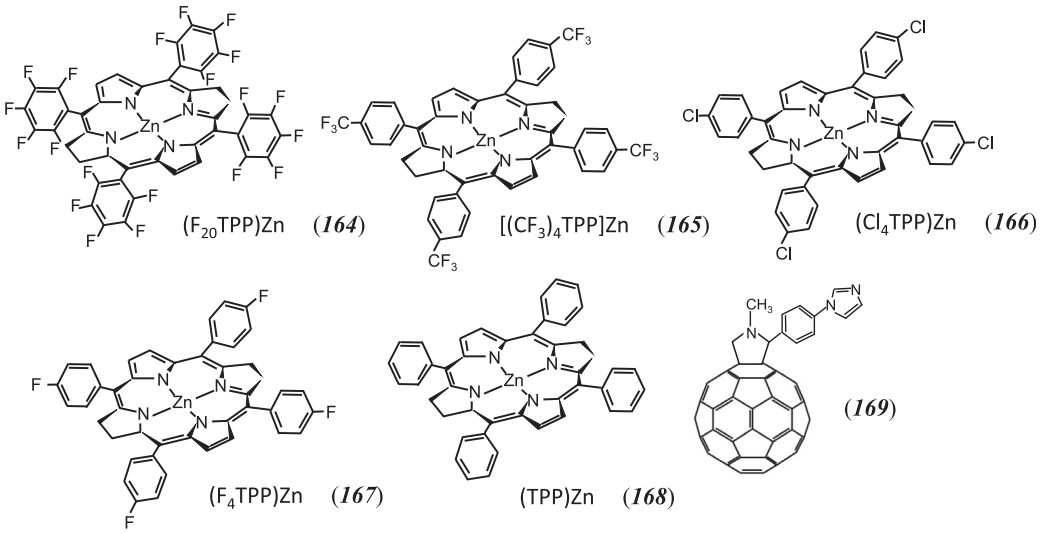

In order to increase the electron-donor ability of the porphyrin moiety and to increase the charge-separated state lifetime, a triad composed of fulleropyrrolidine appended with an imidazole coordinated axially to zinc center of a subphthalocyanine-triphenylamine-zinc porphyrin was synthesized (***170***) [202]. In Fig. 54, voltammograms obtained for the triad (***170***) and free subphthalocyanine-triphenylamine-zinc porphyrin ((***171***) are compared. As is expected, the first oxidation process of the penta-coordinated zinc porphyrin occurs at potentials less positive by 88 mV in comparison to unsubstituted {[5,11,16,21]-tetrakis(pentyl)-21H,23H-porphyrinato}zinc.

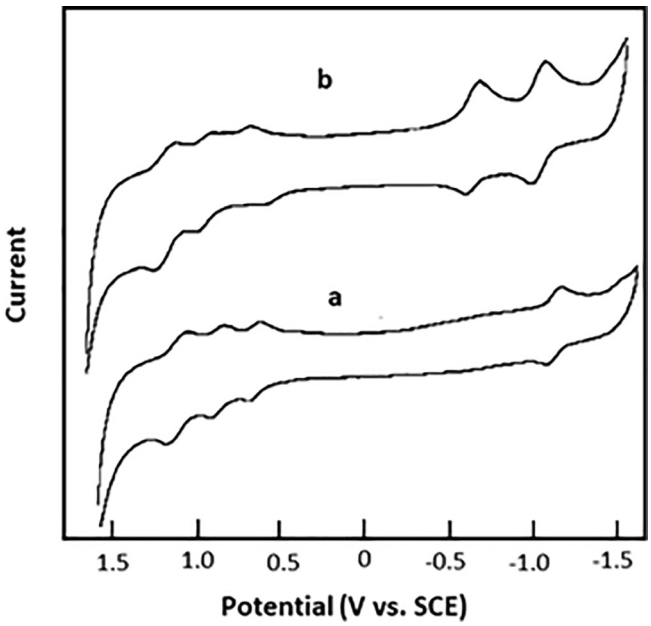

Fig. 54. Cyclic voltammograms of (***170***) and self-assembled (***171***) in CH_2Cl_2 containing 0.1 M $[(n\text{-}Bu)_4N]ClO_4$ a scan rate of 100 mVs^{-1}. Reproduced with permission from Ref. [201]. Copyright © 2010, Wiley-VCH Verlag.

6.3.2. Fullerene–metalloporphyrin complexes with a fullerene moiety covalently linked to the porphyrin ring

Covalent binding of a metalloporphyrin moiety to the fullerene cage allows the production of variety of porphyrin-fullerene dyads, triads, tetrads, *etc*. with different distances and orientations of the electron-donor and electron-acceptor centers along with a variety of different linkers. Examples of relatively simple porphyrin-fullerene dyads are shown below as compounds (***172***) - (***178***) [203–208]. The electrochemical investigation of these dyads was mainly focused on the search for possible intramolecular electronic

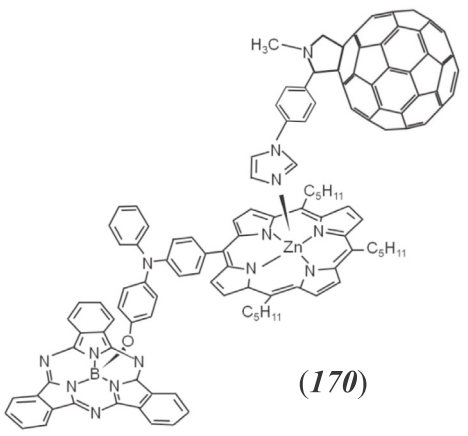

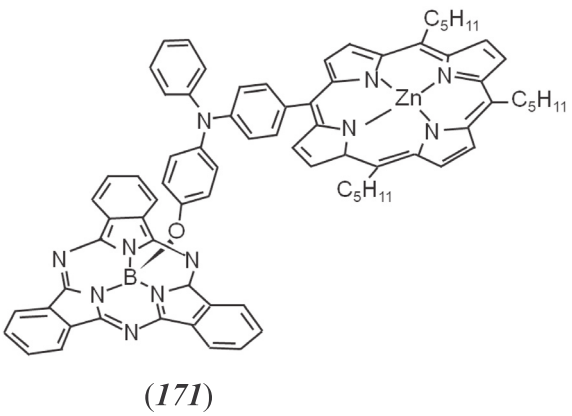

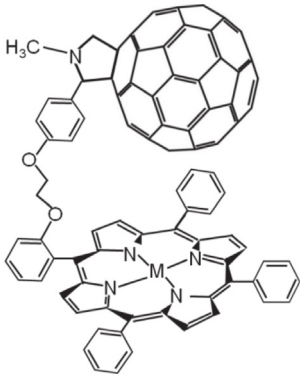

M = Mg (*172*)

M = Zn (*173*)

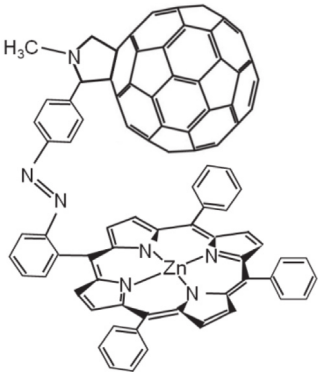

(*174*)

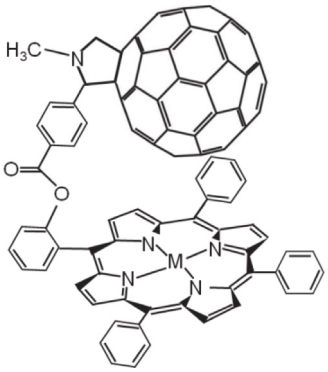

M = Pd (*175*)

M = Pt (*176*)

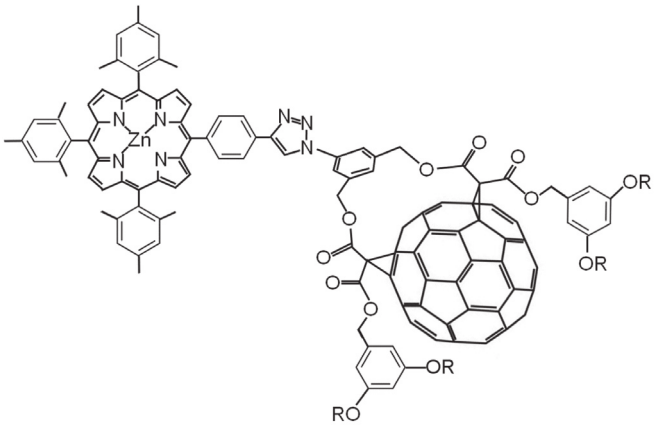

(*177*)

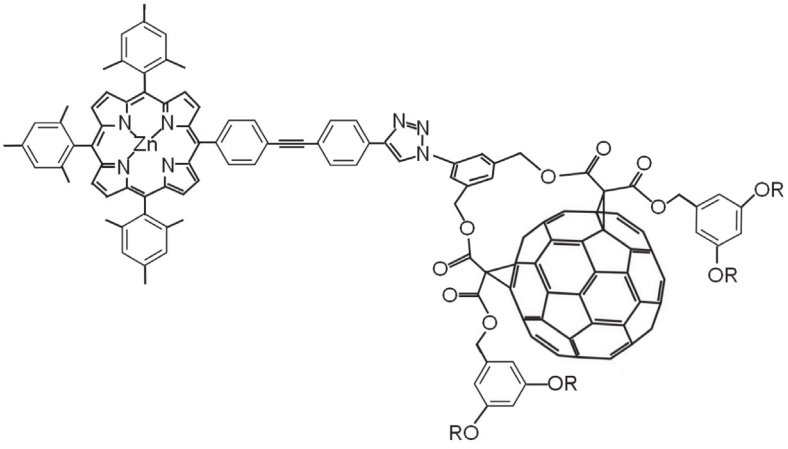

(*178*)

interaction between fullerene cage and the porphyrin moiety and on the determination of the band gap in the ground state. The electrochemical behavior of these dyads is a combination of the electrochemical properties of both components. In the negative potential range, reduction of fullerene moieties is observed. The LUMO is located on the fullerene center (Fig. 55a) and the first reduction steps correspond to the reduction fullerene moiety. The porphyrin-involved charge transfer processes occurs at more negative potentials. The HOMO is located on the porphyrin moiety. Therefore, the porphyrin center is involved in the dyad oxidation processes at positive potentials. In Fig. 55b, the voltammograms of porphyrin-fullerene dyads (***172***) an (***173***) are shown. For both dyads, the first porphyrin oxidation differs from the corresponding oxidation potentials of the pristine metal porphyrins by ca. 30 mV, indicating a weak intramolecular interaction between porphyrin and fullerene redox centers. This interaction and, consequently, the electrochemical properties of the metalloporphyrin derivatives of fullerenes can be changed by axial coordination of ligands (for example pyridine) to the metal center. Such modification results in increase of the distance between metalloporphyrin and fullerene moieties [203]. Similar electrochemical behavior was reported for other fullerene dyads, such as (***177***) and (***178***) [208].

Oligoporphyrins arrays, in which individual porphyrin units are linked together to form extended planar structures, can be covalently bonded to the fullerenes to form the multicomponent arrays (***179***)- (***182***) [209,210]. The fullerene moieties interact relatively strongly (ca. 12 kJ mol^{-1}) with the porphyrin rings leading to the distinct conformation of the multicomponent arrays. Oligoporphyrin arrays exhibit electronic communication due to π-electron conjugation. The voltammetric behavior of dimer (***182***) is shown in Fig. 56 [209]. Both porphyrin units are oxidized separately in one-electron steps. Additionally, peaks related to the fullerene units are recorded in the negative potential range. Formal potentials of all porphyrin-involved redox processes are shifted to more positive potentials with respect to the redox potentials of a corresponding diporphyrin that is not bonded to the fullerene center due to the interaction between the redox centers. Similar effects were observed for other fullerene-polyporphyrin dyads [210]. In Table 17, the redox potentials of fullerene-polyporphyrin dyads are compared to those obtained for reference compounds. The differences in redox potentials for both fullerene-centered reduction processes and porphyrin-involved reduction and oxidation processes indicate electronic interaction between redox centers. These polyporphyrin-fullerene conjugates exhibit high electron capacity. Thus, twelve electrons can be transferred during electrode

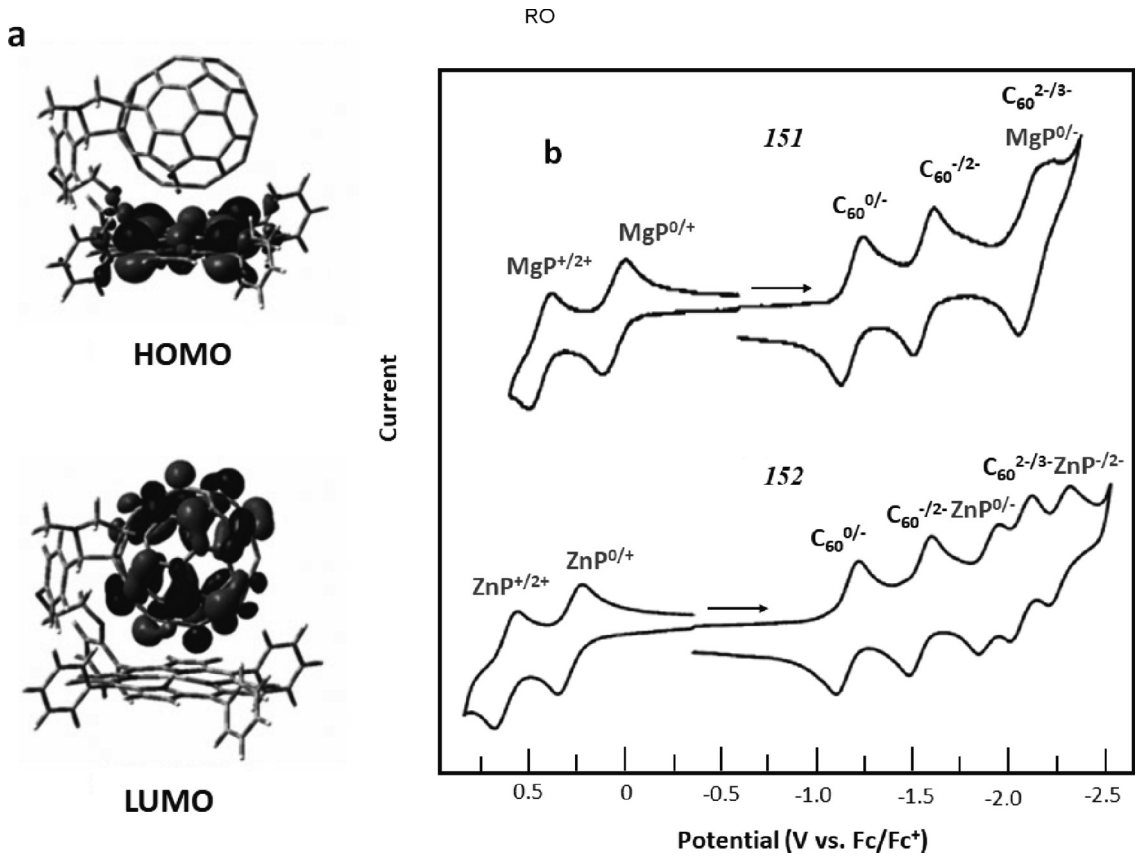

Fig. 55. (a) HOMO and LUMO of dyad (***173***). (b) Cyclic voltammograms of (***173***) and (***174***) (*ca.* 0.05 mM) in *o*-dichlorobenzene containing 0.1 M $[(n\text{-}Bu)_4N]ClO_4$. Scan rate = 100 mV s^{-1}. The site of electron transfer corresponding to each redox couple is indicated on the top of the voltammograms. Reproduced with permission from Ref. [203]. Copyright © 2005, Royal Society of Chemistry.

processes for compound (***180***) within the potential window of the solvent. Dyad (***182***) can exchange up to eighteen electrons during oxidation and reduction [210].

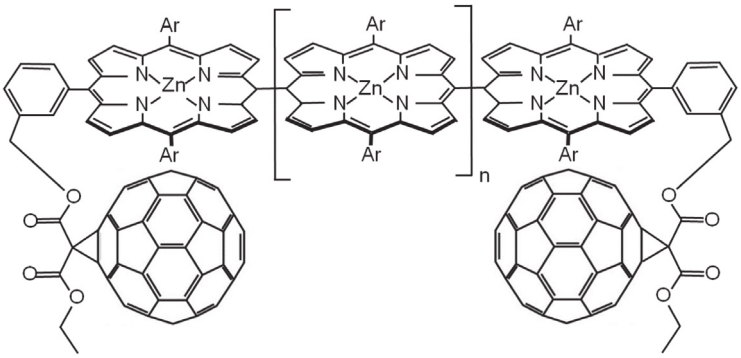

n = 0 (***179***)
n = 1 (***180***)
n = 2 (***181***)

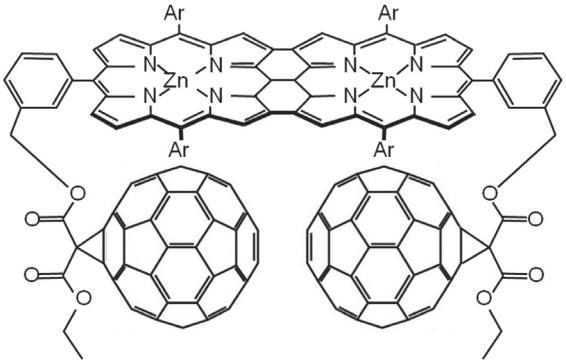

(***182***)

(***183***)

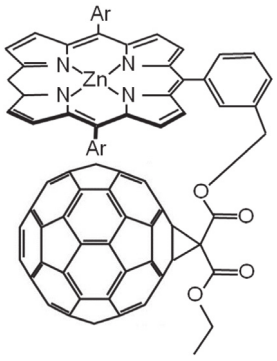

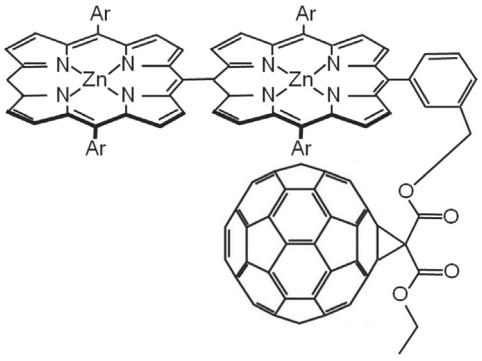

(***184***)

Metal clusters coordinated to the fullerene moiety were also used as a platform to covalently bond metalloporphyrin rings (***185***) – (***188***) [211–213]. The voltammetric behavior of the triad composed of the face-capped $Os_3(CO)_7[CN(CH_2)_3Si(OEt)_3](\mu^3\text{-}\eta^2\text{:}\eta^2\text{:}\eta^2\text{-}C_{60})$, zinc tetraphenylporphyrin and boron dipyrrin moiety (***185***) is shown in Fig. 57 [213]. Similar results were reported for the triad containing ferrocene redox center instead of the boron dipyrrin moiety (***187***) and (***188***) [211]. In Fig. 57, the voltammetric properties of the triad components are shown for comparison. The general cyclic voltammetry feature of the triad (***185***) is a sum of the voltammetric responses of the individual components. The HOMO responsible for the first oxidation step is located on the zinc porphyrin. As can be expected, the LUMO is located on the fullerene cage. Comparison of the voltammetric response of the triad and reference compounds allows assignment of the voltammetric peaks of the triad to individual electrochemical processes as seen in Fig. 57. The values of the redox potentials obtained on the bases of voltammetric measurements for triads (***185***) and (***187***) are summarized in Table 18. In general, the data indicate that there is no significant interaction between the redox-active components of the triad.

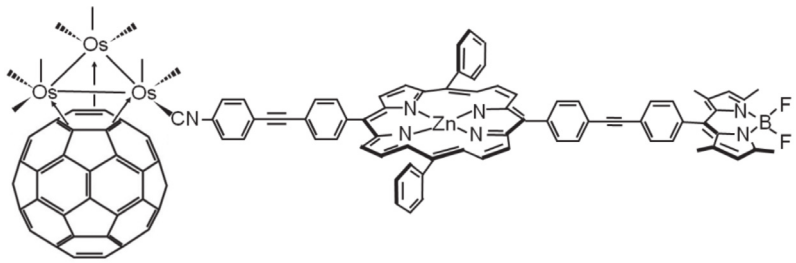

(185)

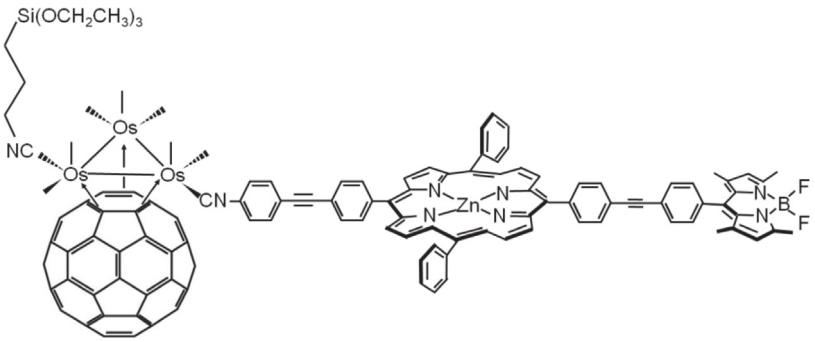

(186)

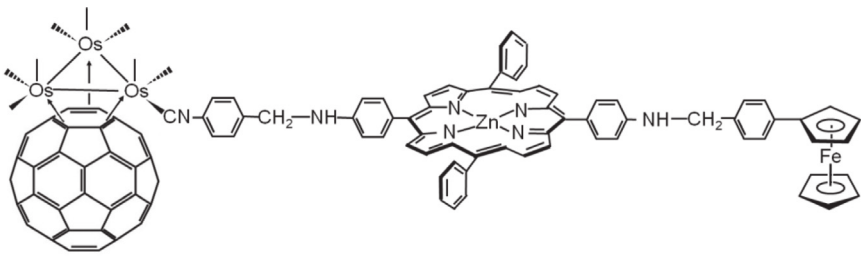

(187)

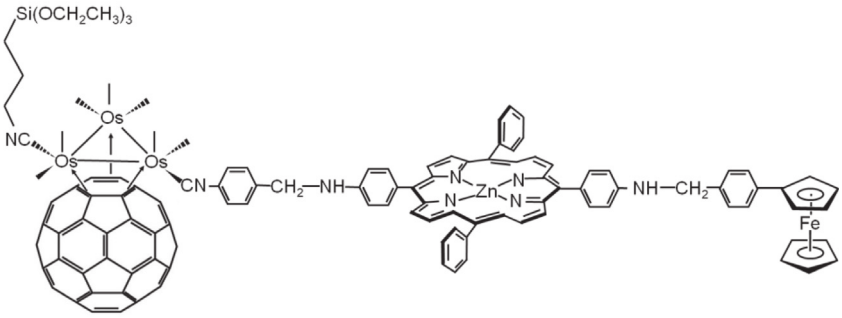

(188)

A covalent modification of the triosmium center with 3-(triethoxysilyl)ethyl [211–213] allows the dyad to be anchored to the surface of ITO to form an electrochemically-active and photochemically-active, highly-ordered layer) (see Fig. 58). The additional stabilization of the layer was achieved by axial coordination of zinc porphyrin units with diazabicyclooctane. The estimated surface coverage was close to the value corresponding to monolayer and confirms the highly ordered structure of the diad at the ITO surface. The voltammetric response of the dyad anchored to the surface of ITO electrode resembles the voltammogram of (***185***) in solution. Three well-resolved redox peaks are observed. First and second peak corresponds to the one-electron reduction localized on C_{60}. The third peak corresponds to the overlapping of triosmium-ferrocene moiety two-electron reduction and the one-electron reduction of porphyrin ring. Three oxidation peaks corresponding to ferrocene and porphyrin moiety oxidation were observed in positive potential range. Such a well-defined response of the fullerene-triosmium-zinc porphyrin dyad covalently anchored on the ITO surface indicates that the electronic structure of the triad is not perturbed during the monolayer formation.

A zinc porphyrin-fullerene dyad was also incorporated into a tetra-octylammonium bromide film at a glassy carbon electrode to form an electrochemical sensor for hydrogen peroxide and nitrite ions [214,215]. In this water-insoluble film, the porphyrin-fullerene conjugate retrains its electrochemical properties. The zinc porphyrin redox centers mediate electron exchange between analytes and the glassy carbon electrode allowing for precise and selective determination of hydrogen peroxide and nitrite ions [214,215].

Echegoyen and co-workers studied the electrochemical properties of [60]fullerene-zinc phthalocyanine dyad (***189***) [216]. The voltammetric behavior of this dyad is almost the sum of the voltammetric behavior of both components, zinc phthalocyanine and the modified fullerene. However, the redox potentials of zinc phthalocyanine and fullerene portions are significantly different from those observed for model compounds. The phthalocyanine-based oxidation and reduction potentials are anodically shifted

while the C_{60}-based reduction processes are cathodically shifted in the dyad. These results indicate some degree in charge transfer from the donating zinc phthalocyanine to the accepting fullerene moiety. Detailed studies of these voltammetric results revealed that both inter- and intra-molecular electronic interactions between both redox-active centers contribute to the changes in redox potentials. The intra-molecular effect dominates for lower charge of the dyad. Conversely, the inter-molecular effect is much more pronounced as the dyad is sequentially reduced [216].

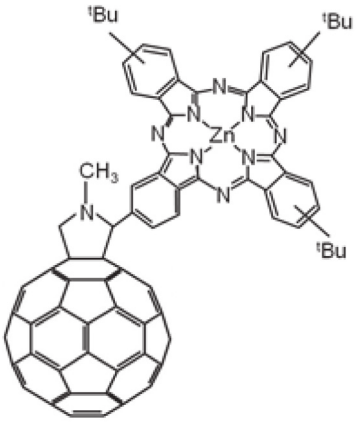

(*189*)

Zinc porphyrin-C_{60} dyad was also used for formation of electro- and photoelectron-active polymeric films [217]. The polymer is formed during oxidation of the monomer (***190***) as shown in Scheme 7. Polymerization occurs by the coupling of two carbazole radical cations. Voltammogram of the polymerization at the electrode surface and the electrochemical response of the polymer film in monomer-free solution are shown in Fig. 59. Dyads incorporated into the polymeric structure retained their electrochemical properties and light harvesting capacity. The possibility of hole- and electron-transport within this polymer with a "double cable" structure was suggested for the newly synthesized material [217].

6.3.3. Endohedral metallofullerenes covalently linked to metalloporphyrins.

A few cases where a metalloporphyrin is linked with an endohedral fullerene have been synthesized and examined electrochemically. Scheme 8 shows one example in which a functionalized version of $Sc_3N@I_h$-C_{80} is coordinated to a zinc phthalocyanine through at pyridyl nitrogen [218]. In *o*-dichlorobenzene solution, the functionalized $Sc_3N@I_h$-C_{80} shows four reversible reduction waves at − 1.04, −1.43, −2.15, and − 2.58 V, whereas $Sc_3N@I_h$-C_{80} itself has three reversible reduction processes occurring at −1.26, −1.62 and −2.37 V. The functionalized $Sc_3N@I_h$-C_{80} exhibits two nearly reversible oxidation processes at + 0.29 and + 0.94 V, while $Sc_3N@I_h$-C_{80} alone displays oxidation waves at 0.59 and 1.09 V. Unfortunately, the redox properties of the dyad itself with the functionalized $Sc_3N@I_h$-C_{80} appended to the zinc phthalocyanine were not reported.

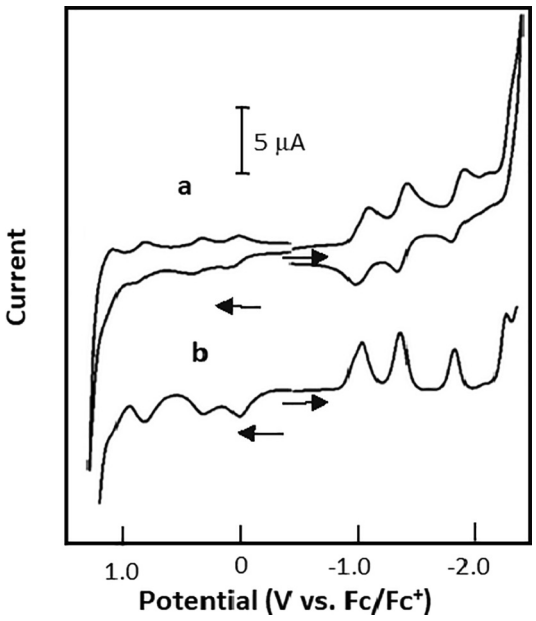

Fig. 56. Cyclic and differential pulse voltammograms of compound (***182***) in CH_2Cl_2 containing $[(n\text{-}Bu)_4N]PF_6$ at 293 K. Glassy carbon electrode. Reproduced with permission from Ref. [209]. Copyright © 2005, Helvetica Chimica Acta Verlag.

The dyad (***191***) utilizes a complex chain to connect a zinc porphyrin on the left to the endohedral fullerene $Sc_3N@I_h$-C_{80} on the right [219]. This dyad exhibits three, one-electron oxidation waves at + 0.28, +0.40 and + 0.55 V versus Fc/Fc^+ in *o*-dichlorobenzene solution. The first and third waves correspond to the first and second oxidations of the zinc porphyrin, while the second wave for the dyad corresponds to the first oxidation of the $Sc_3N@I_h$-C_{80} unit. The dyad (***191***) displays four, one-electron reduction waves at −1.18, −1.56, −1.98, and −2.27 V. The wave at −1.98 corresponds to reduction of the zinc porphyrin, while the other three reductions occur at potentials near those of the $Sc_3N@I_h$-C_{80} moiety.

Table 17
Redox properties of selected oligoporphyrins derivatives of [C_{60}]fullerene and reference compounds ***161*** and ***162*** in 3:1 toluene–acetonitrile solutions containing 0.1 M $[(n\text{-}Bu)_4N]PF_6$.

Compound	Redox potentials in V vs. Fc/Fc^+					
	Reduction			Oxidation of ZnP moiety		Ref.
	R_1	R_2	R_3	O_1	O_2	
(***183***)	−1.06	−1.41	−1.84	+0.36	+0.74	[209]
(***184***)	−0.98	−1.41	−1.84	+0.37 + 0.50	+0.73 + 0.84	[209]
(***179***)	−0.99–1.07	−1.40	−1.85	+0.35 + 0.49	+0.85	[209]
(***180***)	−1.06	−1.42	−1.85	+0.35 + 0.44 + 0.57	+0.83	[209]
(***181***)	−1.04	−1,40	−1.85	+0.33 + 0.47 + 0.61	+0.84	[209]
(***182***)	−0.99–1.09	−1.40	−1,87	+0.03 + 0.34	+0.82	[210]

R_1 first step of fullerene moiety reduction $C_{60}^{0/-}$
R_2 first step of fullerene moiety reduction $C_{60}^{/2-}$
R_3 3e-reduction process for (***184***) C_{60}^{2-}-$(ZnP)_2$/C_{60}^{3-}-$(ZnP)_2^{2-}$
4e-reduction process for (***179***) and (***182***) C_{60}^{2-}-$(ZnP)_2$-C_{60}^{2-}/C_{60}^{3-}-$(ZnP)_2^{2-}$-C_{60}^{3-}
5e-reduction process for (***180***) C_{60}^{2-}-$(ZnP)_3$-C_{60}^{2-}/C_{60}^{3-}-$(ZnP)_3^{3-}$-C_{60}^{3-}
6e-reduction process for (***181***) C_{60}^{2-}-$(ZnP)_4$-C_{60}^{2-}/C_{60}^{3-}-$(ZnP)_4^{4-}$-C_{60}^{3-}
O_1 first oxidation step of zinc porphyrin unit
O_2 second oxidation step of zinc porphyrin unit

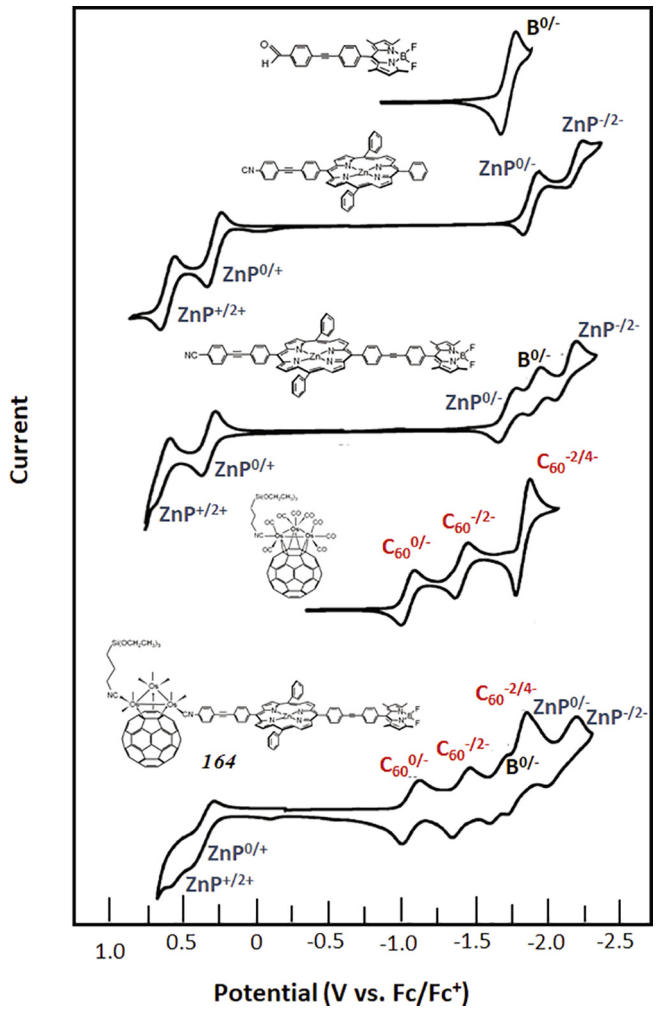

Fig. 57. Cyclic voltammograms of triad (***185***) at the bottom and various reference compounds in dry deoxygenated chlorobenzene containing 0.1 M $[(n\text{-}Bu)_4N]ClO_4$; scan rate 10 mV s^{-1}. Reproduced with permission from Ref. [213]. Copyright © 2010, Wiley-VCH Verlag.

Concluding this chapter of the review, linking porphyrin units to fullerene units through either axial ligation or covalent bonding allows the formation of a variety of structures, from relatively simple dyads to complex, multi-component systems. The electrochemical properties of such structures are generally the sum of the electrochemical properties of individual components. The interaction between fullerene and porphyrin redox centers depends on the distance between these two moieties and their relative orientation. A proper adjustment of both redox components allows intra-molecular electronic interaction and control of electrochemical properties.

6.4. Electrochemistry of other fullerene donor–acceptor systems containing transition metal complexes

A series of iron sulfide derivatives of [60]fullerene, $C_{60}[S_2Fe_2(CO)_6]_n$ where n = 1–6 (***192***), and [70]fullerene, $C_{70}[S_2Fe_2(CO)_6]_n$ where n = 1–3 (***193***), has been synthesized and crystallographically characterized [220]. The iron dimer center, $S_2Fe_2(CO)_6$, is not electroactive in the negative potential range of fullerene reduction. Reduction of the fullerene cage is anodically shifted in comparison to pristine C_{60} or C_{70} because of the electron withdrawing properties of iron dimer center.

The effect of *cis* and *trans* configuration on the electrochemical properties of dyads (***194trans***) and (***194cis***) composed of a C_{60} acceptor and a triphenylamine electron-donor bridged by a platinum(II) acetylide spacer has been investigated by Echegoyen and co-workers [221]. For both compounds the LUMOs are largely localized on the fullerene moiety. They are involved in the reduction processes, which are observed in the negative potential range) (Fig. 60). The fullerene cage reduction potentials depend slightly on the complex geometry. In the case of the *trans* isomer (***194trans***), they are shifted by about 50 – 100 mV toward less negative potentials. The triphenylamine moiety is involved in the first oxidation step, since the HOMO is located on this part of the complex. The LUMO + 1 is largely localized on the platinum center. Therefore, the second, irreversible oxidation process is related to the oxidation of platinum bridge) (Fig. 60). The bonding of the triphenylamine center to the platinum significantly shifts the potential of the oxidation process to less positive values, thus lowering the band gap energy of the dyad. There also a weak electronic communication between the donor and acceptor centers in the ground state [221].

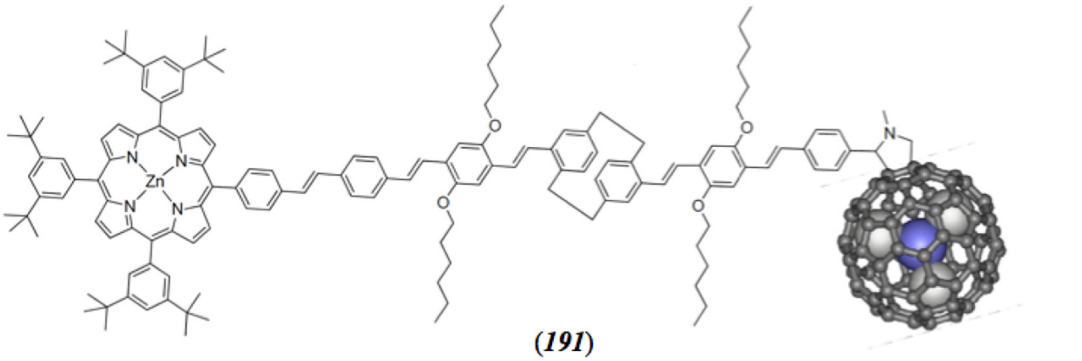

(***191***)

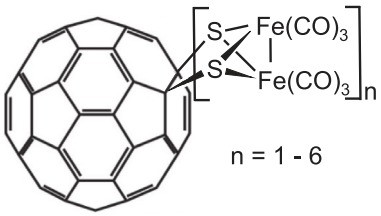

(***192***)

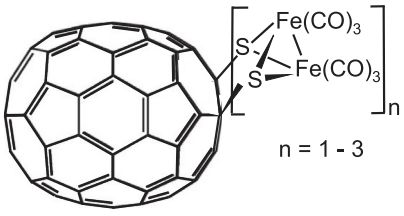

(***193***)

Table 18
Redox properties of triad composed of $Os_3(CO)_7[CN(CH_2)_3Si(OEt)_3](\mu^3\text{-}\eta^2\text{:}\eta^2\text{:}\eta^2\text{-}C_{60})$, zinc tetraphenylporphyrin and boron (***185***) or ferrocene (***187***) moieties in dry chlorobenzene.

Compound	Redox potentials in V vs. Fc/Fc^+									Ref.
	Reduction						Oxidation			
	$C_{60}^{0/-}$	$C_{60}^{-/-2}$	$C_{60}^{-2/-3}$	$B^{0/-}$	$ZnP^{0/-}$	$ZnP^{-/2-}$	Fc/Fc^+	$ZnP^{0/+}$	$ZnP^{+/2+}$	
(***185***)	−1.09	−1.43	−1.82	−1.69	−1.90	−2.12	–	+0.34	+0.51	[213]
(***187***)	−1.10	−1.45	−1.84	–	−1.94	−2.32	0	+0.12	+0.29	[211]

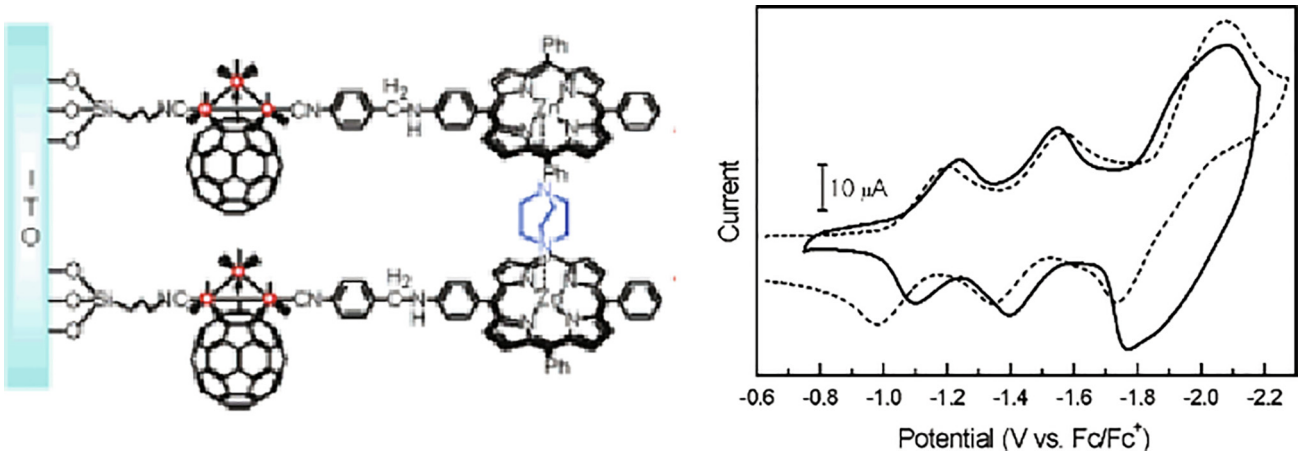

Fig. 58. (a) Schematic molecular structure of the layer of compound fullerene-triosmium-zinc porphyrin dyad at the ITO surface. (b) Cyclic voltammograms of the dyad in chlorobenzene (. . .) and at the surface of ITO (solid) in CH_2Cl_2 with 0.1 M $[(n\text{-}Bu)_4N]PF_6$ as an electrolyte at a scan rate of 0.5 V s^{-1}. Reproduced with permission from Ref. [212]. Copyright © 2005, American Chemical Society.

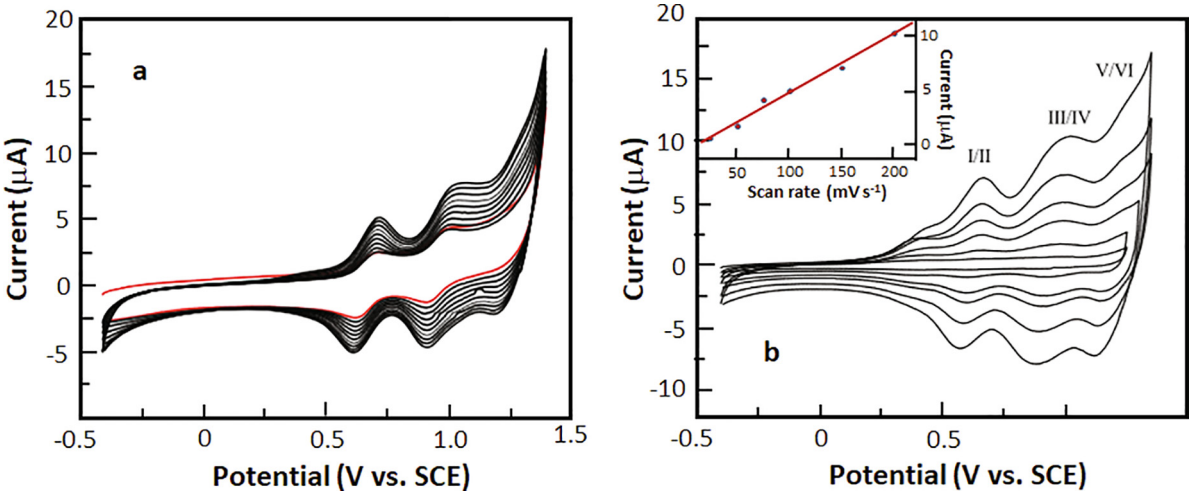

Fig. 59. (a) Ten cyclic successive voltammograms obtained at a scan rate of 100 mV/s in solution containing (***190***). (b) Cyclic voltammograms a (*poly*-***190***) film in solution containing only a support electrolyte. (b-inset) Relation between the oxidation peak currents and the scan rate. All the cyclic voltammogram scans were obtained in *o*-dichlorobenzene containing $[(n\text{-}Bu)_4N]ClO_4$. Pt working electrode. Reproduced with permission from Ref. [217] Copyright © 2013, Elsevier.

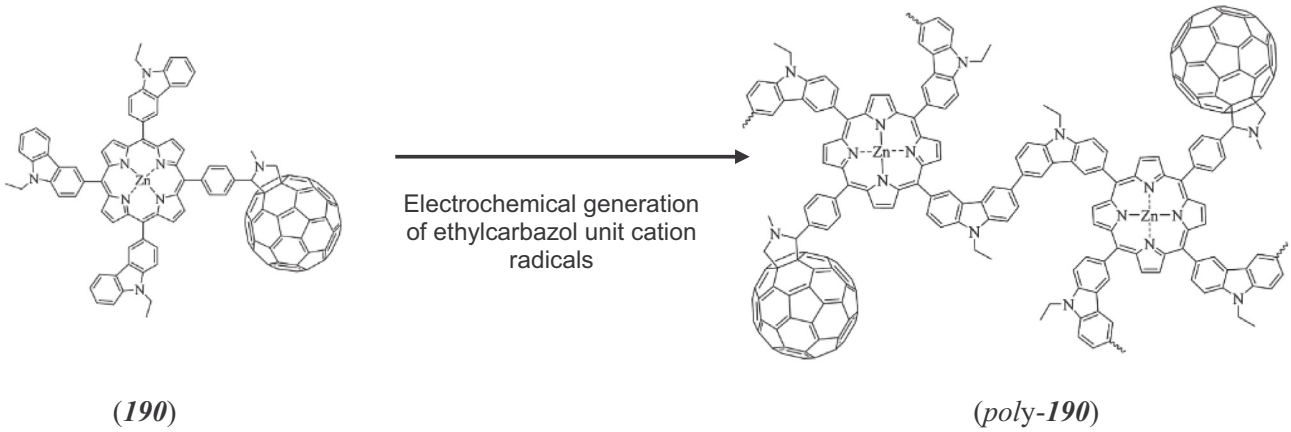

Scheme 7. Electrochemical formation of zinc porphyrin-C_{60} dyad polymer (*poly-**190***).

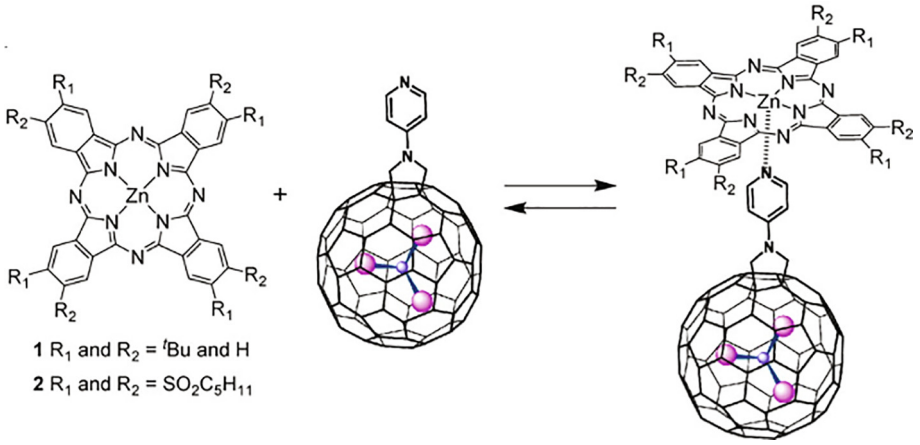

Scheme 8. Formation of zinc phthalocyanine-$Sc_3N@I_h$-C_{80} dyad through axial coordination (Adapted from ref. [218].)

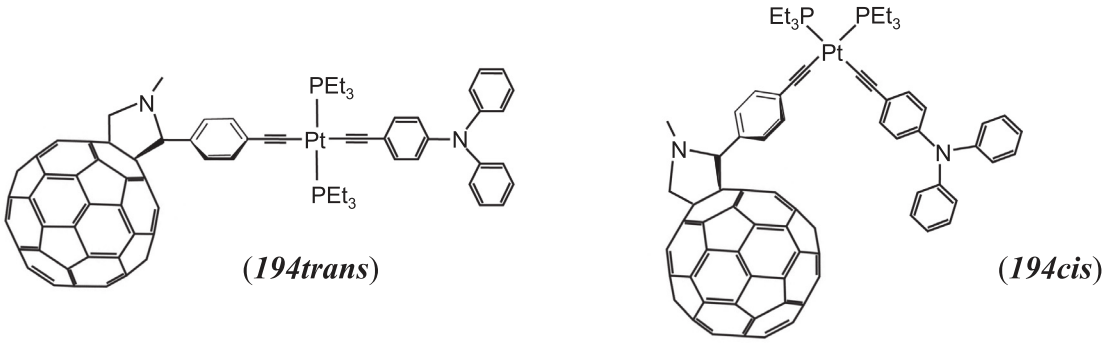

Tri- and *hexa*-platinum clusters were also used to bind fullerene units by means of a 4-ethynyl-benzylpirolidine bridge to form {Pt_3}CC–(1,4)C_6H_4-$C_2H_3N(C_8H_{17})C_{60}$ (***195***) and {Pt_6}(CC–(1,4)C_6H_4-$C_2H_3N(C_8H_{17})C_{60})_2$ (***196***) [222]. The electrochemical properties of these compounds were investigated with cyclic voltammetry and a variety of spectroelectrochemical techniques (UV–Vis, IR and NIR). Experimental results indicated a lack of any electronic communication between the metal clusters and the fullerene moieties. In negative potentials, two reduction steps involving the fullerene cage were observed at potentials more negative than potentials for fullerene reduction. This cathodic potential shift is similar to this one observed for fulleropyrrolidine derivatives of C_{60} due to saturation of the double bond and an increase in the energy of the LUMO. Such behavior indicates a lack of electronic communication between the fullerene cage and the triplatinum cluster. At positive potentials, two, one-electron oxidation processes involving the platinum cluster were observed.

Table 19
Redox properties of salen-C_{60} metal complexes (***199***) in *o*-dichlorobenzene containing 0.1 M $[(n\text{-Bu})_4N]ClO_4$ [224].

Compound	Redox potentials in V vs. decamethylferrocene						
	Reduction					Oxidation	
	$C_{60}^{0/-}$	$C_{60}^{-/-2}$	$C_{60}^{-2/-3}$	M(salen)reduction		Metal oxidation	M(salen) oxidation
salen-C_{60} metal receptor	−0.75	−1.13	−1.66	–		–	+1.03
(***199a***)	−0.73	−1.12	−1.67	−1.55	−1.78	+0.45	–
(***199b***)	−0.71	−1.09	−1.63	–		–	+0.95 +1.01
(***199c***)	−0.68	−1.05	−1.59	−0.32		–	+1.11 +1.34
(***199d***)	−0.71	−1.10	−1.62	−0.63		–	+1.21
(***199e***)	−0.72	−1.10	−1.66	−1.40		+0.63	+1.19
(***199f***)	−0.73	−1.11	−1.65	−1.71		+0.87	+1.30
(***199g***)	−0.74	−1.12	−1.67	−1.48		+0.91	+1.17
(***199i***)	−0.68	−1.08	−1.59	−1.63		+0.99	

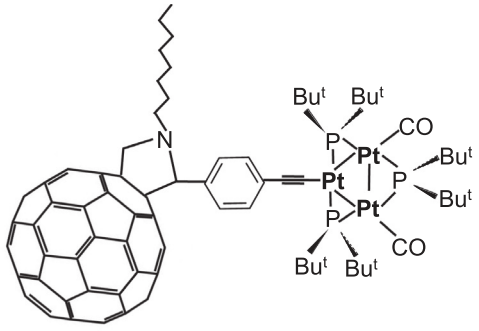

(***195***)

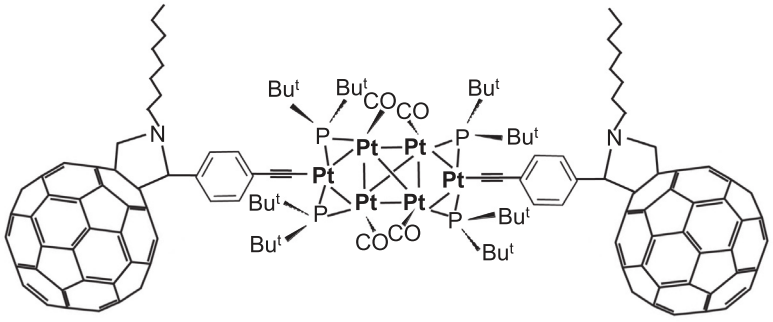

(***196***)

Transition metal ions were also bound to the fullerene moieties through quinolin-8-ol units to form dimeric structures, compounds (***197***) and (***198***) [223]. These complexes are electrochemically active at negative potentials due to reduction of the fullerene moiety. In the positive potential range, the electrochemically irreversible process corresponds to the oxidation of hydroxyquinoline entity. Both, reduction and oxidation of the fullerene derivatives bonded to the metal ions occurs easier in comparison to the free ligands.

A covalently linked salen-[60]fullerene (***199***) binds variety of transition metal cations [224]. The complexes that form exhibit complex electrochemical activity. The electrochemical properties of these systems depend on the binding metal-center and its oxidation state (see Table 19). In addition to the processes of fullerene-based reduction, the metal centers and the salen ligand contribute to the electrode processes. In general, the electronic interaction between fullerene and metal center is not observed in ground state due to the relatively long distance between these redox sites. The

(***197***)

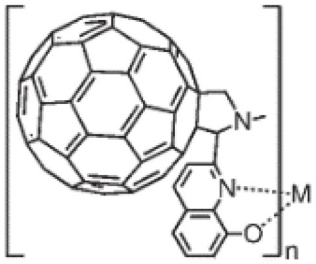

M = Al(III) n = 3; Al**1**$_3$
M = Zn(II) n = 2; Zn**1**$_2$

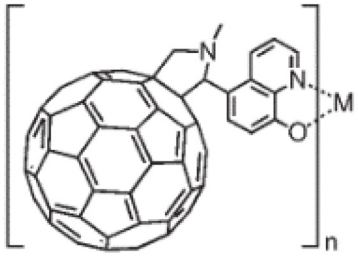

(***198***)

M = Al(III) n = 3; Al**2**$_3$
M = Zn(II) n = 2; Zn**2**$_2$

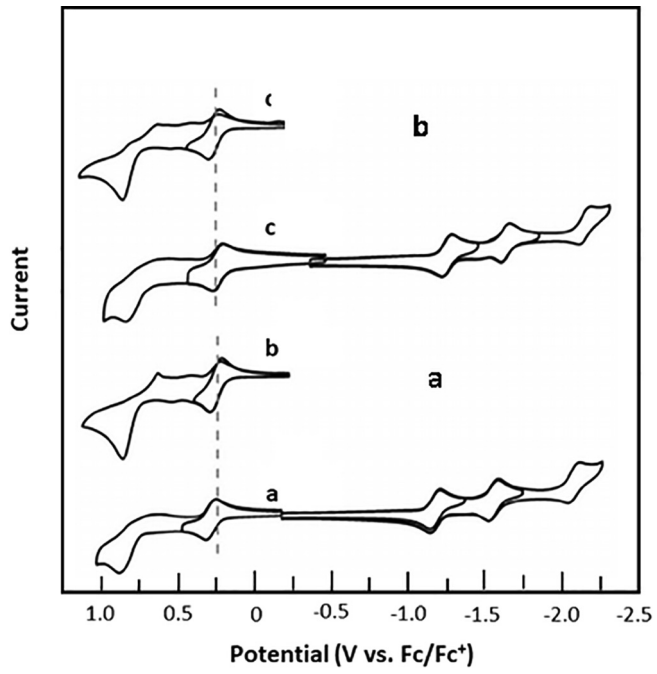

Fig. 60. Cyclic voltammograms of trans (a) and cis (b) triphenylamine-platinum(II) acetylide [60]fullerene triads (***193***) and (***194***) and their corresponding reference compounds in CH_2Cl_2 containing $[(n\text{-}Bu)_4N]$ PF_6 at a scan rate of 100 mVs^{-1} Reproduced with permission from Ref. [221]. Copyright © 2014, Wiley-VCH Verlag.

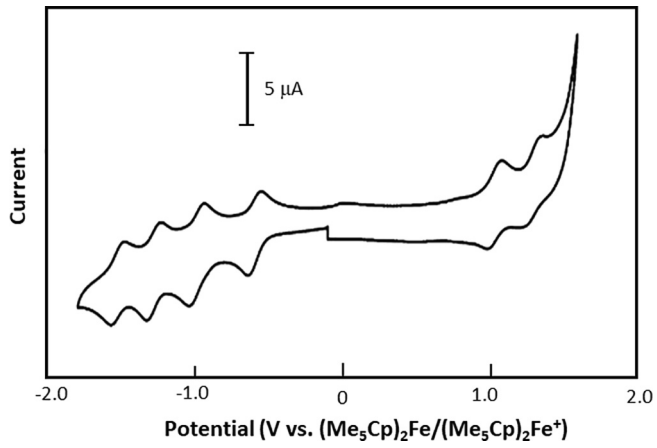

Fig. 61. The cyclic voltammogram of Cu(II)-salen-C_{60} complex (***199g***) in *o*-dichlorobenzene with 0.2 M $[(n\text{-}Bu)_4N]BF_4$ as supporting electrolyte at a scan rate of 0.1 V s^{-1}. Reproduced with permission from Ref. [224]. Copyright © 2013, Wiley-VCH Verlag.

exemplary voltammogram obtained for the Cu(II) complex coordinated by salen-[60]fullerene chelating ligand (***199***) is shown Fig. 61 in [224].

7. Conclusions

Complexes of fullerenes and transition metals are the subject of intensive research from the point of view of basic knowledge and practical applications. For variety of practical applications, the knowledge about their electrochemical properties is required. Therefore significant effort has been paid to the investigation of electrochemical properties of transition metal/fullerene complexes.

Transition metals can be directly coordinated to the C = C bond of the exterior of the fullerene cage in an η^2-fashion. The range of metals that can be coordinated to the fullerene moiety include third, fourth and fifth row of periodic table. The distance of the metal atom to the fullerene cage is limited by the nature of the fullerene-metal bonding. Therefore, the electrochemical performance of these complexes depends on the nature of the metal and the properties of the ligands coordinated to the metal center. Both of these factors influence the contribution of σ and π-back bonding interaction in metal-fullerene bond formation. In η^2-C_{60} complexes of transition metals, the basic electrochemical properties of the fullerene portion remains largely unaltered. Thus, the fullerene cage can be reduced in one-electron steps in the negative potential range. However, the reduction potentials of these processes are shifted in comparison to reduction potentials of pristine C_{60} depending on the nature of coordinated metal and the electron-donating properties of other ligands coordinated to the metal center. In positive potential range, electro-oxidation of metal center is observed. Both electron-transfer processes, oxidation and reduction of η^2-C_{60} complexes are followed by the cleavage of metal-fullerene bond. More stable electrochemical behavior is observed for complexes of metal cluster where multiple bonds to the fullerene can occur. Delocalization of the negative charge located at the fullerene unit onto the fullerene cage and the metallic cluster provides higher stability of these systems during the reduction process. This effect is particularly pronounced in the case of complexes in which fullerene moieties are linked by metal cluster into dimeric structures. In such systems, very effective electronic communication between fullerene units has been reported. The σ-π bonding interaction between metal atoms and fullerene moieties is also responsible for formation of coordination fullerene polymers. These polymers are electrochemically active and conducting in the negative potential range. The electrochemical activity of conducting fullerene polymers determines the potential practical applications of these materials for electrical energy storage, solar energy conversion, chemical and biochemical sensors.

A modification of a fullerene moiety with alkyl or aryl groups as shown in Scheme 1 produces a negatively charged ligand that can

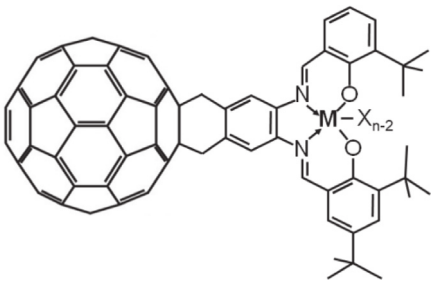

(***199***)

	(*199a*)	(*199b*)	(*199c*)	(*199d*)	(*199e*)	(*199f*)	(*199g*)	(*199h*)
M =	$V^{IV}O$	Cr^{III}	Mn^{II}	Fe^{II}	Ni^{II}	Cu^{II}	Zn^{II}	Pd^{II}
X =	SO_4	Cl	OAc	Cl	OAc	OAc	OAc	OAc
n =	2	3	2	3	2	2	2	2

be coordinated to the variety of metal ions in η^5-fashion. These complexes exhibit a half-sandwich structure with penta-alkylated fullerene anions acting as cyclopentadienide anion. These complexes exhibit electrochemical activity in the negative potential range related to the fullerene cage reduction and in positive potentials due to oxidation of the metal center. The strong electronic interaction between 50 π-electrons fullerene moiety and the metal cyclopentadienide unit significantly influences the redox potentials of electrochemical processes. In contrast to η^2-fullerene complexes, which are unstable during electrochemical reduction and oxidation, the η^5-fullerene metal complexes are much more robust under electrochemical conditions. There is an analogy between electrochemical stability of transition metal olefin complexes and metal cyclopentadienide complexes. The stable redox behavior also allows chemical oxidation of these η^5-fullerene complexes resulting in the formation stable complexes of metals in higher oxidation states. For di- and trinuclear η^5-fullerene complexes of ferrocene and ruthenocene, called as double- or triple-decker buckyocenes, strong electronic communication between metal centers through the C_{60} or C_{70} moieties is observed. Also in this case, the complexes are stable under electrochemical conditions.

Using a ligand covalently attached to the fullerene center to bind a metal is much more versatile approach to the formation of fullerene – transition metal complexes. Transition metal complexes and fullerenes are also excellent building blocks for supramolecular systems Research in this area has been mainly focused on metal complexes of polypyridyl, porphyrin, and cyclopentadienyl derivatives of fullerenes because of their ability to observe photo-induced electron transfer and charge separation in these molecules. The electrochemical behavior of these complexes is usually a combination of the electrochemical properties of the individual components within these dyads and triads. These dyads and triads can be tuned in a controlled manner by changing the architectures of the complexes: the geometry of the complex, the distance of the metal center from the fullerene moiety, the nature of the metal ion, and the solvent. Generally in ground state the electronic interaction between redox active sites is rather weak. Electronic communication between them increases during redox processes and increasing of negative charge on the fullerene moiety. Electrochemical measurements also provide much useful information about energy of the electronic states and allows calculation of the energy of the band gap.

Despite of the large number of experimental results focused on the electrochemical properties of complexes of fullerenes and transition metals, there are still many unresolved issues related to the electrochemical behavior of these compounds. So far, studies have been limited to the electrochemical behavior of fullerene-transition metal complexes in liquid solvents. Recently, some effort has been put into synthesis of dendrimeric and macromolecular structures, which can be applied in solar energy converting systems. A thorough understanding of the electrochemical properties of such systems is very important from the point of view of their practical applications.

Special attention should be also focused on the coordination fullerene polymers in which C_{60} moieties are bonded into macromolecular structures with transition metals in η^2-fashion. Well-ordered, multicomponent systems should provide better capacitance performance. Although progress in his area of studies has occurred, production of novel charge accumulation materials based on transition metal-fullerene polymers and their electrochemical properties is still needed.

Studies of the electrochemical properties of transition metal complexes of endohedral metallofullerenes are in their initial state. Progress in this important both basic and applied field of research, and requires extensive studies in the large-scale production of endohedral metallofullerenes and in transition metals coordination chemistry of these compounds.

More attention should be also focused on the research devoted to the electrochemical properties of η^1-bunded fullerene complexes of transition metals. This area of study is almost completely unexplored.

In most of cases, the electrochemical properties of transition metal-fullerene complexes were limited to qualitative voltammetric experiments and to the assignment of voltammetric signals to the electrochemical processes and their redox potentials determination. More detailed quantitative studies focused on the kinetic studies of the electron transfer processes and chemical reactions associated with electron exchange processes should be also performed. Such studies can provide useful information about the influence of complex structure and the environmental on the electrochemical properties of fullerene complexes of transition metals.

In summary, electrochemical properties of the variety of different fullerene complexes have been investigated. The information gained plays a leading role in both basic and applied areas of research of these compounds. Despite of the progress made in these studies, research on this topic is still an area of active study.

Declaration of Competing Interest

The authors declare that they have no known competing financial interest of personal relationships that could have appeared to influence the work reported in this paper.

Acknowledgements

Portions of this material that were based on research at the University of Bialystok were supported by the National Center of Science (most recently, project no. 2016/21/B/ST5/02496 to KW) and at University of California, Davis they were supported by the National Science Foundation (Grant Grant CHE-1807637).

References

[1] P.J. Fagan, J.C. Calabrese, B. Malone, The chemical nature of buckminsterfullerene (C_{60}) and the characterization of a platinum derivative, Science 252 (1991) 1160–1161.
[2] A.L. Balch, V.J. Catalano, J.W. Lee, M.M. Olmstead, S.R. Parkin, (η^2-C_{70})Ir(CO)Cl(PPh_3)$_2$. The Synthesis and Structure of an Organometallic Derivative of a Higher Fullerene, J. Am. Chem. Soc. 113 (1991) 8953–8954.
[3] A.L. Balch, M.M. Olmstead, Reactions of transition metal complexes with fullerenes (C_{60}, C_{70}, etc.) and related materials, complexes of, Chem. Rev. 98 (1998) 2123–2165.
[4] K. Lee, H. Song, J.T. Park, [60]fullerene−metal cluster complexes: Novel bonding modes and electronic communication, Acc. Chem. Res. 36 (2003) 78–86.
[5] M.R. Axet, O. Dechy-Cabaret, M. Gouygou, P. Serp, Coordination chemistry of carbon surfaces, Coord. Chem. Rev. 308 (2016) 236–345.
[6] P.J. Fagan, J.C. Calabrese, B, Malone, Metal complexes of buckminsterfullerene (C_{60}), Acc. Chem. Res. 25 (1992) 134–142.
[7] Y. Matsuo, Creation of cyclic -electron conjugated systems through the functionalization of fullerenes and synthesis of their multinuclear metal complexes, Bull. Chem. Soc. Jap. 81 (2008) 320–330.
[8] K. Winkler, A.L. Balch, Electrochemically formed two-component films comprised of fullerene and transition metal components, C. R. Chim. 9 (2006) 928–943.
[9] A.L. Balch, K. Winkler, Two-component polymeric materials of fullerenes and the transition metal complexes: A bridge between metal–organic frameworks and conducting polymers, Chem. Rev. 116 (2016) 3812–3882.
[10] M.A. Lebedeva, T.W. Chamberlain, A.N. Khlobystov, Harnessing the synergetic and complementary properties of fullerene and transition metal compounds for nanomaterial applications, Chem. Rev. 115 (2015) 11301–11351.
[11] W. Yan, S.M. Seifermann, P. Pierrat, S. Brase, Synthesis of highly functionalized C_{60} fullerene derivatives and their application in material and life sciences, Org. Biomol. Chem. 13 (2015) 25–54.
[12] M. Prato, [60]Fullerene chemistry for materials science applications, J. Mater. Chem. 7 (1997) 1097–1109.
[13] S.S. Babu, H. Mohwald, T. Nakanishi, Recent progress in morphology control of supramolecular fullerene assemblies and its applications, Chem. Soc. Rev. 39 (2010) 4021–4035.

[14] B.S. Sherigara, W. Kutner, F. D'Souza, Electrocatalytic Properties and Sensor Applications of Fullerenes and Carbon Nanotubes, Electroanalysis 15 (2003) 753–772.
[15] L. Echegoyen, L.E. Echegoyen, Electrochemistry of fullerenes and their derivatives, Acc. Chem. Res. 31 (1998) 593–601.
[16] T. Da Ros, M. Prato, M. Carano, P. Ceroni, F. Paolussi, S. Roffia, Enhanced acceptor character in fullerene derivatives. Synthesis and electrochemical properties of fulleropyrrolidinium salts, J. Am. Chem. Soc. 120 (1998) 11645–11648.
[17] M.B. Illescas, N. Martin, [60]fullerene adducts with improved electron acceptor properties, J. Org. Chem. 65 (2000) 5986–5995.
[18] M.E. El-Khoulya, O. Itoa, P.M. Smith, F. D'Souza, Intermolecular and supramolecular photoinduced electron transfer processes of fullerene–porphyrin/phthalocyanine systems, J. Photochem. Photobiol. C: Photochem. Rev. 5 (2004) 79–104.
[19] F. D'Souza, O. Ito, Photoinduced electron transfer in supramolecular systems of fullerenes functionalized with ligands capable of binding to zinc porphyrins and zinc phthalocyanines, Coord. Chem. Rev. 249 (2005) 1410–1422.
[20] A.S. Konev, A.F. Khlebnikov, O.V. Levil, D.A. Lukyanov, I.M. Zorin, Photocurrent in multilayered assemblies of porphyrin–fullerene covalent dyads: Evidence for channels for charge transport, ChemSusChem 9 (2016) 676–686.
[21] A.L. Balch, A.S. Ginwalla, J.W. Lee, B.C. Noll, M.M. Olmstead, Partial Separation and Structural Characterization of C_{84} Isomers by Crystallization of (^{2}-C_{84})Ir(CO)Cl($P(C_6H_5)_3$)$_2$, J. Am. Chem. Soc. 116 (1994) 2227–2228.
[22] P.W. Fowler, D.E. Manolopoulous, An Atlas of Fullerenes, Clarendon, Oxford, 1995.
[23] R. Taylor, G.J. Langley, A.G. Avent, T.J.S. Dennis, H.W. Kroto, D.M.R. Walton, The minor isomers and IR spectrum of [84]fullerene, J. Chem. Soc. Perkins Trans. 2 (1993) 1029.
[24] M.J.S. Dewar, A review of Complex Theory, Bull. Soc. Chim. Fr. 18 (1951) C71–C79.
[25] J. Chatt, L.A. Duncanson, Olefin co-ordination compounds. Part III. Infra-red spectra and structure: attempted preparation of acetylene complexes, J. Chem. Soc. (1953) 2939–2949.
[26] A.L. Balch, J.W. Lee, B.C. Noll, M.M. Olmstead, A Double Addition Product of C_{60}: C_{60}{Ir(CO)Cl(PMe_2Ph)$_2$}$_2$. Individual Crystallization of Two Conformational Isomers, J. Am. Chem. Soc. 114 (1992) 10984–10985.
[27] A.L. Balch, J.W. Lee, M.M. Olmstead, Isolation and Structural Characterization of a Product of Double Addition to C70: C70{Ir(CO)Cl(PPhMe2) 2}2•3C6H6. Angew. Chem., Internat. Ed. 31 (1992) 1356-1358.
[28] P.J. Fagan, J.C. Calabrese, B. Malone, A Multiply-Substituted Buckminsterfullerene (C_{60}) with an Octahedral Array of Platinum Atoms, J. Am. Chem. Soc. 113 (1991) 9408–9409.
[29] A.L. Balch, L. Hao, M.M. Olmstead, Patterns of Multiple Additions to Fullerene C_{70}: Isolation and Structural Characterization of $[C_{70}\{Pt(PPh_3)_2\}_4$, Angew. Chem., Internat. Ed. 35 (1996) 188–190.
[30] S.-Z. Zhan, G.-H. Zhang, J.-H. Li, J.-L. Liu, S.-H. Zhu, W. Lu, J. Zheng, S.W. Ng, D. Li, Exohedral Cuprofullerene: Sequentially Expanding Metal Olefin Up to a C_{60}@Cu_{24} Rhombicuboctahedron, J. Am. Chem. Soc. 142 (2020) 5943–5947.
[31] K. Lee, H. Song, J.T. Park, 60]Fullerene-Metal Cluster Complexes: Novel Bonding Modes and Electronic Communication, Acc. Chem. Res. 36 (2003) 78–86.
[32] H.-F. Hsu, J.R. Shapley, $Ru_3(CO)_9(\mu_3$-η^2,η^2,η^2-$C_{60})$: A Cluster Face-Capping, Arene-Like Complex of C_{60}, J. Am. Chem. Soc. 118 (1996) 9192–9193.
[33] C.-H. Chen, A. Aghabali, C. Suarez, M.M. Olmstead, A.L. Balch, L. Echegoyen, Synthesis and Characterization of Bis-triruthenium Cluster Derivatives of an All Equatorial [60]Fullerene Tetramalonate, Chem. Commun. 51 (2015) 6489–6492.
[34] E. Nakamura, Bucky ferrocene and ruthenocene: serendipity and discoveries, J. Organometal. Chem. 689 (2004) 4630–4635.
[35] M. Sawamura, Y. Kuninobu, M. Toganoh, Y. Matsuo, M. Yamanaka, E. Nakamura, Hybrid of Ferrocene and Fullerene, J. Am. Chem. Soc. 124 (2002) 9354–9355.
[36] S. Zhang, T.L. Brown, Y. Du, J.R. Shapley, Metalation of C_{60} with Pentacarbonylrhenium Radicals. Reversible Formation of $C_{60}\{Re(CO)_5\}_2$, J. Am. Chem. Soc. 115 (1993) 6705–6709.
[37] F.L. Bowles, M.M. Olmstead, A.L. Balch, Preparation and Crystallographic Characterization of $C_{60}\{\eta^1$-$Ru(CO)_2(\eta^5$-$C_5H_5)\}_2$: A Locally Crowded Organometallic Fullerene Without the Usual η^2-Bonding, J. Am. Chem. Soc. 136 (2014) 3338–3341.
[38] H. Zheng, X. Zhao, S. Sakaki, [2 + 2]-type Reaction of Metal−Metal σ-Bond with Fullerene Forming an η^1-C_{60} Metal Complex: Mechanistic Details of Formation Reaction and Prediction of a New η^1-C_{60} Metal Complex, Inorg. Chem. 56 (2017) 6746–6754.
[39] M.M. Olmstead, K. Maitra, A.L. Balch, Formation of a Curved Silver Nitrate Network That Conforms to the Shape of C_{60} and Encapsulates the Fullerene—Structural Characterization of $C_{60}\{Ag(NO_3)\}_5$, Angew. Chem., Int. Ed. 38 (1999) 231–233.
[40] M. Halim, R.D. Kennedy, M. Suzuki, S.I. Khan, P.L. Diaconescu, Y. Rubin, Complexes of Gold(I), Silver(I), and Copper(I) with Pentaaryl[60]fullerides, J. Am. Chem. Soc. 133 (2011) 6841–6851.
[41] M. Halim, R.D. Kennedy, S.I. Khan, Y. Rubin, Gold(I) Triphenylphosphine Complexes Incorporating Pentaarylfulleride Ligands, Inorg. Chem. 49 (2010) 3974–3976.
[42] A. Rodriguez-Fortea, A.L. Balch, J.M. Poblet, Endohedral metallofullerenes: a unique host-guest association, Chem. Soc. Rev. 40 (2011) 3551–3563.
[43] A.A. Popov, S. Yang, L. Dunsch, Endohedral Fullerenes, Chem. Rev. 113 (2013) 5989–6113.
[44] Endohedral Metallofullerenes: Basics and Applications; X. Lu, L. Echegoyen, A. L. Balch, S. Nagase, T. Akasaka, Eds.; CRC Press: Boca Raton, 2014.
[45] S. Stevenson, G. Rice, T. Glass, K. Harich, F. Cromer, M.R. Jordan, J. Craft, E. Hadju, R. Bible, M.M. Olmstead, K. Maitra, A.J. Fisher, A.L. Balch, H.C. Dorn, Small-bandgap endohedral metallofullerenes in high yield and purity, Nature 401 (1999) 55–57.
[46] S. Stevenson, M.A. Mackey, M.A. Stuart, J.P. Philips, M.L. Easterling, C.J. Chancellor, M.M. Olmstead, A.L. Balch, A Distorted Tetrahedral Metal Oxide Cluster inside an Icosahedral Carbon Cage, Synthesis, Isolation, and Structural Characterization of $Sc_4(\mu_3$-$O)_2$@I_h-C_{80}, J. Am. Chem. Soc. 130 (2008) 11844–11845.
[47] N. Chen, C.M. Beavers, M. Mulet-Gas, A. Rodriguez-Fortea, E.J. Munoz, Y.Y. Li, M.M. Olmstead, J.M. Poblet, L. Echegoyen, A.L. Balch, $Sc_2S@C_2$(10528)-C_{72}: A Dimetallic Sulfide Endohedral Fullerene with a Non-Isolated Pentagon Rule Cage, J. Am. Chem. Soc. 134 (2012) 7851–7860.
[48] T. Watanabe, M.F. Itoh, T. Komuro, H. Okada, T. Sakai, Y. Ono, K. Kawachi, Y. Kasama, H. Tobita, Iridium and Platinum Complexes of $Li^+@C_{60}$, Organometallics 33 (2014) 608–611.
[49] M.-C. Yang, A.K. Sharma, W.M.C. Sameera, K. Morokuma, M.-D. Su, Theoretical Study of Addition Reactions of L_4M(M = Rh, Ir) and L_2M(M = Pd, Pt) to $Li^+@C_{60}$, J. Phys. Chem. A 121 (2017) 2665–2673.
[50] A.L. Balch, V.J. Catalano, J.W. Lee, Accumulating Evidence for the Selective Reactivity of the 6–6 Ring Fusion of C_{60}. Preparation and Structure of (η^2-C_{60})Ir(CO)Cl(PPh_3)$_2$•$5C_6H_6$, Inorg. Chem. 30 (1991) 3980–3981.
[51] S. Aoyagi, K. Miwa, H. Ueno, H. Okada, Y. Matsuo, K. Kokubo, Structure of [60]fullerene with a mobile lithium cation inside, R. Soc. Open Sci. 5 (2018) 180337.
[52] L. Bao, B. Liu, X. Li, C. Pan, Y. Xie, X. Lu, $W(CO)_3(Ph_2PC_2H_4PPh_2)(\eta^2$-$Sc_3N@I_h$-$C_{80}$/$Sc_3N@D_{5h}$-$C_{80})$: regioselective synthesis and crystallographic characterization of air-stable mononuclear complexes of endohedral fullerenes, Dalton Trans. 45 (2016) 11606–11610.
[53] Y.-P. Xie, C. Pan, L. Bao, Z. Slanina, T. Akasaka, X. Lu, Regioselective Coordination of $Re_2(CO)_{10}$ to Y@C_{2v}(9)-C_{82}: An Unprecedented η^1 Complex Stabilized by Intramolecular Electron Transfer, Organometallics 38 (2019) 2259–2263.
[54] C.-H. Chen, W.-Y. Yeh, Y.-H. Liu, G.-H. Lee, $[(\mu$-$H)_3Re_3(CO)_9(\eta^2,\eta^2,\eta^2$-$Sc_2C_2$@$C_{3v}$(8)-$C_{82})]$: Face-Capping Cluster Complex of an Endohedral Fullerene, Angew. Chem. Int. Ed. 51 (2012) 13046–13049.
[55] C.-H. Chen, D.-Y. Lin, W.Y. Yeh, Regiospecific Coordination of Re_3 Clusters with the Sumanene-Type Hexagons on Endohedral Metallofullerenes and Higher Fullerenes That Provides an Efficient Separation Method, Chem. Eur. J. 20 (2014) 5768–5775.
[56] M.D. Meijer, G.P.M. van Klink, G. van Koten, Metal-chelating capacities attached to fullerenes, Coord. Chem. Rev. 230 (2002) 141–163.
[57] Y.-Y. Wu, W.-Y. Yeh, Synthesis of the Diphosphino-Fullerene 1,2,4,15-$(PPh_2)_2(H)_2C_{60}$ and Its Complexation with Triosmium Carbonyl Clusters, Organometallics 30 (2011) 4792–4795.
[58] J.-Y. Yeh, W.-Y. Yeh, Synthesis and metal complexation of a functional fullerene containing amine, phosphine, and pyridine coordinate groups, J. Organometal. Chem. 849–850 (2017) 350–356.
[59] R.C. Haddon, The fullerenes: powerful carbon-based electron acceptors, Phil. Trans. R. Soc. Lond. A. 343 (1993) 53–62.
[60] Q. Xie, E. Pérez-Cordero, L. Echegoyen, Electrochemical Detection of C_{60}^{6-} and C_{70}^{6-}: Enhanced Stability of Fullerides in Solution, J. Am. Chem. Soc. 114 (1992) 3978–3980.
[61] C.A. Reed, R.D. Bolskar, Discrete fulleride anions and fullerenium cations, Chem. Rev. 100 (2000) 1075–1119.
[62] A.J. Christopher, A. Howard, M.S.P. Shaffer, Charged Carbon Nanomaterials: Redox Chemistries of Fullerenes, Carbon Nanotubes, and Graphenes, Chem. Rev. 118 (2018) 7363–7408.
[63] P.W. Stephens, L. Mihaly, P.L. Leet, R.L. Whetten, S.-M. Huang, R. Kaner, F. Deiderich, K. Holczer, Structure of single-phase superconducting K_3C_{60}, Nature 351 (1991) 632–634.
[64] R.C. Haddon, Electronic Structure, Conductivity, and Superconductivity of Alkali Metal Doped C_{60}, Acc. Chem. Res. 25 (1992) 127–133.
[65] O. Gunnarsson, Superconductivity in fullerides, Rev. Mod. Phys. 69 (1997) 575–606.
[66] S.R. Lawrence, C.A. Ohlin, D.B. Cordes, A.M.Z. Slawin, A. Stasch, Hydrocarbon-soluble, hexaanionic fulleride complexes of magnesium, Chem. Sci. 10 (2019) 10755–10764.
[67] Q. Xie, F. Arias, L. Echegoyen, Electrochemically-Reversible, Single-Electron Oxidation of C_{60} and C_{70}, J. Am. Chem. Soc. 115 (1993) 9818–9819.
[68] M. Ricco', D. Pontiroli, M. Mazzani, F. Gianferrari, M. Pagliari, A. Goffredi, M. Brunelli, G. Zandomeneghi, B.H. Meier, T. Shiroka, Fullerenium Salts: A New Class of C_{60}-Based Compounds, J. Am. Chem. Soc. 132 (2010) 2064–2068.
[69] C. Bruno, I. Doubitski, M. Marcaccio, F. Paolucci, D. Paolucci, A. Zaopo, Electrochemical Generation of C_{60}^{2+} and C_{60}^{3+}, J. Am. Chem. Soc. 125 (2003) 15738–15739.
[70] S.A. Lerke, B.A. Parkinson, D.H. Evans, P.J. Fagan, Electrochemical studies on metal derivatives of buckminsterfullerene (C_{60}), J. Am. Chem. Soc. 114 (1992) 7807–7813.

[71] S.A. Lerke, D.H. Evans, P.J. Fagan, Voltammetric study of the oxidation of metal derivatives of buckminsterfullerence (C_{60}), J. Electroanal. Chem. 383 (1995) 127–132.

[72] L.C. Song, P.C. Liu, J.T. Liu, F.H. Su, G.F. Wang, Q.M. Hu, P. Zanello, F. Laschi, M. Fontani, Synthesis, characterization and electrochemical properties of optically active [60]fullerene organotransition metal complexes mer-[(η^2-C_{60})M(CO)$_3${(−)-DIOP}] (M = Mo, W), mer-[(η^2-C_{60})M(CO)$_3${(+)-DIOP}] (M = Mo, W) and [(η^2-C_{60})M{(−)-DIOP}] (M = Pd, Pt) – Crystal structure of [(η^2-C_{60})Pt{(−)-DIOP}], Eur. J. Inorg. Chem. 3201–3210 (2003).

[73] L.C. Song, F.H. Su, Q.M. Hu, E. Grigiotti, P. Zanello, Synthesis, characterization, and electrochemical properties of novel transition metal–fullerene complexes containing di- and tetraphosphane ligands, Eur. J. Inorg. Chem. 422–429 (2006).

[74] A.V. Usatov, S.M. Peregudova, L.I. Denisicich, E.V. Vorontsov, L.E. Vinogradova, Y.N. Novikov, Exohedral mono- and bimetallic hydride complexes of rhodium and iridium with C_{60} and C_{70}: synthesis and electrochemical properties, J. Organomet. Chem. 599 (2000) 87–96.

[75] A.N. Chernega, M.L.H. Green, J. Haggitt, A.H.H. Stephens, New transition-metal derivatives of the fullerene C_{60}, J. Chem. Soc. Dalton Trans. 755–767 (1998).

[76] R.S. Koefod, C. Xu, W. Lu, J.R. Shapley, M.G. Hill, K.R. Mann, An electrochemical and spectroelectrochemical study of an iridium-buckminsterfullerene complex: evidence for C_{60}-localized reductions, J. Phys. Chm. 96 (1992) 2928–2930.

[77] L.I. Denisovich, S.M. Peregudova, A.V. Usatov, A.L. Sigan, Y.N. Novikov, Electrochemical oxidation and reduction of rhodium and iridium complexes with fullerenes C_{60} and C_{70}, Russ. Chem. Bul. 46 (1997) 1251–1257.

[78] S.M. Peregudova, L.I. Denisovich, E.V. Martynova, M.V. Tsikalova, Yu.N. Novikov, Electrochemical oxidation and reduction of osmium and iridium complexes with fullerene C_{60}, Russ. J. Electrochem. 44 (2008) 249–253.

[79] C.H. Chen, C.S. Chen, H.F. Dai, W.Y. Yeh, Synthesis of the phosphino–fullerene PPh_2(o-C_6H_4)(CH_2NMeCH)C_{60} and its function as an η^1-P or η^3-P, C_2 ligand, Dalton Trans. 41 (2012) 3030–3037.

[80] C.H. Chen, W.Y. Yeh, Re–Re bond breaking of (μ-H)$_3$Re$_3$(CO)$_{11}$(NCMe) upon reaction with PPh_2(o-C_6H_4)(CH_2NMeCH)C_{60} to generates monorhenium and dirhenium phosphino–fullerene complexes, Dalton Trans. 42 (2013) 2488–2494.

[81] E. Igartua-Nieves, Y. Ocasio-Delgado, M.D.L.A. Torres-Castillo, O. Rivera-Betancourt, J.A. Rivera-Pagan, D. Rodriguez, G.E. Lopez, J.E. Cortes-Figueroa, Electrochemistry and [60]fullerene displacement reactions of(dihapto-[60]fullerene) pentacarbonyl metal(0) (M=Cr, W), Dalton Trans, 2007, pp. 1293–1299.

[82] P. Zanello, F. Laschi, M. Fontani, L.C. Song, Y.H. Zhu, Redox behavior of the molybdenum and tungsten metallafullerenes Mo(CO)$_3$(dppe)(η^2-C_{60}) (dppe=bis-(1,2-diphenylphosphino)ethane) and W(CO)$_3$(dppb)(η^2-C_{60}) (dppb=bis-(1,2-diphenylphosphino)benzene), J. Organomet. Chem. 593–594 (2000) 7–11.

[83] P. Zanello, F. Laschi, M. Fontani, C. Mealli, A. Ienco, K. Tang, X. Jin, L. Li, Redox behavior of the molybdenum and tungsten metallafullerenes M(η^2-C_{60})(CO)$_2$(phen)(dbm) (phen = 1,10-phenanthroline; dbm = dibutyl maleate): (spectro)electrochemistry and theoretical considerations, J. Chem. Soc. Dalton Trans. 965–970 (1999).

[84] P. Zanello, F. Laschi, A. Cinquantini, M. Fontani, K. Tang, X. Jin, L. Li, The redox behaviour of the family (C_{60})[Mo(CO)$_2$(phen)(dbm)]n (n = 1–3) – A comparison with the analog (η^2-C_{70})[Mo(CO)$_2$(phen)(dbm)] (phen = 1,10-phenanthroline; dbm = dibutyl maleate), Eur. J. Inorg. Chem. 1345–1350 (2000).

[85] J.T. Park, J.J. Cho, H. Song, C.S. Jun, Y. Son, J. Kwak, Electrochemical studies of C_{60}–triosmium complexes: First evidence for a C_{60}-mediated electron transfer to the metal center, Inorg. Chem. 36 (1997) 2698–2699.

[86] J.T. Park, H. Song, J.J. Cho, M.K. Chung, J.H. Lee, I.H. Suh, Synthesis and characterization of η^2-C_{60} and μ_3-η^2, η^2, η^2C_{60} triosmium cluster complexes, Organometallics 17 (1998) 227–236.

[87] H. Song, K. Lee, J.T. Park, M.G. Choi, Synthesis, structure, and electrochemical studies of μ_3-η^2, η^2, η^2C_{60} triosmium complexes, Organometallics 17 (1998) 4477–4483.

[88] K.H. Kim, J. Jung, Y.K. Han, Geometric and electronic structures of Os$_3$(CO)$_9$(μ_3-η^2, η^2, η^2-C_{60}), Os$_3$(CO)$_8$(P(CH$_3$)$_3$)(μ_3-η^2, η^2, η^2-C_{60}), and their anions (Q = −1 to −4): Reduction-induced conversion of to C_{60} – metal complexes, Organometallics 23 (2004) 3865–3869.

[89] Y.J. Cho, H. Song, K. Lee, K. Kim, J. Kwak, S. Kim, J.T. Park, The first observation of four-electron reduction in [60]fullerene-metalcluster self-assembled monolayers (SAMs), Chem. Commun. 2966–2967 (2002).

[90] H. Song, Y. Lee, Z.H. Choi, K. Lee, J.T. Park, J. Kwak, M.G. Choi, Synthesis and characterization of μ_3-η^2, η^2, η^2C_{60} trirhenium hydrido cluster complexes, Organometallics 20 (2001) 3139–3144.

[91] B.K. Park, G. Lee, K.H. Kim, H. Kang, C.Y. Lee, M.A. Miah, J. Jung, Y.K. Han, J.T. Park, Synthetic, electrochemical, and theoretical studies of tetrairidium clusters bearing mono-and bis [60] fullerene ligands, J. Am. Chem. Soc. 128 (2006) 11160–11172.

[92] A.J. Babcock, J. Li, K. Lee, J.R. Shapley, Electrochemistry of carbidopentaruthenium C_{60} complexes and related clusters, Organometallics 21 (2002) 3940–3946.

[93] K. Lee, J.R. Shapley, Face-coordinated C_{60} complexes with carbido pentaruthenium cluster cores including a bimetallic platinum–pentaruthenium complex, Organometallics 17 (1998) 3020–3026.

[94] K. Lee, Y.J. Choi, Y.J. Cho, C.Y. Lee, H. Song, C.H. Lee, Y.S. Lee, J.T. Park, Strong interfullerene electronic communication in a bisfullerene – hexarhodium sandwich complex, J. Am. Chem. Soc. 126 (2004) 9837–9844.

[95] G. Lee, Y.J. Cho, B.K. Park, K. Lee, J.T. Park, Two metal centers bridging two C_{60} cages as a wide passage for efficient interfullerene electronic interaction, J. Am. Chem. Soc. 125 (2003) 13920–13921.

[96] A.L. Balch, D.A. Costa, W.R. Fawcett, K. Winkler, Electronic communication in fullerene dimers. Electrochemical and electron paramagnetic resonance study of the reduction of $C_{120}O$, J. Phys. Chem. 100 (1996) 4823–4827.

[97] J.C. Hummelen, B. Knight, J. Pavlovich, R. Gonzalez, F. Wudl, Isolation of the heterofullerene $C_{59}N$ as its Dimer ($C_{59}N$)$_2$, Science 269 (1995) 1554–1556.

[98] K. Fujiwara, K. Komatsu, Mechanochemical synthesis of a novel C_{60} dimer connected by a silicon bridge and a single bond, Org. Lett. 4 (2002) 1039–1041.

[99] Y. Murata, A. Han, K. Komatsu, Mechanochemical synthesis of a novel C_{60} dimer connected by a germanium bridge and a single bond, Tetrahedron Lett. 44 (2003) 8199–8201.

[100] N. Dragoe, H. Shimotani, M. Hayashi, K. Saigo, A. de Bettencourt-Dias, A.L. Balch, Y. Miyake, Y. Achiba, K. Kitazawa, Electronic interactions in a new fullerene dimer: $C_{122}H_4$, with two methylene bridges, J. Org. Chem. 65 (2000) 3269–3273.

[101] E. Nakamura, M. Sawamura, Chemistry of ^{5}-fullerene metal complexes, Pure Appl. Chem. 73 (2001) 355.

[102] Y. Matsuo, Creation of cyclic π-electron-conjugated systems through the functionalization of fullerenes and synthesis of their multinuclear metal complexes, Bull. Chem. Soc. Jpn. 81 (2008) 320–330.

[103] Y. Matsuo, A. Muramatsu, Y. Kamikawa, T. Kato, E. Nakamura, Lamellar assembly of conical molecules possessing a fullerene apex in crystals and liquid crystals, J. Am. Chem. Soc. 129 (2007) 3052–3053.

[104] D.M. Guildi, G.M.A. Rahman, R. Marczak, Y. Matsuo, M. Yamanaka, E. Nakamura, Sharing orbitals: Ultrafast excited state deactivations with different outcomes in bucky ferrocenes and ruthenocenes, J. Am. Chem. Soc. 128 (2006) 9420–9427.

[105] M. Sawamura, H. Iikura, E. Nakamura, The first pentahaptofullerene metal complexes, J. Am. Chem. Soc. 118 (1996) 12850–12851.

[106] Y.W. Zhong, Y. Matsuo, E. Nakamura, Convergent synthesis of a polyfunctionalized fullerene by regioselective five-fold addition of a functionalized organocopper reagent to C_{60}, Org. Lett. 8 (2006) 1463–1466.

[107] Y. Matsuo, K. Tahara, E. Nakamura, X-ray crystallographic characterization of potassium pentaphenyl [60]fullerene, Chem. Lett. 34 (2005) 1078–1079.

[108] M. Sawamura, Y. Kuninobu, M. Toganoh, Y. Matsuo, M. Yamanaka, E. Nakamura, Hybrid of ferrocene and fullerene, J. Am. Chem. Soc. 124 (2002) 9354–9355.

[109] R.H. Herber, I. Nowik, Y. Matsuo, M. Tohanoh, Y. Kuninobu, E. Nakamura, Mössbauer spectroscopy of bucky ferrocenes: Lattice dynamics and motional anisotropy of the metal atom, Inorg. Chem. 44 (2005) 5629–5635.

[110] M. Toganoh, Y. Matsuo, E. Nakamura, Rhenium-templated regioselective polyhydrogenation reaction of [60]fullerene, Angew. Chem. Int. Ed. 42 (2003) 3530–3532.

[111] M. Toganoh, Y. Matsuo, E. Nakamura, Synthesis of ferrocene/hydrofullerene hybrid and functionalized bucky ferrocenes, J. Am. Chem. Soc. 125 (2003) 13974–13975.

[112] Y. Matsuo, Y. Kuninobu, A.A. Muramatsu, M. Sawamura, E. Nakamura, Synthesis of metal fullerene complexes by the use of fullerene halides, Organometallics 27 (2008) 3403–3409.

[113] Y. Matsuo, A. Iwashita, E. Nakamura, Synthesis and derivatization of iridium (I) and iridium(III) pentamethyl[60]fullerene complexes, Organometallics 24 (2005) 89–95.

[114] M. Sawamura, Y. Kuninobu, E. Nakamura, Half-sandwich metallocene embedded in a spherically extended π-conjugate system. Synthesis, structure, and electrochemistry of Rh(η^5-$C_{60}Me_5$)(CO)$_2$, J. Am. Chem. Soc. 122 (2000) 12407–12408.

[115] Y. Matsuo, E. Nakamura, Ruthenium(II) complexes of pentamethylated [60]fullerene, Alkyl, alkynyl, chloro, isocyanide, and phosphine complexes, Organometallics 22 (2003) 2554–2563.

[116] M.P. Stewart, R. Butterick III, L.G. Sneddon, Y. Matsuo, W.E. Geiger, Voltammetry of half-sandwich manganese group complexes of η^6-$PhC_3B_7H_9$ and η^5-$C_{60}Bn_2PhH_2$, two ligands that are cyclopentadienyl mimicks, Inorg. Chim. Acta 364 (2010) 251–254.

[117] Y. Koninobu, Y. Matsuo, M. Toganoh, M. Saamura, E. Nakamura, Nickel, palladium, and platinum complexes of η^5-cyclopentadienide $C_{60}R_5$ ligands. Kinetic and thermodynamic stabilization effects of the $C_{60}Ph_5$ ligand, Organometallics 23 (2004) 3259–3266.

[118] Y. Matsuo, A. Muramatsu, Y. Kamikawa, T. Kato, E. Nakamura, Synthesis and structural, electrochemical, and stacking properties of conical molecules possessing buckyferrocene on the apex, J. Am. Chem. Soc. 128 (2006) 9586–9587.

[119] Y. Matsuo, T. Fujita, E. Nakamura, Hoop-shaped condensed aromatic systems: Synthesis and structure of iron–and ruthenium–hepta (organo)[60]fullerene complexes, Chem. Asian J. 2 (2007) 948–955.

[120] Y. Matsuo, Y. Kuninobu, S. Ito, E. Nakamura, Synthesis and reactivity of bucky ruthenocene Ru(η^5-$C_{60}Me_5$)(η^5-C_5H_5), Chem. Lett. 33 (2004) 68–69.

[121] Y. Matsuo, M. Maruyama, S.S. Gayathri, T. Uchida, D.M. Guldi, H. Kishida, A. Nakamura, E, Nakamura, -Conjugated multidonor/acceptor arrays of fullerene-cobaltadithiolene-tetrathiafulvalene: from synthesis and structure to electronic interactions, J. Am. Chem. Soc. 131 (2009) 12643–12649.

[122] Y. Matsuo, K. Tahara, E. Nakamura, Synthesis and electrochemistry of double-decker buckyferrocenes, J. Am. Chem. Soc. 128 (2006) 7154–7155.
[123] Y. Matsuo, K. Tahara, T. Fujita, E. Nakamura, Di- and trinuclear [70]fullerene complexes: Syntheses and metal–metal electronic interactions, Angew. Chem. Int. Ed. 48 (2009) 6239–6241.
[124] H. Nagashima, A. Nakaoka, Y. Saito, M. Kato, T. Kawanishi, K. Itoh, $C_{60}Pd_n$: The first organometallic polymer of buckminsterfullerene, J. Chem. Soc., Chem. Commun. (1992) 377–379.
[125] H. Nagashima, Y. Kato, H. Yamaguchi, E. Kimura, T. Kawanishi, M. Kato, Y. Saito, M. Haga, K. Itoh, Synthesis and reactions of organoplatinum compounds of C_{60}, $C_{60}Pt_n$, Chem. Lett. 1207–1210 (1994).
[126] E. Brancewicz, E. Gradzka, A. Basa, K. Winkler, Chemical synthesis and characterization of the C_{60}-Pd polymer spherical nanoparticles, Electrochim. Acta 128 (2014) 91–101.
[127] D.V. Konarev, S.S. Khasanov, Y. Nakano, Y. Nakano, A. Otsuka, H. Yamochi, G. Saito, R.N. Lyubovskaya, Fullerene at an ambient temperature linear coordination fullerene C_{60} polymer $[\{Ni(Me_3P)_2\}(\mu\text{-}\eta^2,\ \eta^2\text{-}C_{60})]_\infty$ bridged by zerovalent nickel atoms, Inorg. Chem. 53 (2014) 11960–11965.
[128] A.L. Balch, D.A. Costa, D.K. Winkler, Formation of redox-active, two-component films by electrochemical reduction of C_{60} and transition metal complexes, J. Am. Chem. Soc. 120 (1998) 9614–9620.
[129] K. Winkler, K. Noworyta, W. Kutner, A.L. Balch, Study of redox active C_{60}/Pd films by simultaneous cyclic voltammetry and piezoelectric microgravimetry at an electrochemical quartz crystal microbalance, J. Electrochem. Soc. 147 (2000) 2597–2603.
[130] E. Grodzka, J. Grabowska, M. Wysocka-Zolopa, K. Winkler, Electrochemical formation and properties of two-component films of transition metal complexes and C_{60} or C_{70}, J. Solid State Electrochem. 12 (2008) 1267–1278.
[131] A. Hayashi, A. de Bettencourt-Dias, A.L. Balch, K. Winkler, Redox-active films formed by electrochemical reduction of solutions of C_{60} and platinum complexes, J. Mater. Chem. 12 (2002) 2116–2122.
[132] K. Winkler, A. de Bettencourt-Dias, A.L. Balch, W. Kutner, K. Noworyta, Recent advances in the Eeectrochemistry of fullerene/transition metal co-polymers, in Fullerenes-Electrochemistry and Photochemistry, S. Fukuzumi, F. D'Souza, D.M. Guldi (eds.) The Electrochemical Society, Inc.: Pennington, 8 (2000) 31−42.
[133] K. Winkler, A. de Bettencourt-Dias, A.L. Balch, Electrochemical studies of C_{60}/Pd films formed by the reduction of C_{60} in the presence of palladium(II) acetate trimer. Effects of varying C_{60}/Pd(II) ratios in the precursor solutions, Chem. Mater. 12 (2000) 1386–1392.
[134] K. Winkler, A. de Bettencourt-Dias, A.L. Balch, Charging processes in electroactive C_{60}/Pd films: Effect of solvent and supporting electrolyte, Chem. Mater. 11 (1999) 2265–2273.
[135] K. Winkler, E. Grodzka, F. D'Souza, A.L. Balch, Two-component films of fullerene and palladium as materials for electrochemical capacitors, J. Electrochem. Soc. 154 (2007) K1–K10.
[136] E. Grodzka, P. Pieta, P. Dluzewski, W. Kutner, K. Winkler, Formation and electrochemical Properties of composites of the C_{60}−Pd polymer and multi-wall carbon nanotubes, Electrochim. Acta 54 (2009) 5621–5628.
[137] P. Pieta, E. Grodzka, K. Winkler, G.M. Venukadasula, F. D'Souza, W. Kutner, Preparation and selected properties of a composite of the C_{60}-Pd conducting polymer and single-wall carbon nanotubes, Phys. Status Solidi B 245 (2008) 2292–2295.
[138] P. Pieta, E. Grodzka, K. Winkler, M. Warczak, A. Sadkowski, G.Z. Zukowska, G. M. Venukadasula, F. D'Souza, W. Kutner, Conductive, capacitive, and viscoelastic properties of a new composite of the C_{60}−Pd conducting polymer and single-wall carbon nanotubes, J. Phys. Chem. B 113 (2009) 6682–6691.
[139] E. Gradzka, K. Winkler, M. Borowska, M.E. Plonska-Brzezinska, L. Echegoyen, Comparison of the electrochemical properties of thin ilms of MWCNTs/C_{60}-Pd, SWCNTs/C_{60}-Pd and ox-CNOs/C_{60}-Pd, Electrochim. Acta 96 (2013) 274–284.
[140] E. Gradzka, E. Brancewicz, K. Winkler, Morphology and capacitance properties of nanostructured composites of carbon nanostructures and C_{60}-Pd nanoparticles, ECS J. Solid State Sci. Technol. 2 (2013) M3151–M3155.
[141] E. Gradzka, M. Wysocka, K. Winkler, In situ conductance studies of two-component C_{60}-Pd polymer, J. Phys. Chem. C 118 (2014) 14061–14072.
[142] J. Goclon, K. Winkler, J.T. Margraf, Theoretical investigation of interactions between palladium and fullerene in polymer, ACS Advances 7 (2017) 2202–2210.
[143] M. Płońska, A. de Bettencourt-Dias, A.L. Balch, K. Winkler, Electropolymerization of 2'-ferrocenylpyrrolidino[3',4';1,2][C_{60}]fullerene in the presence of palladium acetate. Formation of an electroactive fullerene-based film with a covalently attached redox probe, Chem. Mater. 15 (2003) 4122–4131.
[144] M. Wysocka-Zolopa, K. Winkler, R. Caballero, F. Langa, Formation and properties of electroactive fullerene based films with a covalently attached ferrocenyl redox probe, Electrochim. Acta 56 (2011) 5566–5574.
[145] M. Plonska, K. Winkler, S. Gadde, F. D'Souza, A.L. Balch, Redox active two-component films of palladium and covalently linked zinc porphyrin-fullerene dyad, Electroanalysis 18 (2006) 841–848.
[146] M. Wysocka-Zolopa, K. Winkler, S. Gadde, F. D'Souza, Two-component polymer films of palladium and fullerene with covalently linked crown ether voids: effect of cation binding on the redox behavior, J. Solid State Electrochem. 16 (2012) 65–74.
[147] M. Wysocka-Zolopa, K. Winkler, A. Thorn, C.J. Chancellor, A.L. Balch, Electrochemical properties of two-component polymers of palladium and pyrrolidine and piperazine derivatives of C_{60}, Electrochim. Acta 55 (2010) 2010–2021.
[148] E. Grądzka, J. Goclon, S.K. Das, A. Dubis, K. Winkler, F. D'Souza, Polymer network of graphene oxide with covalently attached 2-(4'-hydroxyphenyl)fulleropyrrolidine and palladium: Synthesis, properties and theoretical studies, Mater. Sci. Eng. B 249 (2019) 114406.
[149] F. Cardinali, J.L. Gallani, S. Schergna, M. Maggini, J.F. Nierengarten, An amphiphilic C_{60} derivative with a tris(2,2'-bipyridine)ruthenium(II) polar head group: Synthesis and incorporation in Langmuir films, Tetrahedron Lett. 46 (2005) 2969–5972.
[150] F. Chaignon, J. Torroba, E. Blart, M. Borgstrom, L. Hammarstrom, F. Odobel, Distance-independent photoinduced energy transfer over 1.1 to 2.3 nm in ruthenium trisbipyridine–fullerene assemblies, New J. Chem. 29 (2005) 1272–1284.
[151] M. Maggini, D.M. Guldi, S. Mondini, G. Scorrano, F. Paolucci, P. Ceroni, S. Roffia, Photoinduced electron transfer in a tris(2,2′-bipyridine)-C_{60}-ruthenium(II) dyad: evidence of charge recombination to a fullerene excited state, Chem Eur. J. 4 (1998) 1992–2000.
[152] Z. Zhou, G.H. Sarova, S. Zhang, Z. Ou, F.T. Tat, K.M. Kadish, L. Echegoyen, D.M. Guldi, D.I. Schuster, S.R. Wilson, Fullerene Polypyridine ligands: Synthesis, ruthenium complexes, and electrochemical and photophysical properties, Chem. Eur. J. 12 (2006) 4241–4248.
[153] D. Armspach, E.C. Constable, F. Diederich, C.E. Housecroft, J.F. Nierengarten, Bucky ligands: synthesis, ruthenium(II) complexes, and electrochemical properties, Chem. Eur. J. 4 (1998) 723–733.
[154] M. Maggini, A. Donò, G. Scorrano, M. Prato, Synthesis of a [60]fullerene derivative covalently linked to a ruthenium(II) tris(bipyridine) complex, J. Chem. Soc., Chem. Commun. (1995) 845–846.
[155] A. Valore, M. Balordi, A. Colombo, C. Dragonetti, S. Righetto, D. Roberto, R. Ugo, T. Benincori, G. Rampinini, F. Sannicolo, F. Demartin, Novel ruthenium (II) complexes with substituted 1,10-phenanthroline or 4,5-diazafluorene linked to a fullerene as highly active second order NLO chromophores, Dalton Trans. 39 (2010) 10314–10318.
[156] L. Shu, S. Pyo, J. Rivera, L. Echegoyen, Synthesis and electrochemical properties of a new C_{60}-phenanthroline derivative and its dimeric complex with silver, Inorg. Chim. Acta 292 (1999) 34–40.
[157] N. Armaroli, C. Boudon, D. Felder, J.P. Gisselbrecht, M. Gross, G. Marconi, J.F. Nicoud, J.F. Nierengarten, V. Vicinelli A copper(I) bis-phenanthroline complex buried in fullerene-functionalized dendritic black boxes, Ang. Chem. Int. Ed. 38 (1999) 3730–3733.
[158] J. Zhen, W. Zhou, M. Chen, B. Li, L. Jia, M. Wang, S. Yang, Pyridine-functionalized fullerene additive enabling coordination interactions with $CH_3NH_3PbI_3$ perovskite towards highly efficient bulk heterojunction solar cells, J. Mater. Chem. A 7 (2019) 2754–2763.
[159] P. Yang, S. Chen, Y. Liu, Z. Xiao, L. Ding, A pyridine-functionalized pyrazolinofullerene used as a buffer layer in polymer solar cells, Phys. Chem. Chem. Phys. 15 (2013) 17076–17078.
[160] M.D. Meijer, G.P.M. van Klink, G. van Koten, Metal-chelating capacities attached to fullerenes, Coord. Chem. Rev. 30 (2002) 141–163.
[161] G. Possamai, E. Menna, M. Maggini, M. Carano, M. Marcaccio, F. Paolucci, D.M. Guldi, A. Swartz, Rhenium(I) and ruthenium(II) complexes with a crown-linked methanofullerene ligand: synthesis, electrochemistry and photophysical characterization, Photochem. Photobiol. Sci. 5 (2006) 1154–1164.
[162] W. Yan, S. Menning, G. Brenner-Weiß, T. Muller, P. Pierrat, S. Brase, A hexakis terpyridine-fullerene ligand in six-fold ruthenium, iridium, and iron complexes: Synthesis and electrochemical properties, Chem. Eur. J. 22 (2016) 11522–11526.
[163] D.M. Guldi, M. Maggini, E. Menna, G. Scorrano, P. Ceroni, M. Marcaccio, F. Paolucci, S. Roffia, A photosensitizer dinuclear ruthenium complex: Intramolecular energy transfer to a covalently linked fullerene acceptor, Chem. Eur. J. 7 (2001) 1597–1605.
[164] K. Barthelmes, J. Kübel, A. Winter, M. Wächtler, C. Friebe, B. Dietzek, U.S. Schubert, New ruthenium bis(terpyridine) methanofullerene and pyrrolidinofullerene complexes: Synthesis and electrochemical and photophysical properties, Inorg. Chem. 54 (2015) 3159–3171.
[165] N. Armaroli, F. Diederich, C.O. Dietrich-Buchecker, L. Flamigni, G. Marconi, J.F. Nierengarten, J.P. Sauvage, A copper(I)-complexed rotaxane with two fullerene stoppers: Synthesis, electrochemistry, and photoinduced processes, Chem. Eur. J. 4 (1998) 406–416.
[166] C.C. Phifer, D.R. McMillin, The basis of aryl substituent effects on charge-transfer absorption intensities, Inorg. Chem. 25 (1986) 1329–1333.
[167] A.K. Gushurst, D.R. McMillin, C.O. Dietrich-Buchecker, J.-P. Sauvage, Comparative studies of the photophysical properties of copper phenanthrolines: from $Cu(dmp)^{2+}$ to the copper (I) catenates, Inorg. Chem. 28 (1989) 4070–4072.
[168] J.D. Megiatto Jr., D.I. Schuster, S. Abwandner, G. de Miguel, D.M. Guldi, [2] Catenanes decorated with porphyrin and [60]fullerene groups: Design, convergent synthesis, and photoinduced processes, J. Am. Chem. Soc. 132 (2010) 3847–3862.
[169] E.A. Walsh, J.R. Deye, W. Baas, K. Sullivan, A. Lancaster, K.A. Walters, Synthesis and spectroscopic studies of transition-metal fullerene supramolecular systems, J. Photochem. Photobiol. A: Chem. 260 (2013) 24–36.

[170] S.H. Lee, C.T.L. Chan, K.M.C. Wong, W.H. Lam, W.M. Kwok, V.W.W. Yam, Synthesis and photoinduced electron transfer in platinum (II) bis (N-(4-ethynylphenyl) carbazole) bipyridine fullerene complexes, Dalton Trans. 43 (2014) 17624–17634.
[171] S.H. Lee, C.T.L. Chan, K.M.C. Wong, W.H. Lam, W.M. Kwok, V.W.W. Yam, Design and synthesis of bipyridine platinum (II) bisalkynyl fullerene donor–chromophore–acceptor triads with ultrafast charge separation, J. Am. Chem. Soc. 136 (2014) 10041–10052.
[172] G. Zhou, J. He, I.I. Harruna, K.E. Geckeler, Fullerene and ruthenium dual end-functionalized thermosensitive polymers: Synthesis, characterization, electrochemical properties, and self-assembly, J. Mater. Chem. 18 (2008) 5492–5501.
[173] M. Prato, M. Maggini, C. Giacometti, G. Scorrano, G. Sandona, G. Farnia, Synthesis and electrochemical properties of substituted fulleropyrrolidines, Tetrahedron 52 (1996) 5221–5234.
[174] L. Perez, D.M.S. Isiam, Y. Araki, P. de la Cruz, F. Cardinali, O. Ito, F. Langa, Photoinduced electron transfer in branched bis(ferrocenylacetylene)-C_{60} systems: Influence of the nature of conjugation, Eur. J. Org. Chem. 3535–3543 (2008).
[175] F. D'Souza, M.E. Zandler, P.M. Smith, G.R. Deviprasad, K. Arkady, M. Fujitsuka, O. Ito, A ferrocene−C_{60}−dinitrobenzene triad: Synthesis and computational, electrochemical, and photochemical studies, J. Phys. Chem. A 106 (2002) 649–656.
[176] T.Y. Dong, T. Kambara, D.N. Hendrickson, Mixed-valence 1',6'-dihalobiferrocenium cations: counterions micromodulating intramolecular electron transfer, J. Am. Chem. Soc. 108 (1986) 5857–5865.
[177] Z. Wu, M. Jiang, Fullerene-pyrrolidine biferrocene donor-acceptor triads: Synthesis and effects of fullerene[60] on the electronic communication of the two ferrocene units in biferrocene, Aust. J. Chem. 69 (2015) 440–445.
[178] Z.Y. Wu, R. Zhong, F.Z. Yang, Novel fullerene-based ferrocene dyad and diferrocene triad: Synthesis and effects of introduction of fullerene[60] and phenyl linker on the thermodynamic stability, the magnetic properties and the band structure, J. Organomet. Chem. 840 (2017) 75–81.
[179] B. Bildstein, M. Schweiger, H. Angleitner, H. Kopacka, K. Wurst, K.H. Ongania, M. Fontani, P. Zanello, Tetraferrocenyl[5]cumulene, $(Fc)_2C{=}C{=}C{=}C{=}C(Fc)_2$: Synthesis, electrochemistry, and reactivity, including nickel(0)-promoted [3]ferrocenophane formation and [2+2] cycloaddition with fullerene C_{60}, Organometallics 18 (1999) 4286–4295.
[180] Y. Matsuo, T. Ichiki, S.G. Radhakrishnan, D.M. Guldi, E. Nakamura, Loading pentapod deca(ogano) [60] fullerenes with electron donors: from photophysics to photoelectrochemical bilayers, J. Am. Chem. Soc. 132 (2010) 6342–6348.
[181] L.C. Song, J.T. Liu, Q.M. Hu, G.F. Wang, P. Zanello, M. Fontani, Synthesis, characterization, and electrochemical properties of organotransition metal fullerene derivatives containing dppf ligands. Crystal structures of fac-Mo$(CO)_3$(dppf)(CH_3CN), $W(CO)_4$(dppf), and mer-$W(CO)_3$(dppf)(η^2-C_{60}), Organometallics 19 (2000) 5342–5351.
[182] V.V. Bashilov, T.V. Magdesieva, D.N. Kravchuk, P.V. Petrovskii, A.G. Ginzburg, K.P. Butin, V.I. Sokolov, A new heterobimetallic palladium–[60]fullerene complex with bidentate bis-1, 1′-[P] 2-ferrocene ligand, J. Organomet. Chem. 599 (2000) 37–41.
[183] A. Listorti, G. Accorsi, Y. Rio, N. Armaroli, O. Moudam, A. Gégout, B. Delavaux-Nicot, M. Holler, J.F. Nierengarten, Heteroleptic copper (I) complexes coupled with methano [60] fullerene: Synthesis, electrochemistry, and photophysics, Inorg. Chem. 47 (2008) 6254–6261.
[184] D. Mencel, M. Jevric, E.S. Davies, M. Schroder, A.N. Khlobystov, Triad and cyclic diad compounds of [60]fullerene with metallocenes, Dalton Trans. 42 (2013) 5056–5076.
[185] W.Y. Yeh, S.H. Wu, Functionalization on the tetrairon cluster $Cp_4Fe_4(CO)_4$ with fulleropyrrolidine, Dalton Trans. 42 (2013) 12260–12264.
[186] J.Y. Liu, M.E. El-Khouly, S. Fukuzumi, D.K.P. Ng, Photoinduced electron transfer in a ferrocene–distyryl BODIPY dyad and a ferrocene–distyryl BODIPY–C_{60} triad, Chem. Phys. Chem. 13 (2012) 2030–2036.
[187] V. Bandi, M.E. El-Khouly, E. Ohkubo, V.N. Nesterov, M.E. Zandler, S. Fukuzami, F. D'Souza, Excitation-wavelength-dependent, ultrafast photoinduced electron transfer in bisferrocene/BF_2-chelated-azadipyrromethene/fullerene tetrads, Chem. Eur. J. 19 (2013) 7221–7230.
[188] H. Yamada, H. Imahori, S. Fukuzumi, Photocurrent generation using gold electrodes modified withself-assembled monolayers of a fullerene–porphyrin dyad, J. Mater. Chem. 12 (2002) 2034–2040.
[189] D. Bonifazi, O. Enger, F. Diederich, Supramolecular [60]fullerene chemistry on surfaces, Chem. Soc. Rev. 36 (2007) 390–414.
[190] D. Wróbel, A. Graja, Photoinduced electron transfer processes in fullerene–organic chromophore systems, Coord. Chem. Rev. 255 (2011) 2555–2577.
[191] D.M. Guldi, C. Luo, T. Da Ros, M. Prato, E. Dietel, A. Hirsch, Photoinduced electron transfer in multicomponent arrays of a π-stacked fullerene porphyrin dyad and diazabicyclooctane or a fulleropyrrolidine ligand, Chem. Commun. 375–376 (2000).
[192] D.M. Guldi, C. Luo, A. Swartz, M. Scheloske, A. Hirsch, Self-organisation in photoactive fullerene porphyrin based donor–acceptor ensembles,, Chem. Commun. 1066–1067 (2001).
[193] F. D'Souza, G.R. Deviprasad, M.E. Zandler, V.T. Hoang, K. Arkady, M. van Stipdonk, A. Perera, M.E. El-Khouly, M. Fujitsuka, O. Ito, Spectroscopic, electrochemical, and photochemical studies of self-Assembled via axial coordination zinc porphyrin− fulleropyrrolidine dyads, J. Phys. Chem. A 106 (2002) 3243–3252.
[194] F. D'Souza, G.R. Deviprasad, M.E. Zandler, M.E. El-Khouly, M. Fujitsuka, O. Ito, Electronic interactions and photoinduced electron transfer in covalently linked porphyrin−C_{60}(pyridine) diads and supramolecular triads formed by self-assembling the diads and zinc porphyrin, J. Phys. Chem. B 106 (2002) 4952–4962.
[195] J. Fujisawa, K. Ishii, Y. Ohba, S. Yamauchi, M. Fush, K. Mobius, X- and W-band time-resolved electron paramagnetic resonance studies on radical-excited triplet pairs between metalloporphyrins and axial-ligating nitroxide radicals, J. Phys. Chem. A 101 (1997) 5869–5876.
[196] A. Mateo-Alonso, C. Sooambar, M. Prata, Fullerene photoactive dyads assembled by axial coordination with metals, C.R. Chimie 9 (2006) 944–951.
[197] F.T. Tat, Z. Zhou, S. MacMahon, F. Song, A.L. Rheingold, L. Echegoyen, D.I. Schuster, S.R. Wilson, A new fullerene complexation ligand: N-pyridylfulleropyrrolidine, J. Org. Chem. 69 (2004) 4602–4606.
[198] F. D'Souza, P.M. Smith, L. Rogers, M.E. Zandler, D.M.S. Islam, Y. Araki, O. Ito, Formation, spectral, electrochemical, and photochemical behavior of zinc N-confused porphyrin coordinated to imidazole functionalized fullerene dyads, Inorg. Chem. 45 (2006) 5057–5065.
[199] S.K. Das, B. Song, A. Mahler, V.N. Nesterov, A.K. Wilson, O. Ito, F. D'Souza, Electron transfer studies of high potential zinc porphyrin–fullerene supramolecular dyads, J. Phys. Chem. C 118 (2014) 3994–4006.
[200] C.K.C. Bikram, N.K. Subbaiyan, F. D'Souza, Supramolecular donor–acceptor assembly derived from tetracarbazole–zinc phthalocyanine coordinated to fullerene: Design, synthesis, photochemical, and photoelectrochemical studies, J. Phys. Chem. C 116 (2012) 11964–11972.
[201] F. D'Souza, M.E. El-Khouly, S. Gadde, A.L. McCarty, P.A. Karr, M.E. Zandler, Y. Araki, O. Ito, Self-assembled via axial coordination magnesium porphyrin−imidazole appended fullerene dyad: Spectroscopic, electrochemical, computational, and photochemical studies, J. Phys. Chem. B 109 (2005) 10107–10114.
[202] M.E. El-Khouly, D.K. Ju, K.Y. Kay, F. D'Souza, S. Fukuzumi, Supramolecular tetrad of subphthalocyanine–triphenylamine–zinc porphyrin coordinated to Fullerene as an "antenna-reaction-center" mimic: Formation of a long-lived charge-separated state in nonpolar solvent, Chem. Eur. J. 16 (2010) 6193–6202.
[203] M.E. El-Khouly, Y. Araki, O. Ito, S. Gadde, A.L. McCarty, P.A. Karr, M.E. Zandler, F. D'Souza, Spectral, electrochemical, and photophysical studies of a magnesium porphyrin–fullerene dyad, Phys. Chem. Chem. Phys. 7 (2005) 3163–3171.
[204] D.I. Schuster, K. Li, D.M. Guldi, A. Palkar, L. Echegoyen, C. Stanisky, R.J. Cross, M. Niemi, N.V. Tkachenko, H. Lemmetyinen, Azobenzene-linked porphyrin−fullerene dyads, J. Am. Chem. Soc. 129 (2007) 15973–15982.
[205] C.O. Obondi, G.N. Lim, F. D'Souza, Triplet–triplet excitation transfer in palladium porphyrin–fullerene and platinum porphyrin–fullerene dyads, J. Phys. Chem. C 119 (2015) 176–185.
[206] V. Sannasi, D. Jeyakumar, Synthesis of aziridinofullerene-porphyrin mediated by triethyl phosphite: physicochemical and electrochemical properties, Chem. Select 2 (2017) 9130–9135.
[207] N. Gupta, S. Nagvi, M. Jewariya, S. Chand, R. Kumar, Comparative chargé transfer studies in nonmetallated and matallated porphyrin fullerene dyads, J. Phys. Org. Chem. 30 (2017) e3685.
[208] J. Mohanraj, A. Barbieri, N. Armaroli, M. Vizuete, F. Langa, B. Delavaux-Nicot, M. Vartanian, J. Iehl, Efficient photoinduced energy and electron transfer in Zn^{II}–porphyrin/fullerene dyads with interchromophoric distances up to 2.6 nm and no wire-like connectivity, Chem. Eur. J. 23 (2017) 14200–14212.
[209] D. Bonifazi, G. Accorsi, N. Armaroli, F. Song, A. Palkar, L. Echegoyen, M. Scholl, P. Seiler, B. Jaun, F. Diederich, Oligoporphyrin arrays conjugated to [60]fullerene: preparation, NMR analysis, and photophysical and electrochemical properties, Helv. Chim. Acta 88 (2005) 1839–1884.
[210] N. Armaroli, G. Accorsi, F. Song, A. Palkar, L. Echegoyen, D. Bonifazi, F. Diederich, Photophysical and electrochemical properties of meso, meso-linked oligoporphyrin rods with appended fullerene terminals, Chem. Phys. Chem. 6 (2005) 732–743.
[211] M.H. Lee, J.W. Kim, C.Y. Lee, [60]Fullerene–porphyrin–ferrocene triad self-assembled monolayers (SAMs) for photovoltaic applications, J. Organomet. Chem. 761 (2014) 20–27.
[212] Y.J. Cho, T.K. Ahn, H. Song, K.S. Kim, C.Y. Lee, W.S. Seo, K. Lee, S.K. Kim, D. Kim, J.T. Park, Unusually high performance photovoltaic cell based on a [60]fullerene metal cluster-porphyrin dyad SAM on an ITO electrode, J. Am. Chem. Soc. 127 (2005) 2380–2381.
[213] C.Y. Lee, J.K. Jang, C.H. Kim, J. Jung, B.K. Park, J. Park, W. Choi, Y.K. Han, T. Joo, J. T. Park, Remarkably efficient photocurrent generation based on a [60]fullerene–triosmium cluster/Zn–porphyrin/boron–dipyrrin triad SAM, Chem. Eur. J. 16 (2010) 5586–5599.
[214] H. Wu, S. Fan, X. Jin, H. Zhang, H. Chen, Z. Dai, X. Zou, Construction of a zinc porphyrin–fullerene-derivative based nonenzymatic electrochemical sensor for sensitive sensing of hydrogen peroxide and nitrite, Anal. Chem. 86 (2014) 6285–6290.
[215] S. Fan, J. Yang, T. Wei, J. Zhang, N. Zhang, M. Chai, Zinc porphyrin–fullerene derivative noncovalently functionalized graphene hybrid as interfacial material for electrocatalytic application, Talanta 160 (2016) 713–720.
[216] A. Gouloumis, S.G. Liu, A Sastre, P. Vázquez, L. Echegoyen, T. Torres Synthesis and electrochemical properties of phthalocyanine–fullerene hybrids, Chem. Eur. J. 6 (2000) 3600-3607.
[217] C. Solis, M.B. Ballatore, M.B. Suarez, M.E. Milanesio, E.N. Durantini, M. Santo, T. Dittrich, L. Otero, Miguel Gervaldo, Electrochemical generation of a

molecular heterojunction. A new Zn-porphyrin-fullerene C_{60} polymeric film, Electrochim. Acta 238 (2017) 81–90.
[218] O. Trukhina, M. Rudolf, G. Bottari, T. Akasaka, L. Echegoyen, T. Torres, D.M. Guldi, Bidirectional electron transfer capability in phthalocyanine–$Sc_3N@I_h$–C_{80} Complexes, J. Am. Chem. Soc. 137 (2015) 12914–12922.
[219] S. Wolfrum, J.R. Pinzón, A. Molina-Ontoria, A. Gouloumis, N. Martín, L. Echegoyen, D.M. Guldi, Utilization of $Sc_3N@C_{80}$ in long-range charge transfer reactions, Chem. Commun. 47 (2011) 2270–2272.
[220] M.D. Westmeyer, T.B. Rauchfuss, A.K. Verma, Iron sulfido derivatives of the fullerenes C_{60} and C_{70}, Inorg. Chem. 35 (1996) 7140–7147.
[221] A. Molina-Naria, D.M. Rivera-Nazario, A. Tigreros, A. Ortiz, J.E. Nunez, B. Insuasty, D. Lueders, S. Wolfrum, D.M. Guldi, L. Echegoyen, Geometric influence on intramolecular photoinduced electron transfer in platinum(II) acetylide-linked donor–acceptor assemblies, Chem. Eur. J. 20 (2014) 11111–11119.
[222] V. Bonuccelli, T. Funaioli, P. Leoni, L. Marchetti, S. Zacchini, Bridging molecular clusters and fullerene, Dalton Trans. 42 (2013) 16898–16908.
[223] F. D'Souza, E. Maligaspe, M.E. Zandler, N.K. Subbaiyan, K. Ohkubo, S. Fukuzami, Metal quinolinolate−fullerene(s) donor−acceptor complexes: Evidence for organic LED molecules acting as electron donors in photoinduced electron-transfer reactions, J. Am. Chem. Soc. 130 (2008) 16959–16967.
[224] M.A. Lebedeva, T.W. Chamberlain, E.S. Davies, D. Mancel, B.E. Thomas, M. Suyetin, E. Bichoutskaia, M. Schroder, A.N. Khlobystov, Transition metal complexes of a salen–fullerene diad: redox and catalytically active nanostructures for delivery of metals in nanotubes, Chem. Eur. J. 19 (2013) 11999–12008.